

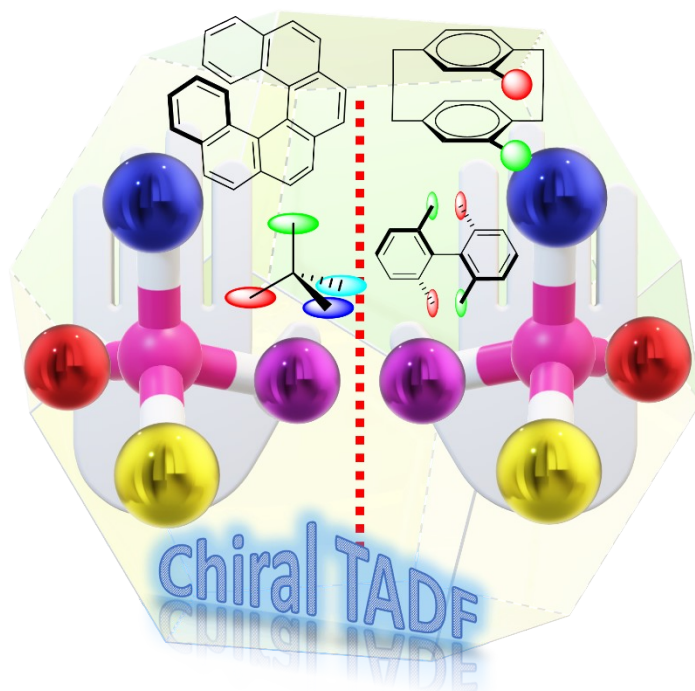
Chirality Inducing Units in Organic TADF Molecules: A Way to Circularly Polarized Luminescence

Diksha Thakur, and Sivakumar Vaidyanathan*

Department of Chemistry, Indian Institute of Technology Hyderabad, Sangareddy, Kandi,
Telangana 502285, India.

* To whom correspondence should be addressed. Email: vsiva@chy.iith.ac.in (Sivakumar Vaidyanathan).

TOC:



Abstract

The circularly polarized luminescence (CPL) emission has become a hot topic due to its applications in optical data storage, optical spintronics, and 3D displays. The CP-OLEDs, being a highly efficient source of CP light, open new possibilities for CP electroluminescence technology in the future. Various types of small and large chiral organic molecules, metal complexes, and macromolecules with decent efficiencies have been developed in this regard. The present literature also includes different approaches for inducing chirality in the organic molecules. TADF technology has been regarded as a promising technique thanks to its 100% internal quantum efficiency and precious metal-free emitters. Therefore, inducing chirality to the TADF molecules to generate CP-EL remains one of the efficient techniques for the future of the CP-OLEDs. This review summarizes various methods or organic moieties utilized in literature to induce chirality in the small organic TADF molecules. We discuss the different moieties to develop the TADF molecule and the organic units to bestow it with the chirality. In addition, their theoretical analysis, photo-physics, chiroptical properties, and chiral-EL efficiencies have also been summarized and discussed. We firmly believe that this review would benefit researchers working in the area of chirality and contribute its share to the future of display technology.

Keywords: circularly polarized; OLED; TADF; chiral; electroluminescence; EQE

1. Introduction

Since the very first report of **organic light emitting diode (OLED)** devices in 1987 this area of research has become a hot topic for future display technology.^[1] OLED comprises of sandwich-type structure with different layers, and the working mechanism includes the recombination of holes and electrons inside the emissive layer to produce exciton (**Figure 1a**). With large number of advantages compared to the current displays and their ability to be easily fabricated on the flexible substrates, OLEDs possess great potential to replace the existing display technology.^[2] Additionally, along with several benefits, the widespread adoption of OLEDs as lighting technology has the potential to save a substantial amount of electricity.^[2] Given the significance of **circularly polarized luminescence (CPL)** in different types of display applications, especially in three-dimensional displays, it has become hot-topic research recently. The CP-OLEDs, being a highly efficient source of CP light, open new possibilities for CP electroluminescence technology in the near future. Numerous kinds of metal complexes, macromolecules, and small- and large-sized chiral organic compounds have been synthesized which provide high efficiency CP-OLEDs. The efficiency of an OLED device is generally expressed in terms of **external quantum efficiency (EQE)** and **internal quantum efficiency (IQE)**. The IQE is defined as the ratio of number of excitons (electron-hole pair) generated inside the device to number excitons given to the device. Similarly, the EQE is defined as the ratio of number of excitons generated outside the device to the number of excitons given to the device. Excitons are typically generated in 25% (singlet excitons) and 75% (triplet excitons) when holes and electrons are introduced into an emissive layer from their respective electrodes.^[3] Since only singlet excitons may be converted into radiative emission in the case of fluorescent emitting materials, only 25% IQE is theoretically feasible.^[3] The very limited value of the IQE led to deeper research in this area in order to find the methods of triplet exciton utilization. The groundbreaking work on phosphorescent OLEDs was done independently by M. A. Baldo and Ma et al, in 1998 and able to harvest the dark triplet exciton to ground state resultant with IQE of 100%.^[4,5] The radiative emissions from triplet excited states to singlet ground states are prohibited, however, spin-orbit coupling enables these transitions in heavy metal complexes.^[6] Increasing singlet excitons concentration with the help of RISC of the triplet excitons produces the third generation of **OLEDs**, the **thermally activated delayed fluorescence (TADF)** (**Figure 1b**).^[7] Since TADF was initially detected in eosin, it is often referred to as E-type delayed fluorescence.^[7] The **reverse intersystem crossing (RISC)** process, which is followed by emission, is enhanced by the absorption of thermal energy in TADF

materials. The 25% of the singlet excitons are responsible for the prompt emission in the transient photoluminescence (PL) decay experiment while 75% comes from delayed fluorescence via RISC.^[3] The slow first excited triplet (T_1) to first excited singlet (S_1) to ground state (S_0) transition, with a lifetime of longer than microseconds, causes the delayed fluorescence, on the other hand, the fast S_1 to S_0 transition with an excited state lifetime of several nanoseconds causes the prompt fluorescence.^[3] The material design strategy of the TADF molecules include involvement of strong donor and acceptor framework. Due to the spatial separation of the HOMO and LUMO, strong donors and acceptors concentrate the HOMO and LUMO on the donor and acceptor moiety, respectively.^[3] The material design method shortening the lifetime for delayed fluorescence is the molecular design to reduce singlet triplet energy gap (ΔE_{ST}).^[3] Increasing the donor and acceptor strength inside the framework and twisted geometry with large angles between the donor and acceptor have been the two major strategies that are used to manipulate the ΔE_{ST} .^[3] The TADF technology is promising method because of its precious metal-free production and 100% IQE. As organic thermally triggered delayed fluorescence emitters have the potential to achieve 100% internal quantum efficiency, they have garnered a lot of attention recently. Faster radiative decay, saturated color purity, and high quantum yields are the outcomes of TADF molecules. These types of molecules have capacity to collect both electro-generated singlet and triplet excitons. Therefore, developing chiral TADF molecules which can generate the CP light with high efficiency is certainly an important strategy to achieve breakthrough in this field.

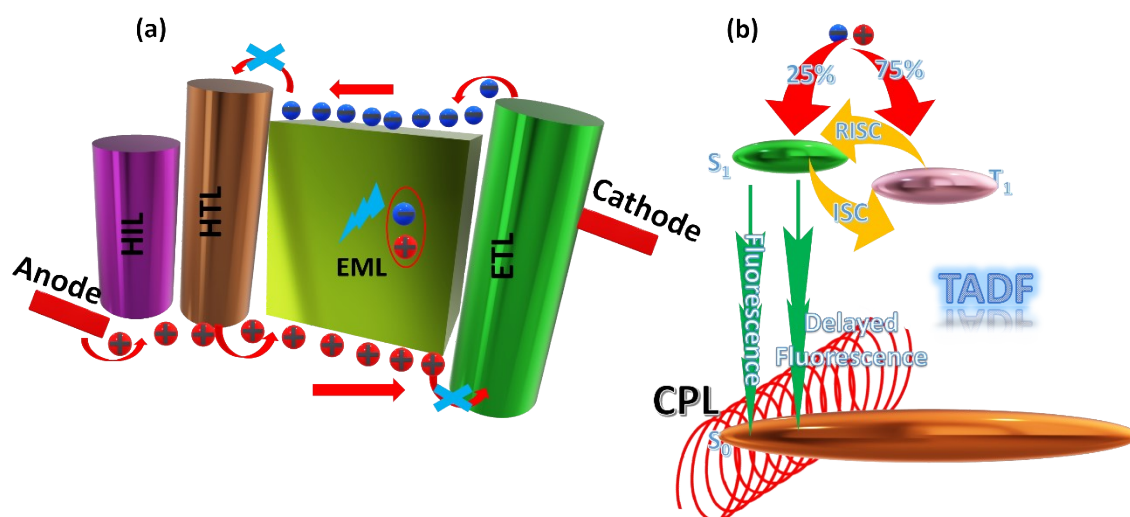


Figure 1. (a) OLED layer structure; (b) TADF mechanism.

Polarized light is a type of light wave where the direction of the light vector's vibration is either constant or varies periodically and it possesses several practical uses in many areas.^[8,9] The light which is coming from normal light source such as Sun, normal light bulbs etc. is the combination of magnetic and electric field propagating in the space. The plane of vibration of electric vector and magnetic vector are perpendicular to each other and perpendicular to the direction of motion of light. Thus, there are two planes perpendicular to each other, one contains electric field vector and the other contains magnetic field vector. The magnetic and electric field vectors can occur in various planes, but these two components would always be perpendicular to each other in case of unpolarized light. When the light is passed through the polariser, the direction of the electric field component would be limited to only one plane. Thus, after passing through the polarizer, the **electromagnetic (EM)** wave is polarized to only one direction which is perpendicular to the direction of propagation of the light. Thus, in case of a linearly polarized light, the electric field component (magnetic field component would always be perpendicular to it) of the light would be limited to only one plane or direction. This is called linearly polarized light. In case of CP light, this EM field of the wave will always have constant magnitude and will rotate circularly at constant rate. This direction of rotation will be perpendicular to the direction of propagation of the EM wave. The CP light can be categorised as **(left-handed circularly polarized) LCP light** and **(right-handed circularly polarized) RCP** light. In case of LCP, the electric field component rotates in the left-hand sense relative to the direction of propagation of light while in case of RCP, the electric field component rotates in the right-hand sense relative to the direction of propagation of light.

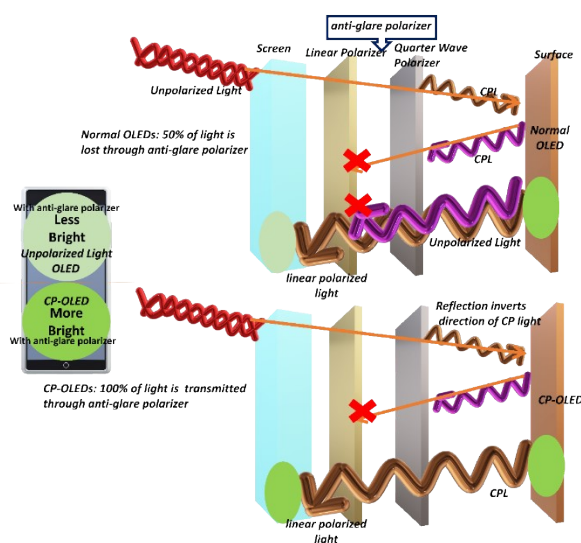


Figure 2. Advantages of CP-OLEDs compared to normal OLEDs [redrawn from 10].^[10]

OLED technology is still in need of improvement for enhancing the efficiency of the devices. Many portable display devices contain anti-glare filters installed in them which are necessary to reduce the amount of light reflection coming from the outside. **Figure 2** clearly compares the light emission intensity by the normal OLED and a CP-OLED.^[10] It is also implied that up to 50% of the electroluminescence (EL) produced by the OLED will be lost when using this kind of filter.^[10] It is necessary to use the anti-glare filter in the display devices to reduce the glare of light from outside. A screen without anti-glare filter will not be visible clearly. An anti-glare filter is the combination of a quarter wave plate and a linear polarizer. When the unpolarized light falls on the emissive surface of a normal OLED, it has to pass through linear polarizer followed by quarter wave polarizer. The linear polarizer will convert unpolarized light to linearly polarized and the quarter wave plate would change linearly polarized light to CP light. This CP light falls on the emissive metallic surface and gets reflected. The reflection of the CP light inverts the direction of polarization. Thus, this inverted CP light cannot return through the anti-glare filter as it allows only one type of CP light to pass through it (either LCP or RCP). This explains the necessity of the anti-glare filter in the display devices as it makes the picture clearer by reducing the glare of the outside light. A normal OLED which emits an unpolarized light suffers loss of light energy as the linear polarizer present in the anti-glare filter polarizes this emitted light to one plane. Whereas a CP light can really save energy in these cases and can flow through these filters with less attenuation.^[11]

Owing to many potential uses in displays and photonic technologies, CP light has drawn a lot of interest recently.^[11] The nonpolarized light may be easily converted into CP light by constantly passing it via a linear polarizer and quarter-wave plate, but this approach typically has complicated device design and brightness loss.^[11] The CPL may also be produced directly from chiral luminescent materials. The ground state and excited state characteristics of chiral luminous materials are often described using the CD and CPL, respectively. The ground state refers to absorption and the excited state refers to emission. In order to measure the CD spectra, LCP and RCP light is thrown upon the optically active material. The chiral molecules exhibit different extent of absorption of LCP and RCP light. The CD experiment analyses these differences by passing LCP and RCP light through a chiral sample. Thus, the optically active sample transmits different degrees of elliptically polarized light. This phenomenon is called CD and has been depicted in (**Figure 3a**). The chiroptical spectroscopies are widely used to measure the performance of the chiral isomers. In CD spectroscopy, the molar absorption coefficient of chiral luminous materials varies as LCP and RCP light passes through them. As

mentioned earlier, the difference in molar absorption coefficient is used to compute the CD intensity. It is measured by the absorption dissymmetry factor, g_{abs} , defined as $2(A_L - A_R)/(A_L + A_R)$.^[10] This is also described as $\Delta\varepsilon/\varepsilon$ and it does not depend on the solution concentration. A_L and A_R refer to absorption coefficient of LCP and RCP light.^[10]

The excited state characteristics of the optically active molecule are assessed using CPL spectroscopy. The luminescence intensity difference between LCP and RCP light is measured using CPL spectroscopy. **Figure 3b** depicts the basic principle of the CPL spectroscopy. The optically active material is excited with the help of non-polarized light. The optically active molecule interacts with the non-polarized light and decays to ground state by emitting one type of CP light (either LCP or RCP) in high intensity. There is also luminous dissymmetry factor, g_{lum} , which is used to measure the extent of the CPL.^[10,12] In the following equations, I_L/I_R refer to intensity of LCP/RCP light.

$$g_{\text{lum}} = 2(I_L - I_R)/(I_L + I_R)$$

$$g_{\text{lum}} = 0, \text{ non-polarized light}$$

$$g_{\text{lum}} = +2, \text{ fully left-handed CPL}$$

$$g_{\text{lum}} = -2, \text{ fully right-handed CPL}$$

Theoretically the dissymmetry factor can be associated to the electric and magnetic transition dipole moments. The following equation provides a theoretical expression for the g_{lum} factor.^[13]

$$g_{\text{lum}} = 4(|\mu||m| \cos \theta)/(|\mu|^2 + |m|^2)$$

The electric and magnetic transition dipole moments are represented by μ and m , respectively. The θ indicates the angle between these two vectors. The organic molecular compounds often have a higher $|\mu|$ value than $|m|$; therefore, the above equation can be written as follows.^[13]

$$g_{\text{lum}} = 4(|m| \cos \theta)/|\mu|$$

Chiral materials with magnetic dipole-allowed and electric dipole-forbidden transitions have the highest g_{lum} values. Lanthanide complexes are preferred for studying CPL phenomena because of their Laporte forbidden f to f transitions and high luminescence dissymmetry factor ($|g_{\text{lum}}| > 1$).^[10] Till date lanthanide complexes have the highest known (cesium tetrakis(3-heptafluoro-butylryl-(+)-camphorato) Eu(III) complexes) g_{lum} value of around 1.3.^[14]

Small chiral organic compounds have recently gained popularity as emitters due to their high luminescence quantum yields. Prior research found that the emission dissymmetry of CP light from a chiral emissive small molecule is often proportionate to and less than the absorption dissymmetry. Therefore, low selectivity in CP light absorption might result in low emission dissymmetry.^[15]

One major challenge in developing CPL materials is achieving a larger dissymmetry factor. Duan et. al. in 2019 achieved CP emission with a boosted dissymmetry factor by adjusting the solvent content and the morphology of the chiral emissive small molecules (*R*- or *S*-SPAn).^[16] They observed that it was possible to gain kinetic control over the attachment of chiral emitter (*R*- or *S*-SPAn) into different nanostructures with 0D nanospheres, 2D nanoflakes, and 3D stacked nanoflakes by varying the water percentage in the mixed THF/H₂O. Each one of these nanostructures composition was CPL active. They observed that the dissymmetry factors of the nanostructures were notably higher than those of the molecules and increased even more in various morphologies, ranging from 0D nanospheres to 2D flakes to 3D nanoflakes. They claimed that the excimer's intense luminescence caused by excellent packing might account for the increased g_{lum} value. This approach made it possible to produce organic nanomaterials with a greater dissymmetry factor while utilizing the same chiral small molecules and simply altering the supramolecular structures.

Samu et al. reported that increasing the chromophoric size can increase the dissymmetry factor.^[15,17] They reported a molecule of an aromatic chromophore and a nearby chiral center. In such a situation, the molecule's chirality was not strongly related to the chromophore. As a result, there is little asymmetry in the chromophore. For instance, at 205 nm, phenylethylammonium perchlorate had a very low dissymmetry value of $|g_{abs}|=8\times 10^{-5}$. They observed that by increasing the chromophore's size to a naphthyl ring, the g -factor might be raised to more than doubling the dissymmetry, $|g_{abs}|=2\times 10^{-4}$ at 222 nm.

Nitschke et. al. reported that the length of the self-assembled helical metallopolymers affected their g -factors.^[18] The free enantiopure monomers did not absorb their CD spectra in the disassembled state as the chiral center was far from the quinoline-based chromophore. Quinoline motifs self-assemble and display bands in the CD spectrum. They also coordinate to CuI ions to create a double helix of conjugated strands. They observed that the $|g_{abs}|$ of the metal-to-ligand charge-transfer and $\pi-\pi^*$ absorption bands increased from around 0.4×10^{-3} to 1.9×10^{-3} as a function of the metallopolymer length. They claimed that this length dependency

might be explained by increased exciton delocalization along the helically coiled backbone. Thus, increase in molecular size would be helpful in increasing the dissymmetry of the chirality.

As mentioned above that the CPL can be generated with the help of chiral luminescent or chiral TADF molecules, therefore, the question arises what are the various methods which are helpful in synthesizing the chiral TADF molecules. There are two types of design strategies for synthesizing chiral TADF molecules (**Figure 4**). The first approach is called chiral perturbation strategy. In chiral perturbation approach, a TADF unit is connected with the chiral unit. These two units together make a complete set of chiral luminescent molecule. The purpose of the TADF unit is to bestow the molecule with the fluorescent properties while the chiral unit serves as the chirality inducer. The chiral units may possess the axial, helical, planar or central chirality. This type of molecule is the basis for CP-OLEDs, which often have high EQEs but low EL dissymmetry factor. This might be because of the relative separation between the chiral and luminous centres. The second approach to construct the chiral molecule is the intrinsic or inherent chirality in the TADF molecule itself. This type of chiral TADF molecule have high values of the EL dissymmetry factor but it requires the resolution of the enantiomers from the mixture.^[10]

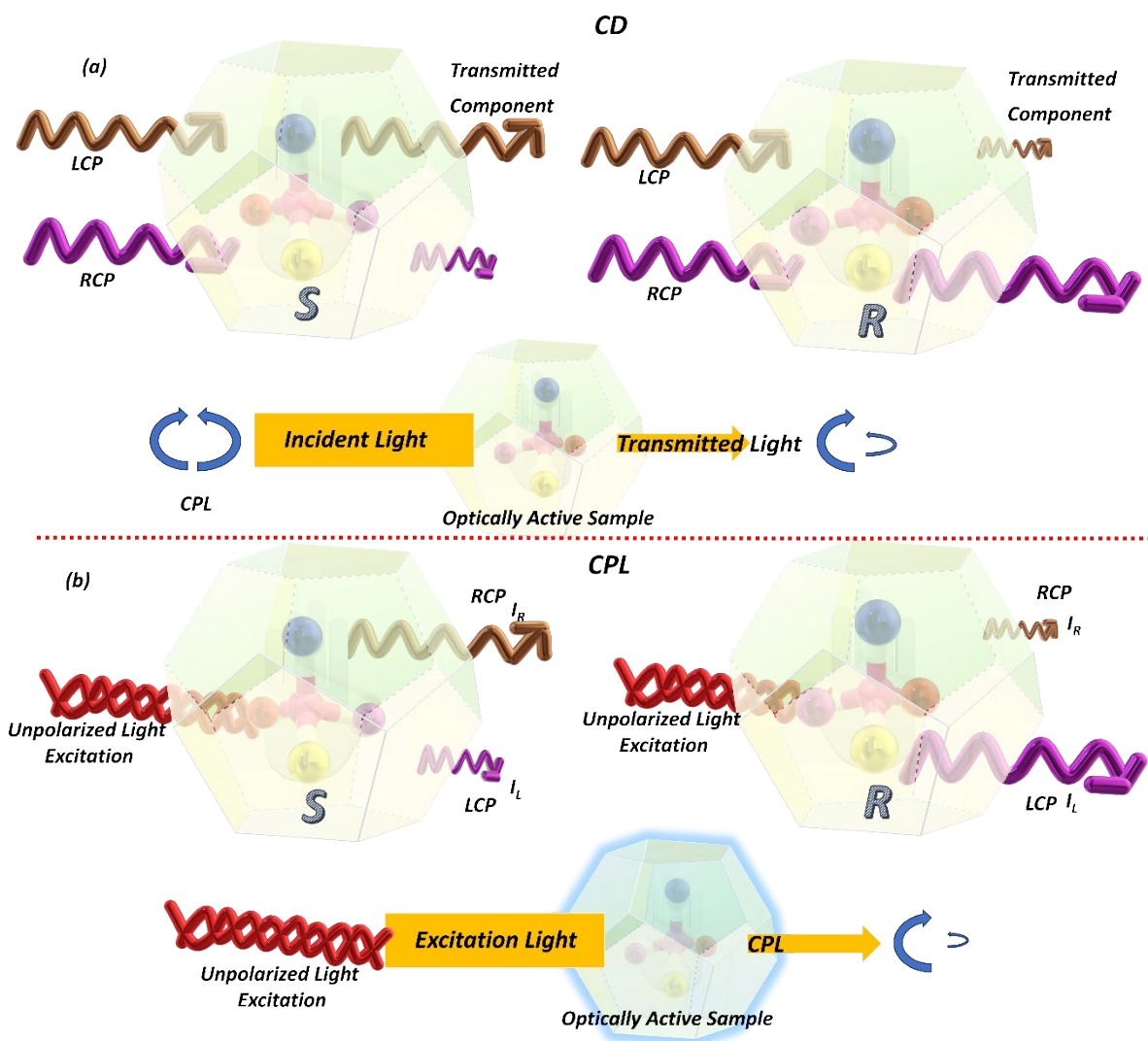


Figure 3. Illustration of (a) CD and (b) CPL phenomenon [redrawn from 10].^[10]

In the present review article, efforts have been made to categorize the chiral TADF molecule according to the chiral organic moieties or units (Asymmetric carbon, paracyclophane, biphenyl, helicene, 1,2-diaminocyclohexane, binaphthol, and octahydrobinaphthol are some of these organic moieties) that are used to impart chirality to the organic molecules. **Figure 5** depicts the classification method that has been used for the present review. We have also summarized their chiroptical properties, theoretical analysis, and chiral-EL efficiencies in addition to their photo-physics. In addition, the basic requirements of the TADF molecules, such as a small singlet-triplet energy gap for an efficient RISC process have also been explained. The strong donor-acceptor organic units having large dihedral angle or a π -spacer between them is one of the design strategies for developing TADF molecules. The present

review article explains various carbazole and phenothiazine decorated donor units and the cyano substituted acceptor moieties present in the organic TADF molecules.

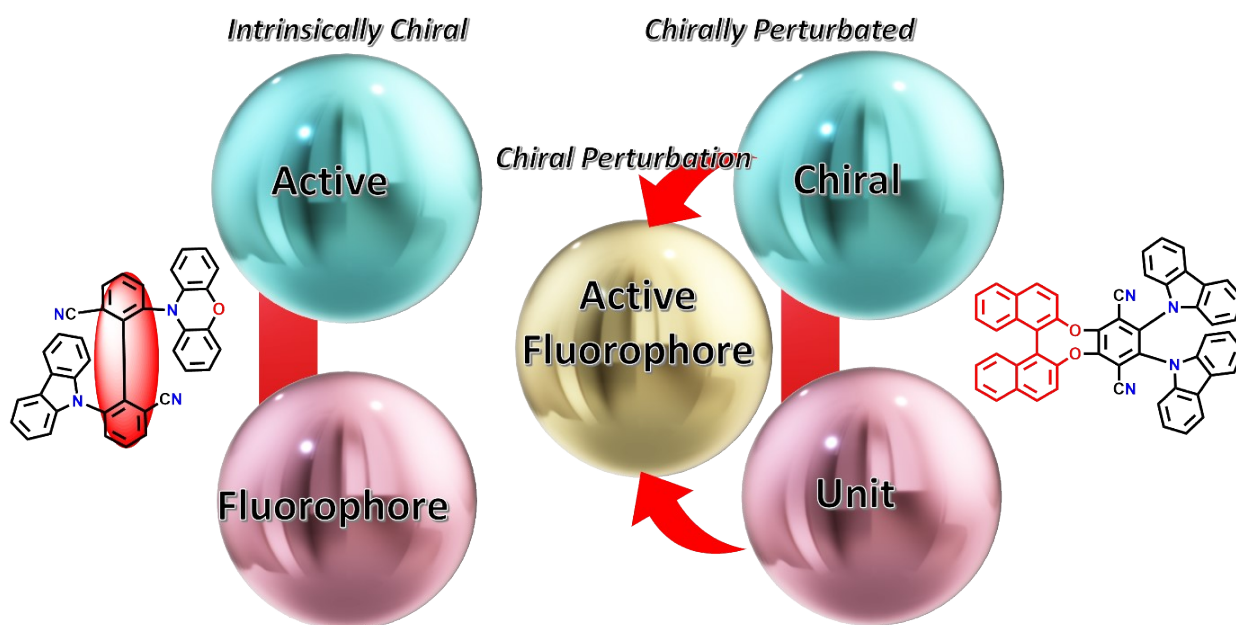


Figure 4. Design strategies of chiral TADF molecules. [redrawn from 10]^[10]

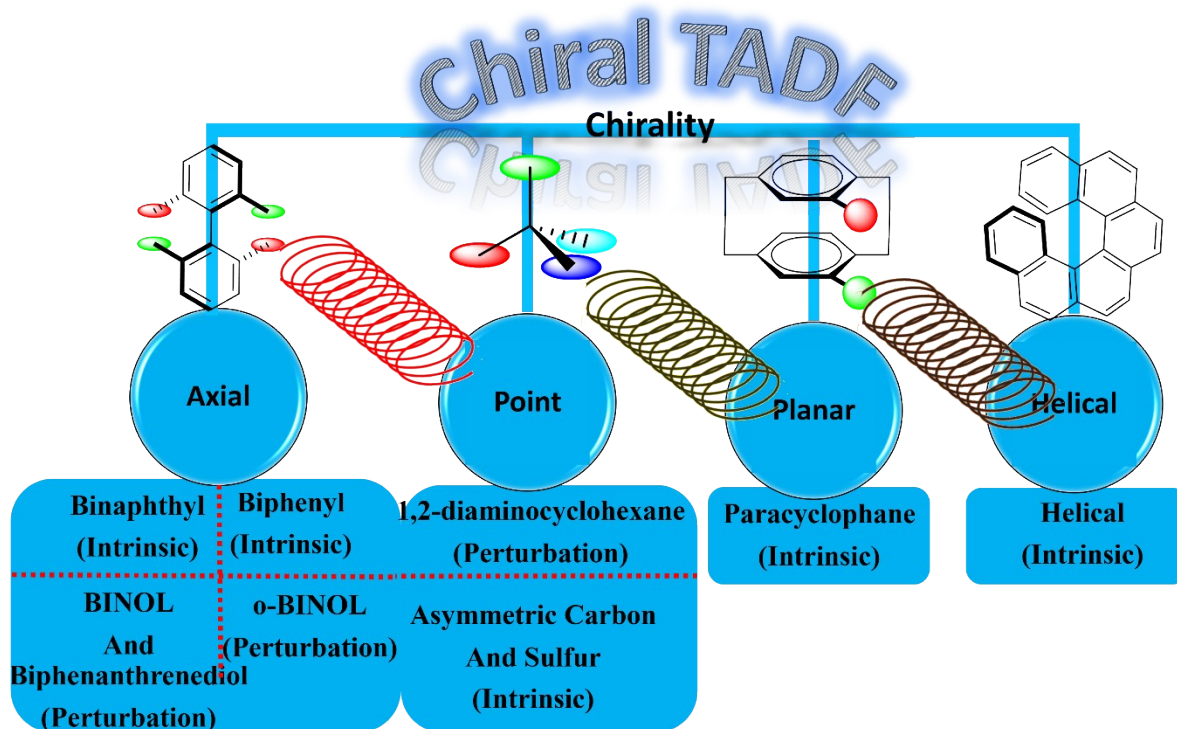


Figure 5. Classification of chiral TADF molecules.

2. Molecular designs for chiral TADF based on different units

2.1. 1,1'-Bi-2-naphthol (BINOL) based chiral TADF molecules

The first TADF material was reported in 2016 with the help of chiral perturbation strategy.^[19] The main focus is to connect a chiral unit to the TADF molecule which can bestow it with chirality. The TADF unit consisted of two carbazole directly connected to the benzene ring containing two cyano moieties while the chiral unit was 1,1'-Bi-2-naphthol (BINOL). The enantiopure molecules ((*R*)-1 and (*S*)-1) was synthesized using an efficient one-pot sequential process (**Figure 6**). It has been shown that both isomers of 1 with high enantiomeric excess and high yield was successfully synthesised via starting with enantiopure BINOL. Spatial separation of HOMO-LUMO is an important parameter for a TADF molecule. It has been observed through DFT calculations that the HOMO was mostly on the carbazole units and the LUMO on the terephthalonitrile. The presently observed spatial separation of HOMO and LUMO might indicate modest ΔE_{ST} . The chiral unit BINOL unit did not contain any frontier orbital coefficients. Although the chiral component was not directly engaged in the frontier, orbital, molecule 1 exhibited ECD and CPL activity, indicating effective chiral influence. The difference in sign between ECD and CPL measurements indicated a change in geometry between the basic state and S1. The developed molecule 1 depicted green emission with PLQY of 28% in aerated solution and 53% in inert atmosphere solution, respectively. These molecular structures depicted CPL with a luminescence dissymmetry factor, $|g_{lum}|$, of 1.3×10^{-3} . An OLED with an EQE_{max} of up to 9.1% has been achieved using these chiral dopants. **Table 1** summarizes different chiroptical properties of BINOL-based chiral TADF molecules.

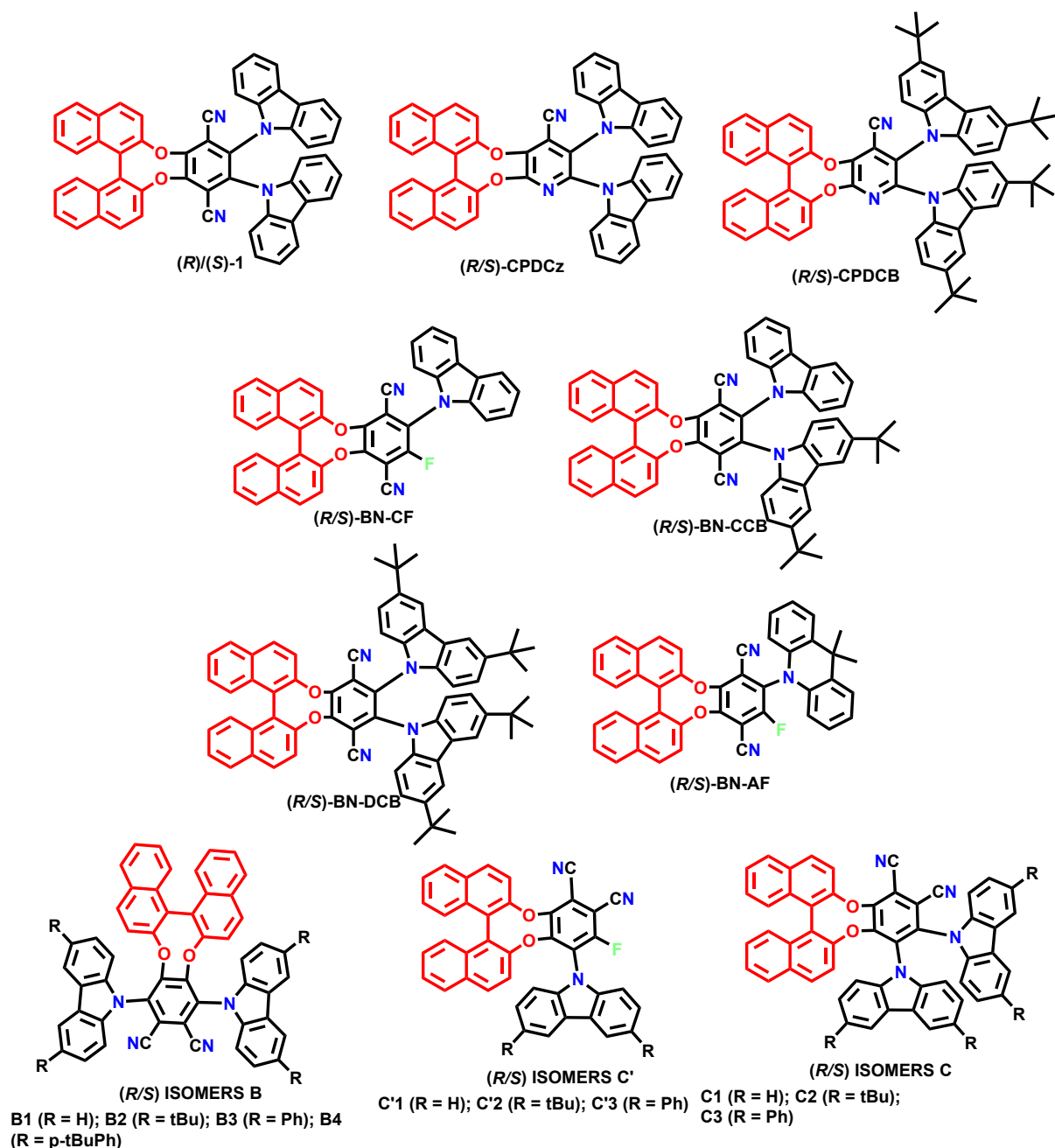


Figure 6. 1,1'-Bi-2-naphthol (BINOL) based chiral TADF molecules.^[19-22]

A numerous binaphthalene-based enantiomers with aggregation-induced emission (AIE) and TADF features ((*R/S*)-BN-AF, (*R/S*)-BN-CF, (*R/S*)-BN-DCB, and (*R/S*)-BN-CCB) has been designed and synthesized by Tang's group in 2018 (**Figure 6**).^[20] The chiral unit BINOL was connected in all four pairs of enantiomers which perturbed the TADF molecule with axial chirality. The synthetic design involved the two cyano units attached on the aryl group as the strong acceptor and carbazole or 9,10-dihydroacridine derivative as the donor. Through DFT calculations, it has been observed that the HOMOs were occupying the electron-donating carbazole and 9,9-dimethyl-9,10-dihydroacridine moieties and LUMOs were mostly found on

the central phenyl with cyano substitution, such a distinct distribution of HOMO and LUMO electron clouds encouraged lowering of ΔE_{ST} . The single crystals for the synthesized compounds confirmed the twisted geometries and observed a large torsion angle between the donor unit and acceptor unit which resulted in separation of HOMO and LUMO leading to small ΔE_{ST} . The torsion angle between the carbazole and phenyl rings in (*R*)-BN-CF was 46°, resulting in minimal electronic coupling and effective separation of the HOMO and LUMO. Small ΔE_{ST} and the RISC process were promoted, resulting in a molecule with notable delayed fluorescence properties. (*S*)-BN-DCB and (*S*)-BN-AF had a similar twisted conformation in their single crystal structures. (*S*)-BN-AF exhibited a torsion angle of 74° between its dimethyl-acridine unit and phenyl ring. Twisted conformations with weak intermolecular contacts effectively reduced exciton annihilation. Multiple C-H \cdots π and C-H \cdots N interactions in the crystal lattice could stiffen and lock intramolecular rotations, making molecules highly emissive in their crystal state. Tuneable emission (green to red) was observed due to the twisted intramolecular charge transfer phenomenon in the developed compounds depending on the polarity of the solvent. The synthesized compounds exhibited an AIE phenomenon as they emitted intense light in their solid powders. Increasing the water fraction from 70% to 99% resulted in a 48-fold increase in emission intensity for (*S*)-BN-CF and a significant blueshift of up to 46 nm with a peak at 506 nm. The aggregates in higher water amounts restricted intramolecular rotational and vibrational movements in molecularly dispersed solutions. This prevented nonradiative decay of the excited state, resulting in high luminous emission. (*S*)-BN-CCB and (*S*)-BN-DCB emitted up to 64.9-fold and 30.9-fold from water fraction = 60% to water fraction = 95%, respectively. The multi-layer doped and non-doped devices (CPOLEDs) was fabricated using the developed compounds. These CPOLEDs depicted high EL dissymmetry factors (g_{EL}) for doped and non-doped devices (Table 1). The EQE for (*S*)/(*R*)-BN-CF in CPOLED was as high as 9.3% and 3.5%, with g_{EL} values of +0.026/−0.021 and +0.06/−0.06, respectively. Unlike doped CPOLEDs, non-doped CPOLEDs exhibited greater g_{EL} and lower current efficiency roll-off due to a larger AIE impact.

Further in 2019, solution-processible TADF enantiomeric pairs were developed that showed high CPEL in the fabricated CP-OLEDs.^[21] The various units comprising these molecular structures included BINOL, carbazoles and cyanopyridine. The BINOL unit was responsible for CP emission induction via chiral perturbation, high stability against racemization upon photo-excitation and strong conjugation effects. The designed molecules consisted of cyanopyridine as an acceptor and carbazole ((*R/S*)-CPDCz)/di-tert-butyl-carbazole ((*R/S*)-

CPDCB) which were known for their high triplet energies (**Figure 6**). These designed enantiomers in high yields were easily prepared using one-pot sequential synthesis process. The synthesized materials possessed decent features like good solubility, intense emission, and mirror-image circular dichroism. The DFT calculations of the molecules displayed that LUMO was populated over the acceptor, cyanopyridine, and the chiral group BINOL had a very less contribution to both the HOMO and LUMO. Thus, the usage of a cyanopyridine derivative did not affect the HOMO-LUMO distribution, i.e., it was similar in the case of dicyano-substituted derivatives, indicating that the BINOL unit was not involved. The TADF molecules are supposed to have the distinct separation of the HOMO and LUMO for realizing reduced ΔE_{ST} . A slight overlap of the HOMO and LUMO on the cyanopyridine with overlap extent of around 33% was observed. This small overlap extent was significant for the high efficiency of the developed molecule and high PLQY. This was the reason the synthesized molecules could achieve high absolute PLQY as well as high solution-state PLQY. Solution-processed and vacuum-deposited OLEDs were fabricated. The CP-OLEDs based on these TADF molecules exhibited good CPEL signals with g_{EL} of 6×10^{-4} / -8.6×10^{-4} (dry-process (*R/S*) devices with EQE of 12.4% (*S*-CPDCB)) and higher g_{EL} of 3.5×10^{-3} / -3.9×10^{-3} (solution-processed (*R/S*) TADF devices with EQE of 10.6% (*S*-CPDCB)).

The effect of isomerism in the chiral unit BINOL based TADF molecules was explored in 2020.^[22] To identify the crucial structural and electrical characteristics that would allow for the maximum chiral disruption while maintaining the TADF characteristics. Three series of chiral TADF molecules namely B, C, and C' (**Figure 6**) were designed and synthesised. A phthalonitrile moiety served as the acceptor unit in molecule B having BINOL connected at positions 4 and 5, and carbazole derivatives at positions 3 and 6. In case of compounds C and C', the BINOL was connected at position 3 and 4. In the case of the C series of compounds, two carbazoles were coupled in positions 5 and 6. In contrast, for C' series of compounds, just one carbazole derivative was introduced in position 5. They expected a short distance between the chiral unit and the TADF chromophore's frontier orbitals with the designed architecture. Thus, an increase in the effect of chiral perturbation on the TADF D-A-D system was expected. Furthermore, due to steric congestion between the D-A-D system and the chiral unit, the system might assume a twisted conformation, improving its chiroptical features. Geometry optimization showed that non-covalent interactions between hydrogens in positions 3 and 3' of the BINOL moiety and carbazole aromatic rings limit free rotations in this architecture. DFT calculations depicted that HOMO and LUMO were mostly situated on donor and acceptor

units, respectively. The BINOL unit did not have any kind of distribution of frontier molecular orbitals. All the synthesized materials exhibited moderate quantum yields and aggregation-induced emission enhancement properties. The PMMA matrix of the compounds revealed bi-exponential luminous decays which validated the TADF characteristics of each of those molecules. The magnetic and electric transition dipole moments were analysed with the help of DFT calculations. The DFT calculations anticipated that compound B have a favourable orientation and B1 showed the highest g_{lum} value for CP-TADF molecules based on chiral perturbation strategy (3×10^{-3}).

Wang et al. in 2024 used the chiral perturbation technique to develop an enantiomeric pair of liquid-crystalline CP-TADF molecules (*R/S*)-4 **Figure 7**.^[23] Organic molecules have a relatively big electric transition dipole moment and a small magnetic transition dipole moment, making it challenging to get high g_{lum} values. Achieving high emission efficiencies and huge g_{lum} values in a single molecule is a significant task. They proposed a liquid-crystalline CP-TADF molecule as a solution to this issue. The developed molecule showed strong green emission comparable to the emission core of the CP-TADF, indicating that the addition of the mesogenic moieties had no impact on the emission characteristics. A distinct delayed emission component was seen in thin film and solution. The g_{lum} values in the doped film reached 0.1, which was two orders of magnitude greater than the values obtained for the native chromophore. (*R/S*)-4 displayed symmetrical CD and CPL signals as films. This phenomenon showed that g_{lum} amplification was positively impacted by liquid crystallinity. With (*R/S*)-4 as the dopants, the solution-processed, sensitized OLED attained an impressive maximum EQE of 21.2%.

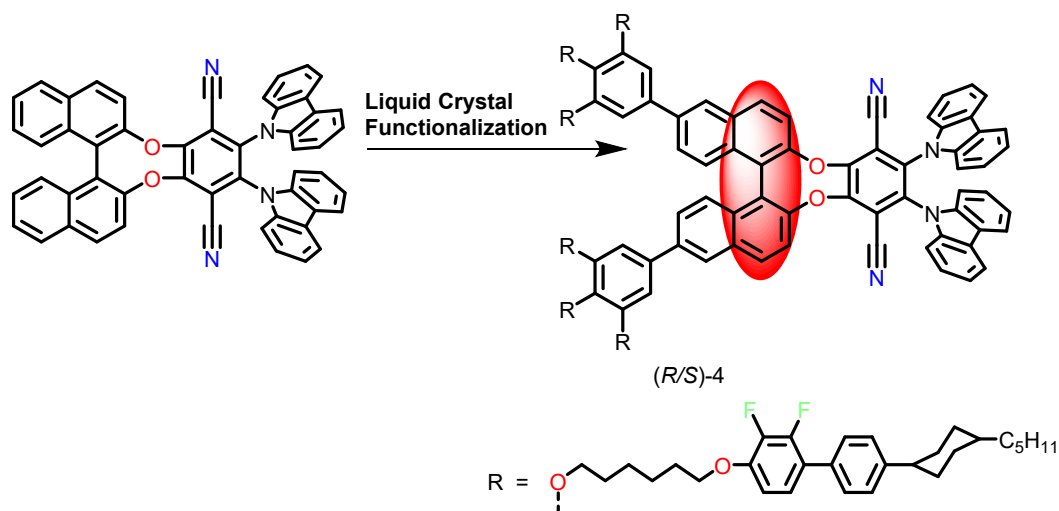
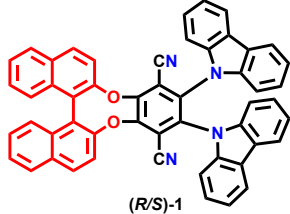
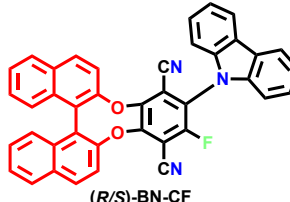
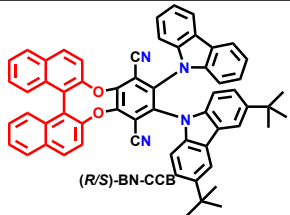
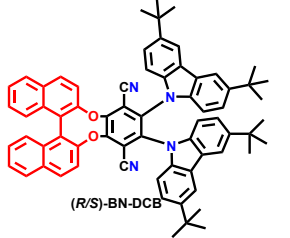
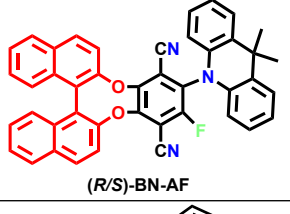
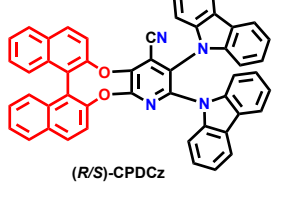
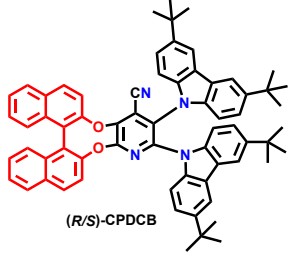
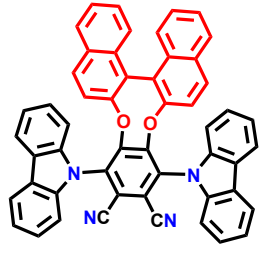
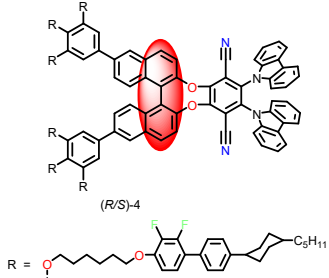
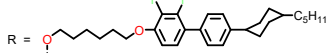


Figure 7. Chemical structure for (*R/S*)-4 molecule.^[23]

Table 1. Chiroptical properties of BINOL-based chiral TADF molecules.

Compound	EQE _{max} (%) (Isomer used as emitter)	Luminescence dissymmetry factor	Electroluminescence dissymmetry factor	Reference
 (R/S)-1	9.1 (S)	$ g_{lum} = 1.3 \times 10^{-3}$	-	[19]
 (R/S)-BN-CF	9.3 (S)	$g_{PL} = 0.041$ (S) $g_{PL} = -0.042$ (R) (Neat film)	$g_{EL} = 0.06$ (S) $g_{EL} = -0.06$ (R)	[20]
 (R/S)-BN-CCB	6.3 (S)	$g_{PL} = 0.038$ (S) $g_{PL} = -0.03$ (R) (Neat film)	$g_{EL} = 0.054$ (S) $g_{EL} = -0.063$ (R)	[20]
 (R/S)-BN-DCB	3.5 (S)	$g_{PL} = 0.03$ (S) $g_{PL} = -0.031$ (R) (Neat film)	$g_{EL} = 0.067$ (S) $g_{EL} = -0.082$ (R)	[20]
 (R/S)-BN-AF	1.7 (S)	$g_{PL} = 0.02$ (S) $g_{PL} = -0.02$ (R) (Neat film)	$g_{EL} = 0.084$ (S) $g_{EL} = -0.091$ (R)	[20]
 (R/S)-CPDCz	10.1/8.4 (S) (Solution/Vacuum-process)	$g_{PL} = 3.7 \times 10^{-4} / -3.3 \times 10^{-4}$ (R/S) (Neat film)	$g_{EL} = 2.5 \times 10^{-3} / -3.7 \times 10^{-3}$ (Solution-process) (R/S) $g_{EL} = 4.0 \times 10^{-4} / -5.5 \times 10^{-4}$ (Vacuum-process) (R/S)	[21]

 <p>(R/S)-CPDCB</p>	10.6/12.4 (S) (Solution/Vacuum-process)	$g_{PL} = 5.8 \times 10^{-4} / -4.0 \times 10^{-4}$ (R/S) (Neat film)	$g_{EL} = 3.5 \times 10^{-3} / -3.9 \times 10^{-3}$ (Solution-process) (R/S) $g_{EL} = 6.0 \times 10^{-4} / -8.6 \times 10^{-4}$ (Vacuum-process) (R/S)	[21]
 <p>(R/S)-B1</p>	-	$g_{lum} = 3 \times 10^{-3}$	-	[22]
 <p>(R/S)-4</p> <p>R = </p>	21.1 (R)	$g_{PL} = 0.8 \times 10^{-1} / -1.1 \times 10^{-1}$ (S)	-	[23]

2.2. Octahydro-binaphthol (o-BINOL) based chiral TADF molecules

Zheng's group reported a TADF material using chiral perturbation techniques and their goal was to use a chiral unit that could confer chirality to the TADF molecule.^[24] Here, octahydro-binaphthol (o-BINOL) used as a chiral unit. The TADF molecule consisted of two carbazole molecules that were directly attached to a benzene ring that had two cyano moieties. The enantiopure molecules ((R/S)-OBN-Cz) was synthesized using an efficient two step synthetic process by substitution of o-BINOL and carbazole with tetrafluoroterephthalonitrile (**Figure 8**). The enantiomers of (R/S)-OBN-Cz were revealed to assume a twisted shape with complete mirror symmetry with the help of single-crystal X-ray diffraction investigation. The DFT calculations for the synthesized enantiomers revealed that the LUMOs are primarily found on the phenyl and cyano units while the HOMOs were populated over carbazole unit. A clear spatial separation between the HOMO and LUMO was observed, which is necessary for small ΔE_{ST} gap. The small overlap of frontier molecular orbitals on the benzene ring which was enough for the high luminescence efficiency. For (R/S)-OBN-Cz, the theoretical ΔE_{ST} gap calculated by TD-DFT using the B3LYP functional was 0.064 eV, which was close to the value

determined by experimental data. A noticeable fluctuation in emission intensities and peaks in THF/water experiment with varied water fractions for *R*-OBN-Cz was observed, which indicated its TICT property and the aggregation-induced emission. The lifetime of the delayed component of (*R*)-OBN-Cz got significantly reduced by oxygen in the oxygen-filled toluene solution compared to the nitrogen atmosphere which further proved that (*R*)-OBN-Cz was depicting a TADF property. A small experimental ΔE_{ST} of 0.037 eV with high quantum yields of 92% and high CP-PL with dissymmetry factors ($|g_{PL}|$) of $\sim 2.0 \times 10^{-3}$ in thin film has been achieved. The fabricated CP-OLED device showed high maximum EQE of 32.6% and CP-EL signals with a $\sim |g_{EL}|$ of $\approx 2.0 \times 10^{-3}$. **Table 2** summarizes different chiroptical properties of o-BINOL-based chiral TADF molecules.

Further in 2019, same group again combined a chiral source and the luminophore skeleton to make a chiral TADF molecule.^[25] The chiral unit octahydro-binaphthol (o-BINOL) was utilized for perturbing the TADF unit with chirality. Two diphenylamine groups were directly joined to a benzene ring that possessed two cyano moieties to form the TADF molecule having a donor-acceptor molecular framework. Two-step synthesis method was used to synthesize enantiopure molecules ((*R/S*)-OBN-DPA) by substitution of o-BINOL and diphenylamine with tetrafluoroterephthalonitrile (**Figure 8**). The enantiomers exhibited perfect mirror symmetry and a twisted conformation due to steric hindrance from sixteen peripheral hydrogen atoms in cyclohexane parts. This suppressed molecule accumulation and reduced intermolecular interactions, resulting in low-efficiency roll-off at high current density. It has been predicted that the frontier molecular orbital distribution found that LUMOs were mostly found on the phenyl and cyano moieties. In contrast, the HOMOs were primarily dispersed on the diphenylamine units. The efficient up-conversion was observed from triplet to singlet energy levels might be accomplished by utilizing the effective spatial electronic separation of the HOMO-LUMO. This spatial separation between HOMO and LUMO led to modest ΔE_{ST} . A slight spatial overlap between the HOMO- LUMO at the benzene ring was found that would help to achieve high luminescence efficiency. A small ΔE_{ST} of 0.09 eV was obtained by calculating the first singlet and first triplet energy levels from the low-temperature fluorescence and phosphorescence spectra at 77K. This small ΔE_{ST} was responsible for better RISC from triplet to singlet state. The (*R*)-OBN-DPA compound exhibited an AIE effect. An enhancement in emission intensity at 99% water fraction was observed due to aggregation of molecules. The decent fluorescence nature of (*R*)-OBN-DPA in the solid state could make this material as an excellent AIE-active emitter. The (*R/S*)-OBN-DPA enantiomers displayed significant Cotton

effects and mirror-image CD bands before 350 nm, indicating chiral OBN unit absorption. The CD signals at 450 nm were caused by the twisted intramolecular charge transfer absorption of the D-A electronic structure from the TADF skeleton. This demonstrated effective chirality transfer from the chiral OBN unit to the TADF skeleton in its ground state. These developed chiral TADF enantiomers exhibited intense CP-PL with dissymmetry factors ($|g_{PL}|$) about $\sim 2.0 \times 10^{-3}$ in the films and a high PLQY of 84.67%. The doped as well as doped and non-doped CP-OLEDs were fabricated. The un-doped CP-OLEDs could accomplish $|g_{EL}|$ up to $\sim 2.9 \times 10^{-3}$.

In 2021, a TADF material ((*S/R*)-OBN-tBuCz) based on o-BINOL chiral unit (**Figure 8**) was developed.^[26] The chiral unit o-BINOL was fused with the tert-butylcarbazole cyanobenzene luminophore framework. The exterior sixteen hydrogen atoms in the cyclohexane part of the o-BINOL and the tertiary butyl group were responsible for increasing the steric hindrance and lessen the intermolecular stacking effect. The developed chiral molecules depicted green light emission at around 523 nm, a high PLQY of 85.2% and a low ΔE_{ST} of 0.05 eV with TADF characteristics. Circular dichroism (CD) and CPL spectra were used to study the chiroptical properties of (*S/R*)-OBN-tBuCz enantiomers in the ground and excited states. The strong CP luminescent signals with g_{PL} values of $+8.6 \times 10^{-4}$ and -6.5×10^{-4} in toluene solution were observed for (*S*) and (*R*)-OBN-tBuCz, respectively. The CP-OLEDs were fabricated using these enantiomers as chiral emitters because of their effective TADF and CPL characteristics. The CP-OLEDs based on (*S/R*)-OBN-tBuCz depicted a turn-on voltage of 3.9 V, a maximum brightness of 27709 cd/m², a maximum EQE of 12.4% and g_{EL} signal of 1.57×10^{-3} and -0.90×10^{-3} , respectively.

Further, a 5,5,10,10-tetraoxide acceptor, carbazole/ditert-butylcarbazole donors and a stable chiral octahydro-binaphthol unit were used to synthesize chiral (*R/S*)-OBS-Cz and (*R/S*)-OBS-TCz with axial chirality (**Figure 8**).^[27] The DFT calculations of the enantiomer revealed that the electronic clouds of the HOMO and the LUMO of the (*R*)-OBSCz and (*R*)-OBS-TCz molecules were situated over carbazole/ditert-butylcarbazole units and tetraoxide units, respectively. At the phenyl bridge, a minor overlap of HOMO and LUMO can be seen, which would help the radiative decay for high luminescence efficiency. The -tBu group enhanced carbazole's electron-donating capacity, leading to a higher HOMO energy level in (*R*)-OBSTCz. The computed findings suggested that both compounds could impact the TADF phenomena through an effective RISC mechanism. Weak absorption bands at 338-440 nm indicated twisted intramolecular charge transfer by electron transitions from donor to acceptor.

(*R*)-OBS-TCz had bathochromically shifted absorption peaks in the same transition mode as (*R*)-OBS-Cz. The PL spectra of (*R*)-OBS-Cz centered at 504 nm in toluene solution. Substitution of the -tBu group resulted in a redshifted emission peak about 520 nm for (*R*)-OBS-TCz. Cotton effects (325-400 nm) and CPL signals (425-650 nm) were mostly caused by the TICT process, indicating that (*R/S*)-OBN chirality was successfully transferred into the TADF core in both ground and excited states. The enantiomers exhibited symmetrical CD and CPL spectra. The developed chiral compounds depicted CP PL with dissymmetry factors ($|g_{PL}|$) of 8.7×10^{-4} (*R/S*-OBS-Cz) and 6.4×10^{-4} ((*R/S*)-OBS-TCz) in co-doped films. These compounds also displayed TADF features with small singlet-triplet energy gaps of 0.04 and 0.05 eV. A high PLQYs of the enantiomers *R*-OBS-Cz (0.68) and (*R*)-OBS-TCz (0.56) was observed in toluene solutions. In solid state co-doped films, higher quantum efficiencies were observed, which could be credited to the restricted rotation in the solid state. The high PLQY was advantageous for achieving high device performance. As the temperature increased from 100 to 298 K, the lifetime decay of (*R/S*)-OBSCz and (*R/S*)-OBS-TCz in doped film got shortened. This property indicated the presence of TADF characteristics in the developed molecules. The CP-OLEDs were fabricated by using these enantiomers, which demonstrated good device performances with a maximum EQE of 20.3% and CPEL characteristics with a $|g_{EL}|$ factor of up to 1.0×10^{-3} .

Li²⁸ group in 2021 proposed a design for circularly polarized multi-resonance TADF emitters. In first step, carbazole and boron-based MR-TADF emitter (DtBuCzB) were chosen.^[28] The B-substituted phenyl ring's para-carbon position was further modified by adding the peripheral electron-withdrawing group benzonitrile. These acceptor benzonitrile units served as chromophores. The chiral perturbation technique was used by attaching chiral (*R/S*)-OBN units to acceptor benzonitrile moieties to achieve CP luminescence. Thus, the synthesis of two sets of green emissive CP-MR-TADF enantiomers ((*R/S*)-OBN-4CN-BN and (*R/S*)-OBN-2CN-BN) was completed (**Figure 8**). The DFT calculations depicted that the HOMOs of the both molecules were mostly dispersed on the nitrogen and carbon atoms in the ortho/para locations. The HOMO distribution was similar to the parent molecule DtBuCzB. The LUMOs extended to the outer benzonitrile units and were mostly centered on the carbon and boron atoms in the ortho/para locations. The narrow FWHM was maintained by this frontier molecular orbital distribution. The addition of benzonitrile to the para-carbon position of the B-substituted phenyl ring dispersed the electron density and prevented the confined LUMO population. Thus, this type of insertion of increased the intra-molecular charge transfer strength. The ΔE_{ST} values

for (*R*)-OBN-2CN-BN (0.12 eV) and (*R*)-OBN-4CNBN (0.13 eV) were determined to be small which enabled effective RISC of excitons from T_1 to S_1 . Both (*R*)-OBN-2CNBN and (*R*)-OBN-4CN-BN exhibited double-exponential decay with prompt lifetimes of 9.8 and 10.0 ns while the delayed fluorescence decay was having lifetimes of 95.3 and 97.4 microseconds. It was found that the percentage of the delayed component increased as the temperature rose from 80 to 320 K, which supported the TADF. The fabricated the OLEDs using these molecules as emitters showed intense green EL and a maximum EQEs of 29.4% and 24.5%, respectively. The CP-OLEDs also clearly showed CPEL signals with g_{EL} of $+1.43 \times 10^{-3}$ / -1.27×10^{-3} ((*R/S*)-OBN-2CN-BN) and $+4.60 \times 10^{-4}$ / -4.76×10^{-4} ((*R/S*)-OBN-4CN-BN).

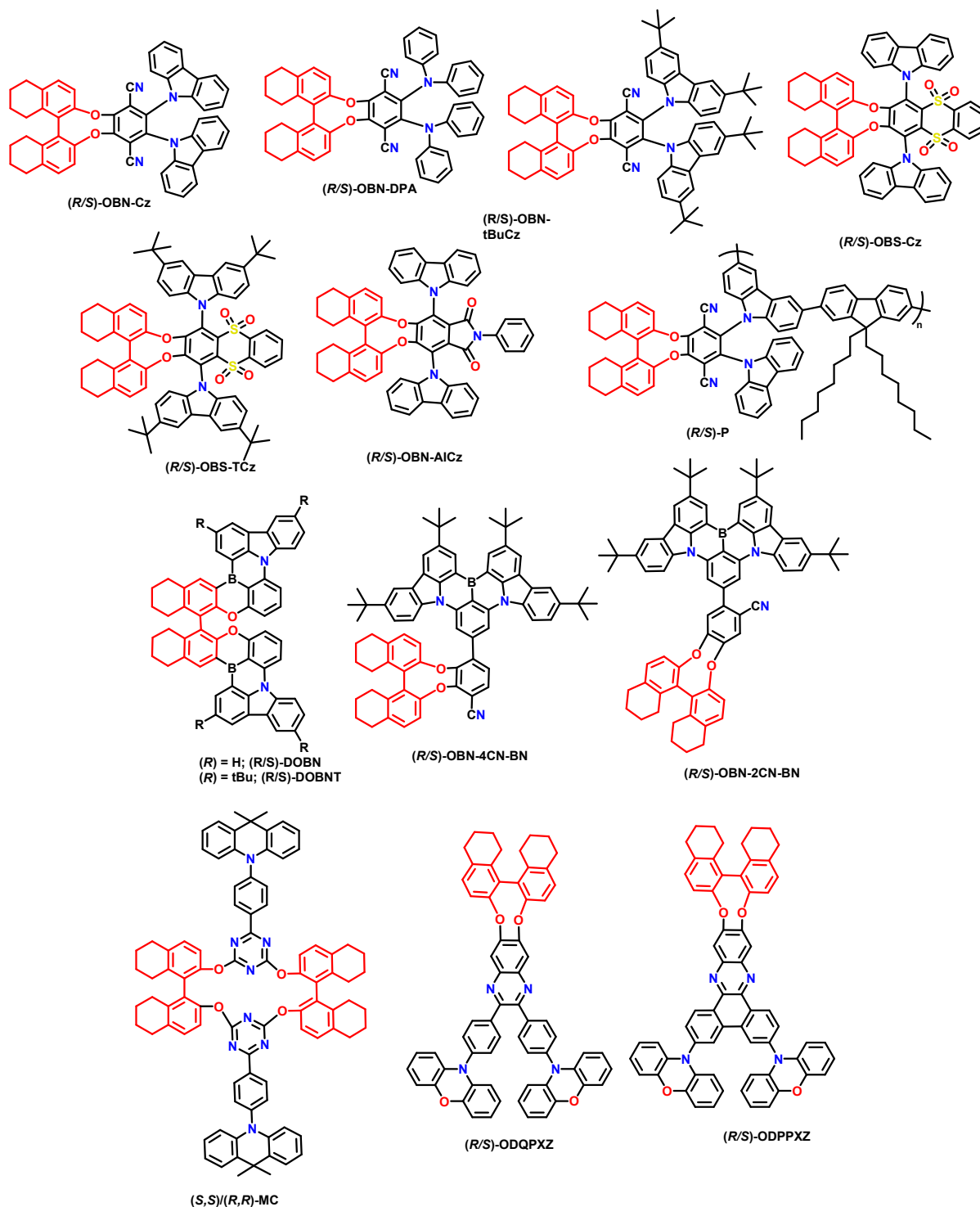


Figure 8. Octahydro-binaphthol (o-BINOL) based chiral TADF molecules.^[24-33]

Further, in 2021, octahydro-binaphthol (chiral *(R/S)*-OBN) was inserted into the TADF molecule to create two pairs of enantiomers (*(R/S)*-ODPPXZ and (*(R/S)*-ODQPXZ with CPPL and TADF characteristics (**Figure 8**).^[29] The phenoxazine moiety was used as a donor for the (*(R/S)*-ODQPXZ isomers, whereas 2,3-diphenylquinoxaline was used as an acceptor. The (*(R/S)*-ODPPXZ isomers were synthesized using a robust dibenzo[a,c]phenazine acceptor, in which

the two rotatable phenyl groups were joined by an additional single bond to produce a rigid coplanar dibenzo[a,c]phenazine moiety. These two pairs of chiral TADF molecules were created using a two-step method. The first step was the replacement of bromine atoms with phenoxazine donors through Pd-catalyzed C–N cross-coupling reactions. While the second step was the nucleophilic substitution ring closure with the OBN units. Due to significant steric hindrance, the dihedral angles between two phenoxazine units and benzene rings in (*R/S*)-ODQPXZ were 81°/82°, whereas the angles between the donors and the central quinaline plane were 41°/42°. A higher twisted angle of 85°/85° between phenoxazine and central plane for (*R/S*)-ODPPXZ was seen. In case of (*R/S*)-ODPPXZ with a rigid coplanar dibenzo[a,c]phenazine unit. The DFT calculation predicted that their HOMOs were situated on phenoxazine units. In contrast, the LUMOs were mostly found on the acceptor units, with a minor extension to the O atoms of the OBN unit. The minimal overlap between LUMO and HOMO on the neighbouring benzene ring caused an incredibly small ΔE_{ST} value of 0.181 ((*R/S*)-ODQPXZ) and 0.002 ((*R/S*)-ODPPXZ). Both the molecules exhibited the decomposition temperature above 400 °C. A little overlap between the PL and absorption spectra was observed which was responsible for high PLQY for both molecules. A notable aggregation-induced emission feature was also implied by the elevated emission intensities with an increasing water ratio in the THF/water experiment. The experimentally calculated ΔE_{ST} values were 0.16 eV ((*R*)-ODQPXZ) and 0.07 eV ((*R*)-ODPPXZ), respectively, indicating their quick RISC rate. For (*R*)-ODQPXZ and (*R*)-ODPPXZ neat films, the measured prompt/delayed fluorescence lifetimes were 20.3 ns/2.2 microseconds and 16.3 ns/1.1 microseconds. The CP-OLEDs were fabricated by using developed enantiomers as emitters. The CP-OLEDs exhibited CPEL signals with a $|g_{EL}|/EQE$ values of $6.0 \times 10^{-4}/28.3\%$ ((*R*)-ODQPXZ) and $2.4 \times 10^{-3}/20.3\%$ ((*R*)-ODPPXZ).

Chen's group, in 2022, developed a pair of aromatic-imide-substituted TADF enantiomers, known as (*R/S*)-OBN-AICz by connecting a chiral unit to the luminophore (**Figure 8**).^[30] The chiral unit o-BINOL was used to induce chirality to the TADF molecule. The final molecule was synthesized by nucleophilic substitution reaction of the carbazole and the chiral intermediate. The DFT calculations depicted that the HOMO was mostly concentrated on the electron-donor carbazole moieties while the LUMO was populated over the aromatic-imide units. The distinct separation of HOMO and LUMO was responsible for small ΔE_{ST} which was beneficial for RISC. The DFT calculations for the compound OBN-AICz's predicted the HOMO and LUMO energy levels were at 5.43 and 2.31 eV, respectively. It was found that the

chiral unit did not contribute to either the HOMOs or the LUMOs but the clear signals of CD and CPL were detected because of chiral disruption by *o*-BINOL. The single crystal of the synthesized molecule showed that there existed high torsion angle between the acceptor and donor which made effective spatial separation of the HOMO and LUMO. The enantiomers showed exceptional thermal stability, with (*R*)-OBN-AICz having a decomposition temperature of 419 °C. It was found that (*R*)-OBN-AICz was weakly emissive in pure THF solution and the emission intensity drastically decreased as the amount of water in the system rose from 0% to 60% along with the red shift in the peak maxima. The strong twisted intramolecular charge transfer process and enhanced intersystem crossing rate arose by the increasing polarity of solvent might be responsible for this. The water percentage was raised from 70% to 90%, there occurred a considerable blue-shift in the emission peak and a PL emission enhancement was observed. The PL intensity of (*R*)-OBN-AICz was found to be increased by 2.1 times from pure THF to water fraction of 90% in the THF water experiment. The aggregate state of the enantiomer in THF caused restriction in intramolecular rotational motion which resulted in the enhancement of the radiative decay. These outcomes illustrated the AIE characteristics of (*R*)-OBN-AICz. The ΔE_{ST} value of (*R*)-OBN-AICz was 0.08 eV based on the onset wavelengths of its phosphorescence and fluorescence spectra measured at 77 K. This small singlet-triplet energy gap enhanced the RISC process from first triplet to first singlet state. The room temperature transient PL decay curves of the mCBP doped film displayed a two-exponential decay. The delayed fluorescence lifetime of the (*R*)-OBN-AICz as 4.0 microseconds was found. Also, the photophysical characteristics of (*S*)-OBN-AICz were also investigated, and it was found that the photophysical properties of the (*S*)-OBN-AICz were comparable to those of (*R*)-OBN-AICz. The chiral emitters depicted effective TADF and AIE characteristics with small singlet-triplet energy gap of 0.08 eV and a high PLQY of 81%. The synthesized enantiomers had a distinct mirror image ECD band in toluene. Cotton's effects below 325 nm are likely due to the chiral OBN moiety's absorption. The modest Cotton effects seen in the long-wavelength region were attributed to the absorption of the ICT band from the carbazole donor to the aromatic-imide moiety. The spectra of (*R*)-OBN-AICz and (*S*)-OBN-AICz in toluene demonstrated chiroptical characteristics in the excited state. In toluene solution, the TADF enantiomers displayed CPL activity with dissymmetry factor $|g_{PL}|$ as high as $\sim 2.6 \times 10^{-3}$. The CP-OLEDs were fabricated with $E_{QE_{max}}$ of 19% and maximum brightness of 24790 cd/m².

In the same year, the synthesis of two new chiral conjugated polymers, (*R*)-P and (*S*)-P, was reported from a pair of CP-TADF enantiomers (**Figure 8**).^[31] To chirally disrupt the TADF unit, the chiral unit o-BINOL was used. The carbazole as a donor and the aryl group with two cyano units as an acceptor was used in the molecule. Both the developed materials depicted the small ΔE_{ST} of 0.045 and 0.061 eV and high PLQYs of 72 and 76%, respectively. Through DFT calculations, the distribution of frontier molecular orbitals was predicted. For optimization and computation, two repetition units of (*R*)-P/(*S*)-P with end-capping groups were selected. The distribution of the LUMOs on the acceptor moieties was comparable to that of the monomers. However, the HOMO was populated over whole conjugated main chain of the polymer. The second carbazole moiety of each repeat unit away from the main chain had no HOMO distribution. The conjugation copolymerization should greatly impact the photophysical features and TADF properties of the polymer. Also, (*R*)-P and (*S*)-P in solution and film states both produced strong mirror-image CP luminescence signals with dissymmetry factors ($|g_{lum}|$) up to 1.9×10^{-3} (In mCP doped films). Cotton effects were seen in the CD spectra of (*R*)-P and (*S*)-P in a toluene solution (at around 332 nm). The axial chiral binaphthyl units caused chirality to be imparted throughout the whole polymer chain. They observed that the g value for CPL emission enhanced for mCP-doped films relative to non-doped films. The rise in g values may be due to the degree of order in polymer structures in doped films after annealing. The fabricated CP polymer light-emitting diodes (CP-PLED) with (*R*)-P and (*S*)-P could achieve $E_{QE_{max}}$ of 14.9 and 15.8% and emission peaks at 546 and 544 nm, respectively. Also, the CP-LED devices made with (*R*)-P and (*S*)-P, respectively, showed strong CP-EL signals with g_{EL} of -1.5×10^{-3} and $+1.6 \times 10^{-3}$.

In 2022, macrocyclic enantiomers (*S*, *S*)-MC and (*R*, *R*)-MC were developed using perturbing unit o-BINOL and a triazine-based TADF molecular framework (**Figure 8**).^[32] Dimethyldihydroacridine as the donor and triazine as the acceptor was used in the emitters. From single crystal structure, it has been observed that there existed large dihedral angle between acceptor and donor (almost 90°), which helped to separate the HOMO and LUMO. In addition, a packing unit cell comprising both enantiomers revealed several C-H interactions and hydrogen bonds also been noticed. The o-BINOL unit might be exploited as both a chirality inducing unit and a steric barrier to lessen the exciton annihilation of the enantiomers in an aggregation state. With the help of DFT calculations, it has been found that the LUMOs were primarily dispersed on the triazine acceptors, whilst the HOMOs were primarily distributed on the dimethyldihydroacridine moieties. The distinct separation between HOMO and LUMO led

to small ΔE_{ST} gap. The calculated singlet and triplet energy levels were 2.46 and 2.45 eV which resulted in small ΔE_{ST} gap of 0.01 eV. The DFT calculations displayed that o-BINOL was not involved in the frontier orbital electronic distribution but it bestowed the TADF units to exhibit CD and CPL activities. The AIE properties were observed for the developed enantiomers ((*S,S*)-MC) through THF/water experiment. With a rise in water fraction from 0% to 99%), the emission intensity of (*S,S*)-MC improved considerably. The delayed fluorescence lifetime of (*S,S*)-MC steadily increased, with an increase in water fraction also observed. This demonstrated that this chiral macrocycle had a delayed fluorescence because of aggregation. The AIE property of (*S,S*)-MC led to a PLQY of 65.6% in the air and a high PLQY of 79.7% under vacuum in a film state. The macrocyclic enantiomers depicted CPL and mirror-imaged circular dichroism signals with a dissymmetry factor ($|g_{PL}|$) of 2.2×10^{-3} in toluene solution. The solution-processed CP-OLEDs based on macrocyclic isomers showed $E_{QE_{max}}$ of up to 17.1% and CPEL characteristics with $|g_{EL}|$ of up to 1.7×10^{-3} .

A steric hindrance-assisted dual-core strategy was adopted in 2022 to prepare CP-MR-TADF materials.^[33] The two carbazole and boron-based mono-cores were constructed through single bond and achieved ultra-blue emission and CPL properties. With the two hindered luminous cores, a stable chiral configuration was created by directly connecting the two mono-cores at a precise point with a single bond. ((*R/S*)-DOBN and (*R/S*)-DOBNT) (**Figure 8**). The steric hindrance reduced the conjugation between the two connected centres. The developed molecules, (*R/S*)-DOBN and (*R/S*)-DOBNT, could achieve good PLQYs of 0.91 and 0.96 along with emission peaks at 453 and 459 nm, respectively. These molecules possessed good thermal stability with decomposition temperatures above 400 °C. Through DFT calculations predicted that the HOMO and LUMO were populated over dual-core structures. Both the developed compounds exhibited clear HOMO/LUMO distributions caused by the MR effect, primarily on the ortho and para carbon atoms and each nitrogen and boron atom. When comparing (*R*)-DOBNT to (*R*)-DOBN, the HOMO energy level was lowered by 0.12 eV due to the extra tert-butyl group. The LUMO/LUMO+1 and HOMO/HOMO-1 of (*R*)-DOBNT and (*R*)-DOBN exhibited comparable MR effects and almost resembled the HOMO/LUMO energy levels of their corresponding monochromes. The S_1/T_1 energy levels of (*R*)-DOBN and (*R*)-DOBNT were inferred to be 2.87/2.73 and 2.80/2.68 eV, respectively. This provided ΔE_{ST} data of 0.14 and 0.12 eV, respectively, which were enough for the exciton up conversion from T_1 to S_1 . The characteristic TADF properties of these materials were indicated by the delayed lifetime component becoming quicker as temperature increased. The prompt and delayed components

were (*R*)-DOBNT-doped films 5.2 ns/51.8 microseconds ((*R*)-DOBN), and 4.5 ns/122.2 microseconds ((*R*)-DOBNT), based on an analysis of the TRPL signals obtained at 300 K. The fabricated CP-OLEDs with these emitters showed EQEs of 23.9% ((*R*)-DOBN) and 25.6% ((*R*)-DOBNT) with CIE coordinates of (0.14, 0.10) and (0.13, 0.12), respectively. The CP-OLEDs achieved a clear CPEL characters with $|g_{EL}|$ factors $\approx 10^{-3}$.

Xiang et al. in 2023 developed a pair of chiral biphenoxazine dyes based on octahydro-binaphthalene ((*R/S*)-BIPNX-TRZ) (**Figure 9**).^[34] The developed compound comprised of the axial chirality containing electron-donating unit biphenoxazine and two electron-accepting 2,4,6-triphenyl-*S*-triazineine fragments. This donor and acceptor system generated a tri-propeller-type structure allowing charge separation and A-D-D-A charge transfer. This produced aggregation-induced yellow-green TADF with 25.2% and 57.6% quantum yields for neat and doped films, respectively. They were used as emitters in solution-processed CP-OLEDs, achieving external quantum efficiency, and dissymmetry factor of up to 11.3%, and 0.88×10^{-3} . Additionally, semi-transparent electrodes could increase the dissymmetry factor to 1.69×10^{-3} .

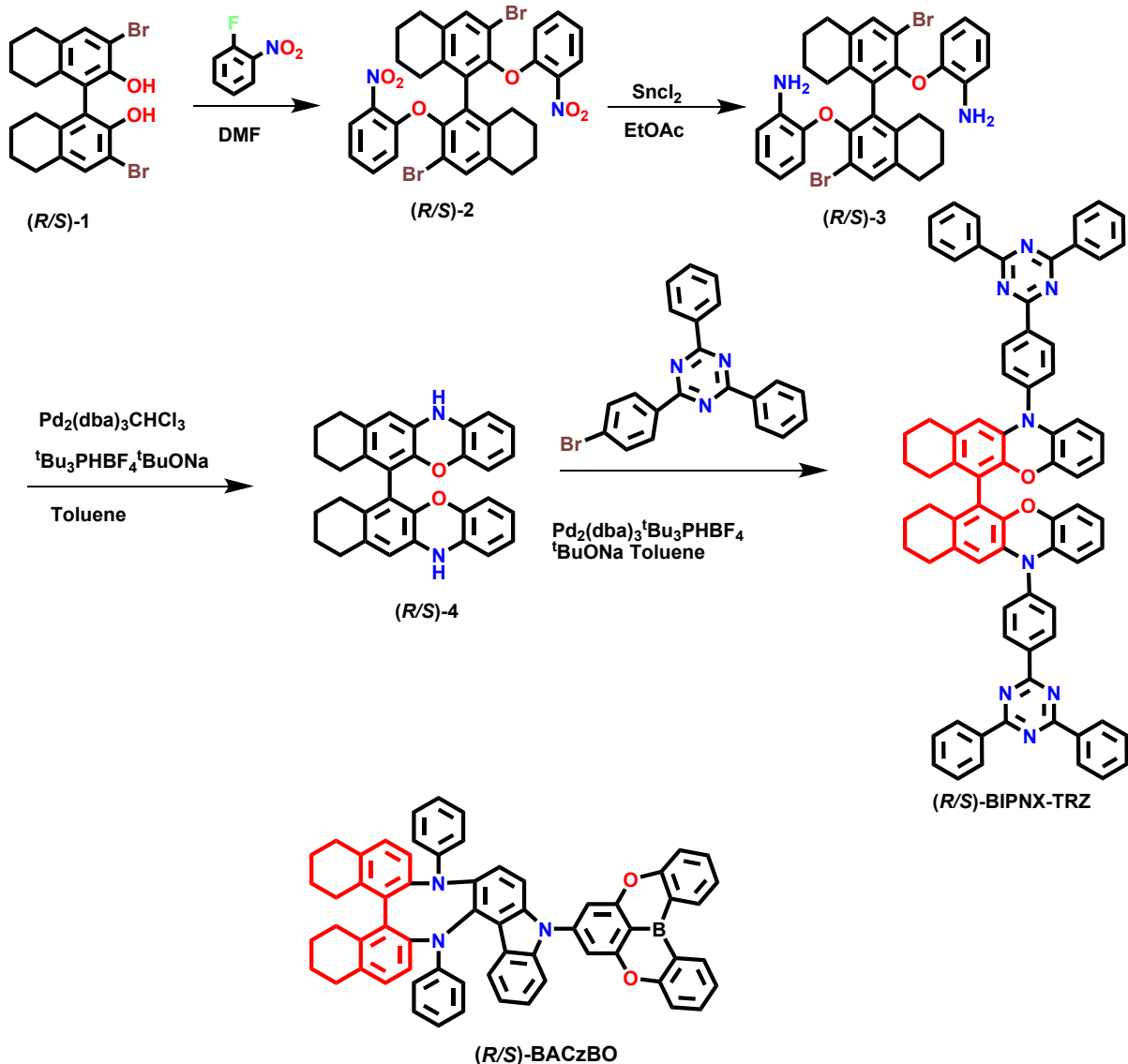


Figure 9. Chemical structures of some octahydrobinaphthalene based chiral molecules.^[34-35]

Yang et al. in 2024 merged a precisely tailored chiral donor with the hybrid properties of long/short-range charge-transfer excitations to synthesize CP-TADF emitters ((R/S)-BACzBO, **Figure 9**) for use in high-performance OLEDs.^[35] Combining electron-rich carbazole fragments with commercially available chiral octahydro-[1,10-binaphthalene]-2,20-diamine, the new chiral donor improved the compatibility with a wide range of acceptors and played a key role in shaping their FMOs. Their strategic design achieved amazing results, including a significant g_{PL} of over 1.6×10^{-3} , a high quantum yield of up to 98%, and a fast reverse ISC rate of 1.41×10^6 s. The use of these chiral dopants in OLEDs resulted in a high maximum EQE of 37.4%

Chen et al. in 2024 explored novel design methodologies for chiral TADF-active polymers and developed two chiral TADF polymer-based emitters: (R) and (S)-pSACODP (**Figure 10**).^[36]

These chiral polymers emitted yellowish-green light in toluene and exhibited mirror-imaged CPL signals. The g_{abs} values for (*R*)- and (*S*)-pSACODP at 365 nm were -1.1×10^{-3} and 1.1×10^{-3} , respectively. Their mirror-image CPL signals in the toluene solution depicted the g_{lum} values as -1.0×10^{-3} and 1.0×10^{-3} , respectively. They also fabricated the PLED devices using these polymers as emitters. The devices achieved impressive EL performances with maximum EQEs of 12.0% (*R*) and 11.7% (*S*). Additionally, CPEL signals were identified from devices with g_{EL} values of -1.1×10^{-3} (*R*) and 1.3×10^{-3} (*S*) at 561 nm.

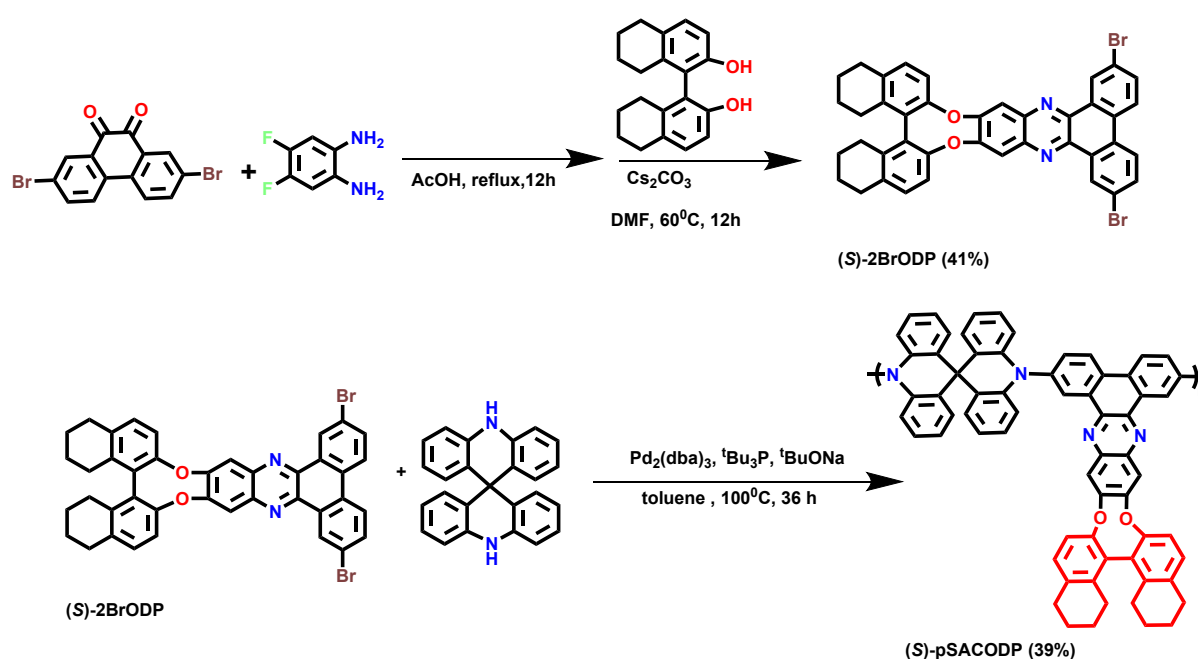
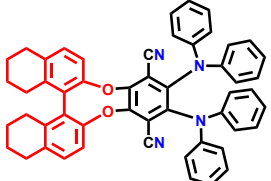
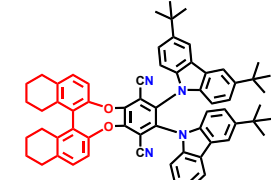
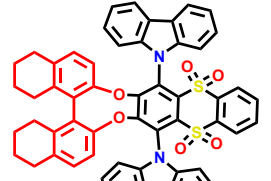
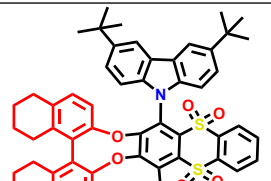
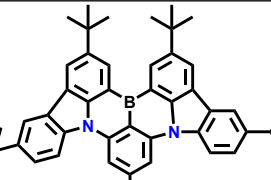
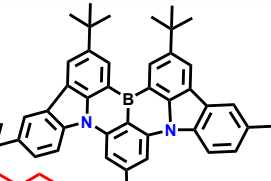
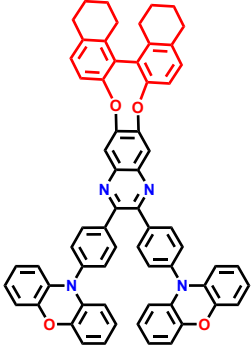
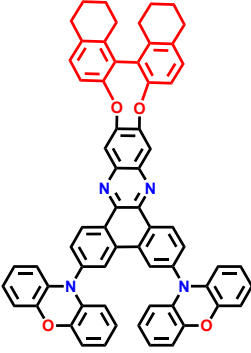
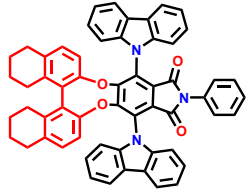
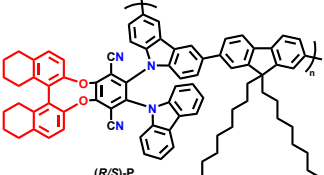
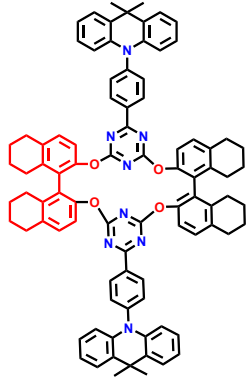


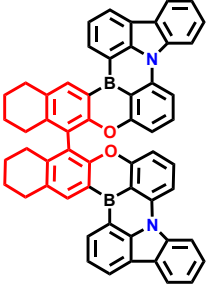
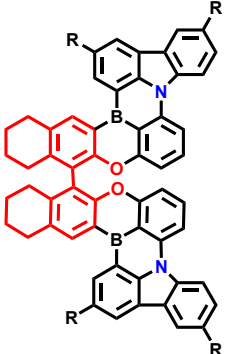
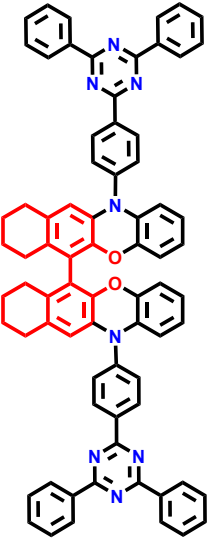
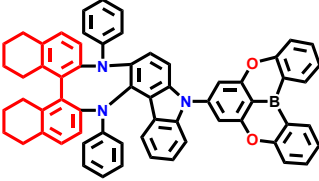
Figure 10. Synthetic scheme for octahydrobinaphthalene based chiral molecule.^[36]

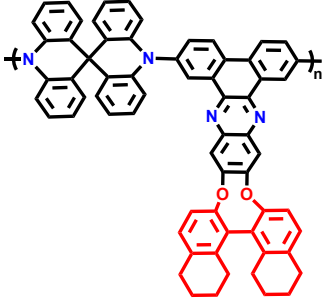
Table 2. Chiroptical properties of o-BINOL-based chiral TADF molecules.

Compound	EQE_{max} (%) (Isomer used as emitter)	Luminescence dissymmetry factor	Electroluminescence dissymmetry factor	Reference
 (<i>R/S</i>)-OBN-Cz	32.6 (<i>R</i>)	$g_{\text{PL}} = -2 \times 10^{-3} / 2.14 \times 10^{-3}$ (<i>R/S</i>) (Neat film)	$g_{\text{EL}} = -1.94 \times 10^{-3} / 2.30 \times 10^{-3}$ (<i>R/S</i>) (Doped Device)	[24]

 <p>(R/S)-OBN-DPA</p>	12.3 (R) Doped	$g_{PL} = 2.52 \times 10^{-3} / -1.96 \times 10^{-3}$ (R/S) (Neat film)	$g_{EL} = 2.9 \times 10^{-3} / -2.2 \times 10^{-3}$ (R/S) (Non-doped Device)	[25]
 <p>(R/S)-OBN-tBuCz</p>	12.4	$g_{PL} = -6.5 \times 10^{-4} / 8.6 \times 10^{-4}$ (R/S) (Toluene)	$g_{EL} = -0.90 \times 10^{-3} / 1.57 \times 10^{-3}$ (Solution-process) (R/S)	[26]
 <p>(R/S)-OBS-Cz</p>	15 (R)	$ g_{PL} = 8.7 \times 10^{-4}$ (Neat film)	$g_{EL} = 0.8 \times 10^{-3} / -1.0 \times 10^{-3}$ (R/S)	[27]
 <p>(R/S)-OBS-tCz</p>	20.3 (R)	$ g_{PL} = 6.4 \times 10^{-4}$ (Neat film)	$g_{EL} = 0.5 \times 10^{-3} / -0.4 \times 10^{-3}$ (R/S)	[27]
 <p>(R/S)-OBN-2CN-BN</p>	29.4 (R)	$g_{PL} = 9.0 \times 10^{-4} / -9.1 \times 10^{-4}$ (R/S) (doped films)	$g_{EL} = 1.43 \times 10^{-3} / -1.27 \times 10^{-3}$ (R/S)	[28]
 <p>(R/S)-OBN-4CN-BN</p>	24.5 (R)	$g_{PL} = 8.0 \times 10^{-4} / -10.4 \times 10^{-4}$ (R/S) (doped films)	$g_{EL} = 4.60 \times 10^{-4} / -4.76 \times 10^{-4}$ (R/S)	[28]

 <p>(R/S)-ODQPXZ</p>	28.3 (R)	$g_{PL} = -4.6 \times 10^{-4} / 4 \times 10^{-4}$ (R/S) (thin films)	$ g_{EL} = 6 \times 10^{-4}$	[29]
 <p>(R/S)-ODPPXZ</p>	20.3 (R)	$g_{PL} = -1.4 \times 10^{-3} / 1.9 \times 10^{-3}$ (R/S) (thin films)	$ g_{EL} = 2.4 \times 10^{-4}$	[29]
 <p>(R/S)-OBN-AICz</p>	19 (R)	$g_{PL} = 2.6 \times 10^{-3} / -2.4 \times 10^{-3}$ (R/S) (Toluene and thin films)	$g_{EL} = 4.7 \times 10^{-4} / -6.5 \times 10^{-4}$ (R/S)	[30]
 <p>(R/S)-P</p>	14.9 (R)	$ g_{PL} = 1.9 \times 10^{-3}$ (Doped film)	$g_{EL} = -1.5 \times 10^{-3} / 1.6 \times 10^{-3}$ (R/S)	[31]
 <p>(S,S)/(R,R)-MC</p>	17.1 (R,R)	$ g_{PL} = 2.2 \times 10^{-3}$ (Toluene)	$g_{EL} = 1.5 \times 10^{-3} / -1.7 \times 10^{-3}$ (R/S)	[32]

 <p>(R/S)-DOBNT</p>	23.9 (R)	$ g_{PL} = 1 \times 10^{-3}$ (Solid film)	$g_{EL} = -0.9 \times 10^{-3} / 0.9 \times 10^{-3}$ (R/S)	[33]
 <p>R = tBu; (R/S)-DOBNT</p>	25.6 (R)	$ g_{PL} = 0.9 \times 10^{-3}$ (Solid film)	$g_{EL} = -1.0 \times 10^{-3} / 0.9 \times 10^{-3}$ (R/S)	[33]
 <p>(R/S)-BIPNX-TRZ</p>	11.3 (S)	$ g_{PL} = 1.80 \times 10^{-3}$ (Powder)	$g_{EL} = -0.84 \times 10^{-3} / 0.88 \times 10^{-3}$ (R/S)	[34]
 <p>(R/S)-BACzBO</p>	37.4 (R)	$ g_{PL} = 1.6 \times 10^{-3}$	$g_{EL} = 3.5 \times 10^{-4} / -3.9 \times 10^{-4}$ (R/S)	[35]

 <p>pSACODP</p>	12 (R)	$g_{\text{lum}}^{\text{=}}$ $-1.0 \times 10^{-3} / 1.0 \times 10^{-3}$ (R/S)	$g_{\text{EL}}^{\text{=}}$ $-1.1 \times 10^{-3} / 1.3 \times 10^{-3}$ (R/S)	[36]
--	-----------	--	---	------

CPL emitters have problematic chiral separation and poor photoluminescence quantum yield. Wu et al. in 2024 introduced the chiral 4,4'-biphenanthrene-3,3'-diol unit to a TADF framework and developed two enantiomers: (*R/S*)-*o*-DCzBPNCN and (*R/S*)-*p*-DCzBPNCN (**Figure 11**).^[37] They synthesized these enantiomers using (*R/S*)-BIPOL unit in a carbazole-cyano-based TADF framework. The BIPOL-based emitters had highly twisted conformations and substantial torsion angles between the donor and acceptor. This resulted in small singlet-triplet energy gaps of 0.05 and 0.17 eV for *o*-DCzBPNCN and *p*-DCzBPNCN. The reversed ISC) rates of *o*-DCzBPNCN and *p*-DCzBPNCN were $2.11 \times 10^6 \text{ s}^{-1}$ and $2.90 \times 10^5 \text{ s}^{-1}$, respectively. In doped films, (*R/S*)-*o*-DCzBPNCN showed a g_{PL} of $-1.94 \times 10^{-2} / 1.91 \times 10^{-2}$.

Recently, donor-acceptor cage arrangements offered a new design technique for identifying efficient CP-TADF emitters.^[38] Zhang et al. in 2024 reported the example of a chiral donor-acceptor cage (DA-2) (**Figure 11**) that exhibited efficient CP-TADF with $|g_{\text{lum}}|$ values up to 2.1×10^{-3} and PLQY of 32%. The anchoring rotation of the donor induces chirality in DA-2, resulting in racemic M/P-DA-2 with clockwise and anti-clockwise rotations. The charge transfer interaction between the donor and acceptor in DA-2 resulted in a small ΔE_{ST} of 0.051 eV, facilitating the reverse ISC process promoting TADF. These charge transfer interactions also caused quasi-parallel transition electric and magnetic dipole moments.

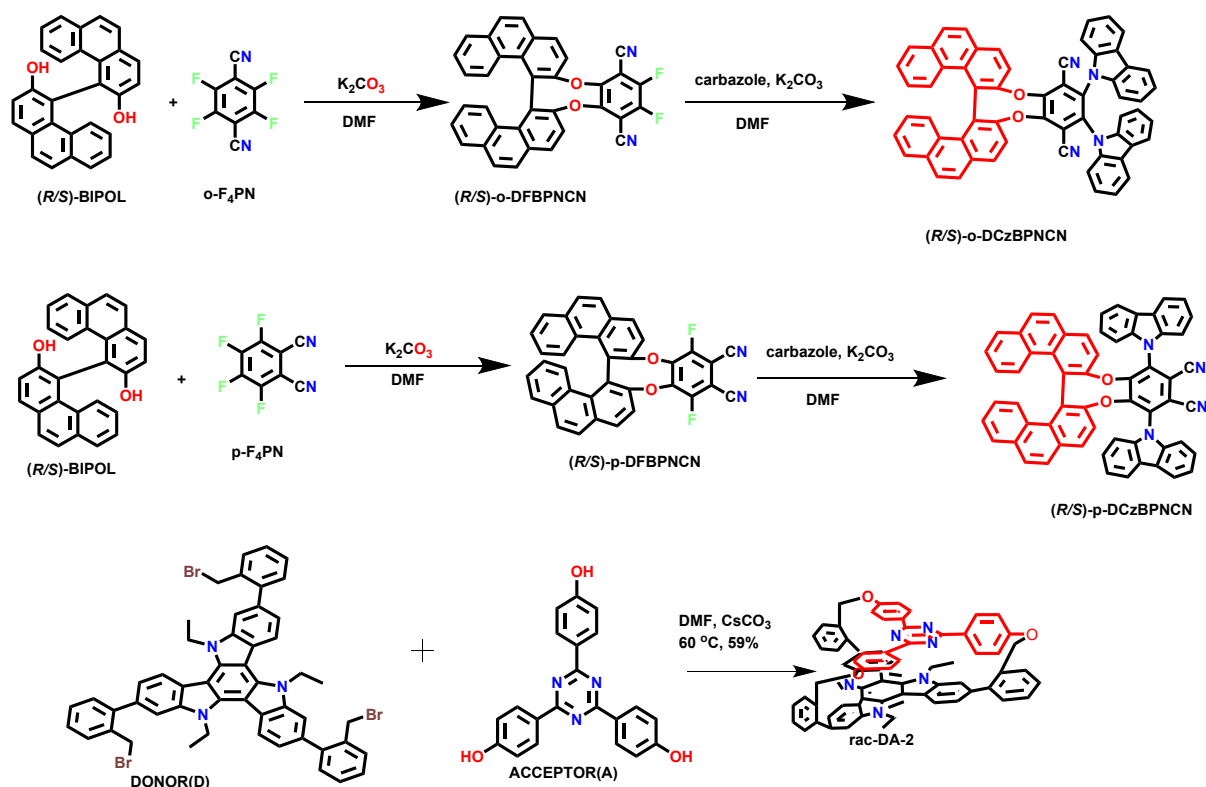


Figure 11. Synthetic scheme for some chiral TADF molecules.^[37-38]

2.3. Biphenyl based chiral TADF molecules

Zheng's group in 2020 developed a pair of axially chiral enantiomers based on cyano-carbazole and CN- phenoxazine, namely (*R/S*)-BPPOACZ (**Figure 12**).^[39] A three-step procedure was used including the Ullmann coupling reaction (Cu-catalyzed) and nucleophilic substitution with carbazole and phenoxazine. The optically pure (*R/S*)-BPPOACZ enantiomers with enantiomeric excesses >99% were achieved. An axially chiral biphenyl unit was used to link the donors and acceptors in the TADF skeleton.

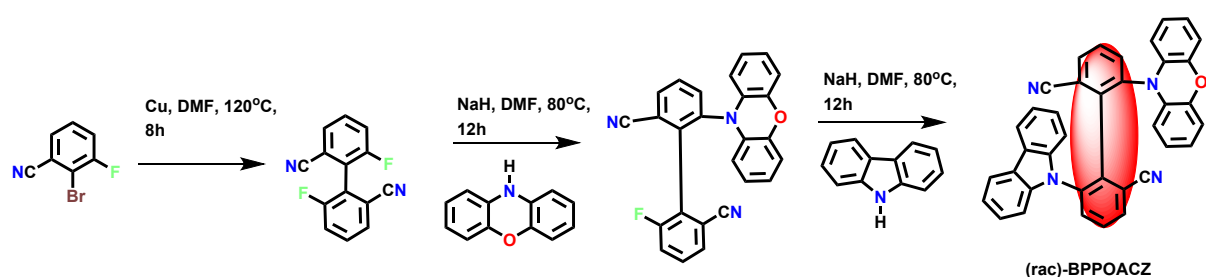


Figure 12. Synthetic scheme of some biphenyl-based chiral TADF molecule.^[39]

The two pairs of donors and acceptors on either side of the biphenyl unit hindered racemization of the axially chiral biphenyl unit by creating torsion between the two phenyl rings. The twist

between the biphenyl units stabilized the donor-acceptor structures in the two TADF cores. The DFT calculations observed that the HOMO was mostly positioned on the phenoxazine moiety, whereas the LUMO was primarily placed on the biphenyl rings and cyano units. This type of distribution was beneficial for low ΔE_{ST} . The greater electronic circular dichroism and CPL activities might result from the chiral biphenyl component being clearly involved in the HOMO/LUMO distribution. In toluene with inert environment, the enantiomers exhibited low ΔE_{ST} values of 0.04 eV and high PLQY of 86.10%. The biphenyl unit participated in the HOMO/LUMO distribution which induced the CPL characteristics in the molecule. The maximal value of $|g_{PL}|$ was $\sim 9.7 \times 10^{-3}$ in toluene and $\sim 1.8 \times 10^{-2}$ in doped film. The developed molecule ((*S*)-BPPOACZ) displayed a CPEL signal with a $|g_{EL}|$ of 4.5×10^{-3} and EQE_{max} up to 17.8% in CP-OLEDs. **Table 3** summarizes different chiroptical properties of biphenyl-based chiral TADF molecules.

Further, in 2020, a TADF emitter (4tBuCzPN) having axial chirality was developed by linking two identical TADF emitters (2tBuCzPN) (**Figure 13**)^[40] and observed that 4tBuCzPN was thermally more superior to 2tBuCzPN with a decomposition temperature of 498 °C. The two tBuCz units, two CN units in the central biphenyl moiety and the large conjugation brought on by the direct linkage between two phenyl moieties might be the causes of the increased thermal stability of 4tBuCzPN. The DFT calculations depicted that the CN and central biphenyl moieties could attract the LUMO population while the majority of the HOMO was present on tBuCz units. Due to the twisted conformation created by the dual-core emitter design, emitter 4tBuCzPN demonstrated an effective HOMO and LUMO separation. This effective separation between HOMO and LUMO resulted in high charge transfer characteristics of 4tBuCzPN with lower ΔE_{ST} . The first singlet and first triplet energies for 2tBuCzPN and 4tBuCzPN, respectively, were calculated to be 3.53 and 3.11 eV and 2.88 and 2.70 eV, respectively. Thus, 2tBuCzPN and 4tBuCzPN had theoretical ΔE_{ST} values of 0.42 eV and 0.18 eV, respectively. The ΔE_{ST} and PLQY of 4tBuCzPN with a twisted rigid conformation were found to be lesser than those of 2tBuCzPN. The experimental ΔE_{ST} value of 4tBuCzPN was 0.05 eV, significantly lower than the ΔE_{ST} value of 2tBuCzPN, 0.33 eV. The device based on 4tBuCzPN, in particular, had a high EQE of 20.8% compared to the EQE of 2tBuCzPN based device (5.3%). The high-performance liquid chromatography was used to resolve the enantiomers (+)-4tBuCzPN and (-)-4tBuCzPN, which showed mirror-image circular dichroism and CPL characteristics (**Figure 14**). The g_{lum} values of (+)-4tBuCzPN and (-)-4tBuCzPN in toluene were $+5.4 \times 10^{-3}$ and -5.0×10^{-3} , respectively. The CPEL signals of the TADF enantiomers were

not observed because racemization of those enantiomers took place during vacuum evaporation.

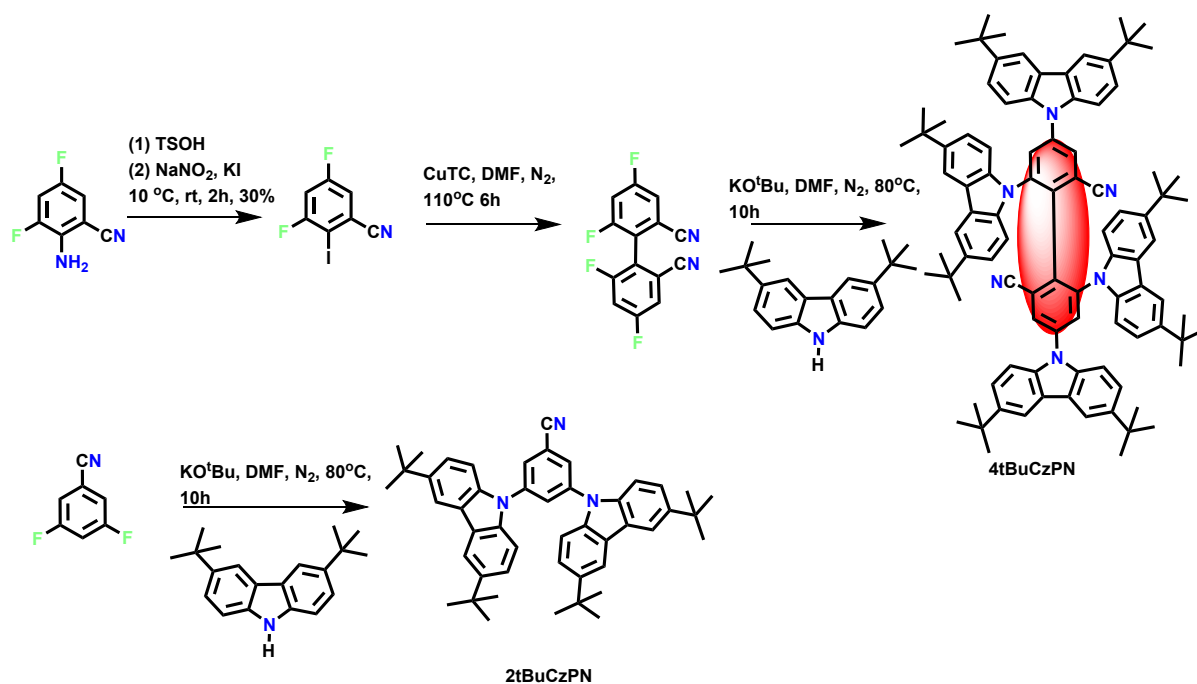


Figure 13. Synthetic scheme of some biphenyl-based chiral TADF molecule.^[40]

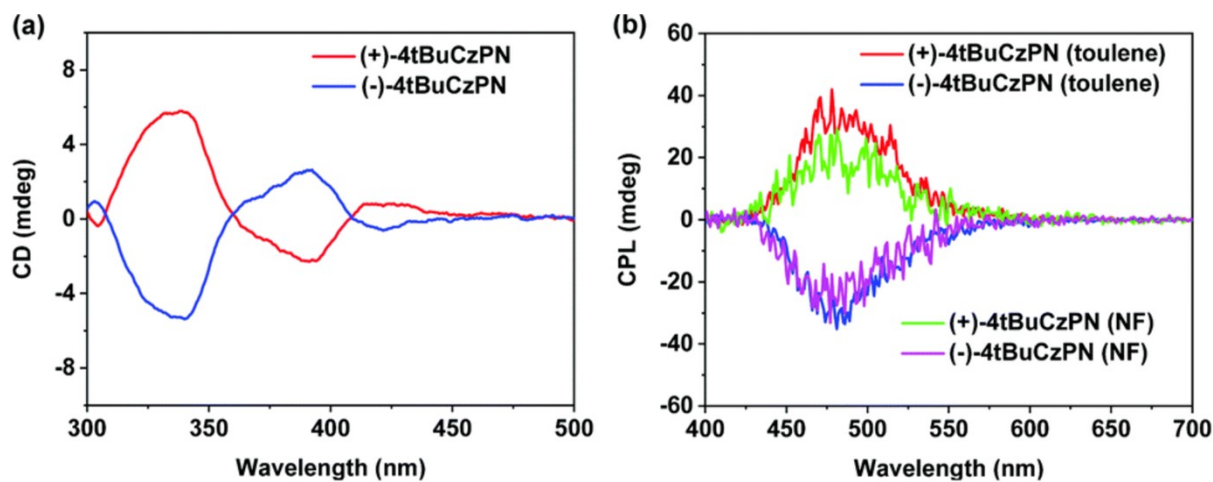


Figure 14. (a) CD spectra of (+)-4tBuCzPN and (-)-4tBuCzPN in toluene (1.0×10^{-5} M). (b) CPL spectra of (+)-4tBuCzPN and (-)-4tBuCzPN in toluene and neat films.^[40]

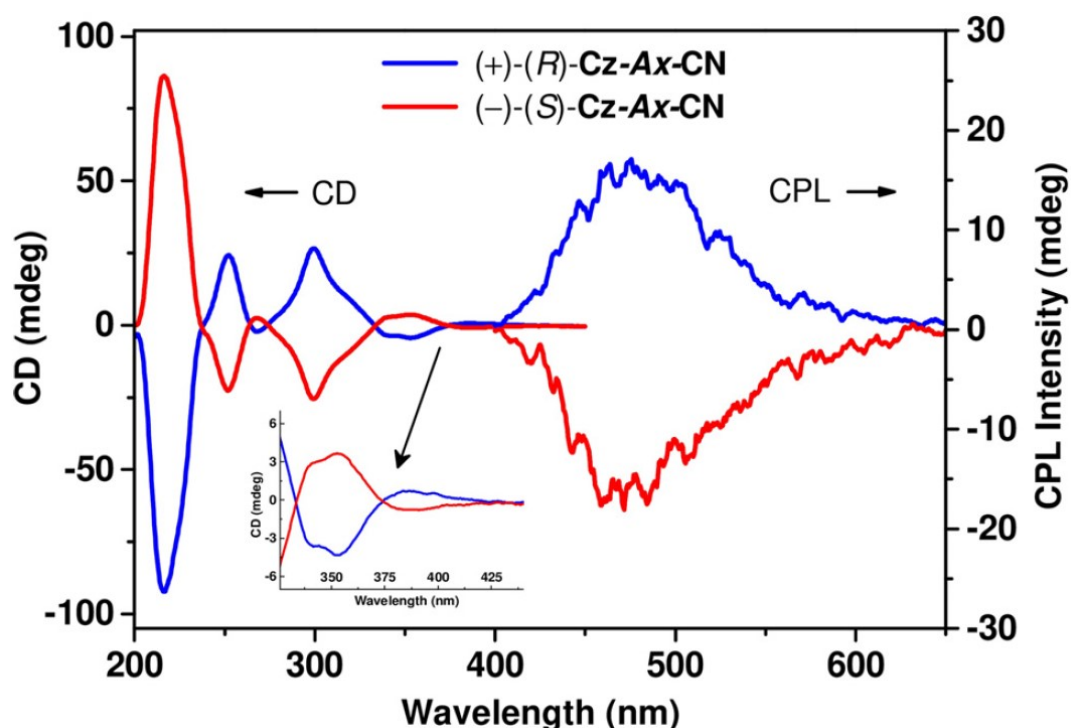
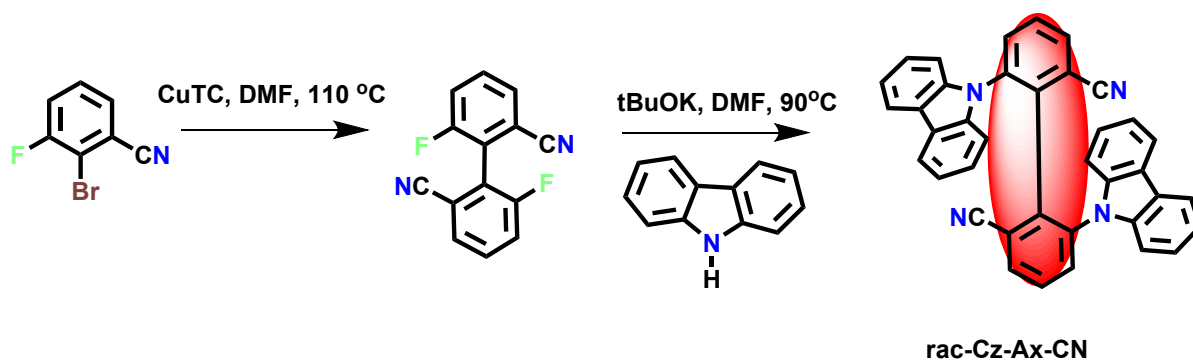


Figure 15. Synthetic scheme of some biphenyl based chiral TADF molecule (above); CD and CPL spectra of (-)-(S)-Cz-Ax-CN and (+)-(R)-Cz-Ax-CN in film states (below).^[41]

An axially chiral TADF-active material with CPPL properties was synthesized by combining two fluorophores ((*R*) and (*S*)-Cz-Ax-CN) (**Figure 15**).^[41] The design concept of the molecule included the biphenyl unit with cyano and carbazole units attached on the ortho position of each phenyl ring. The copper-catalyzed halogenated benzonitrile coupling reaction and a carbazole substitution process was used to synthesize the molecule and the enantiomers were purified by chiral HPLC with ee>99%. The emitters exhibited axial chirality with high conversion barriers as the symmetry axis was surrounded by sterically hindered groups. This was advantageous since it allows for the production of a g_{lum} . DFT calculations predicted that the carbazole unit was encompassing the HOMO, whereas the CN modified phenyl ring was

containing the LUMO energy levels. The ΔE_{ST} value of Cz-Ax-CN was 0.096 eV which was small enough for RISC process. The complete axial skeleton was covered by the electronic distribution which was beneficial for their superior CD and CPL activity. The single crystals revealed that the molecule had an axially chiral skeleton, with a dihedral angle of 64° . The huge dihedral angle disrupted the π -conjugation of the whole molecule. The $CH\cdots\pi$ distance between the cyano group on one fluorophore and the carbazole on the other was small enough to guarantee intramolecular spatial charge transfer. It was found that the emission intensities significantly rose when the water concentration in THF:water experiment was increased to 99%. This indicated that aggregation-induced emission was present in the enantiomers. The emission spectra of the doped *S* isomer were examined at 77 K with fluorescence and phosphorescence bands coming at 460 and 465 nm, respectively. The measured S_1 and T_1 energy levels were 2.696 and 2.667 eV, respectively, and the ΔE_{ST} value was 0.029 eV. The transient PL curve exhibited two exponential decays at 300 K, which were attributed to prompt fluorescence (30 ns) and delayed component (12.6 microseconds). The temperature increased from 100 K to 300 K, the delayed component of the transient PL slowly increased. This suggested that a steady increase in temperature would result in a favourable RISC of excitons from T_1 to S_1 . A clear mirror image CD spectrum showed alternating positive and negative Cotton effects; the strong Cotton effects in short wavelength ranges were attributed to absorption brought on by the intramolecular charge transfer of the π -system (**Figure 15, below**). The CPL spectra of the enantiomers showed mirror-image patterns, with g_{lum} values of $+4.5 \times 10^{-3}$ for *R* isomer and -4.8×10^{-3} for *S* isomer. The CP-OLEDs were fabricated by using the developed enantiomers as the emitters. The CP-OLEDs based on these enantiomers exhibited CPEL characteristics with g_{EL} values of -1.2×10^{-2} (*S* isomer) and $+1.4 \times 10^{-2}$ (*R* isomer). The devices depicted the bright blue EL at 468 nm with EQE_{max} values of up to 12.7%.

Zheng's group in 2021 developed two new blue CP-TADF emitters, M-BPCZ4 and P-BPCZ4. The biphenyl unit was a chiral source and a π bridge (**Figure 16**).^[42] The design concept of the M-BPCZ4 was similar to the molecule developed by Chen et al. in 2020. Chen et al. in 2020 developed, 4tBuCzPN, an axially chiral TADF emitter with a dual emitting core (**Figure 13**). Their work was a comparison of photophysical and efficiency values between the single core and the dual core molecules. The 4tBuCzPN based OLED had a substantially higher PLQY (74%) and EQE (20.8%) than the OLED based on TADF emitter 2tBuCzPN, which had PLQY of 29% and EQE of 5.3%. The design concept of both materials by Zheng et al. included the

biphenyl unit with cyano and carbazole units attached on the ortho position of each phenyl ring. Two more carbazole units were attached in the meta position of each phenyl ring (P-BPCZ4) and in para position of each phenyl ring (M-BPCZ4). The Ullmann coupling reaction (Cu-catalyzed) from difluoro-2-iodobenzonitrile was used to synthesize these molecules, which were then substituted with carbazole by a nucleophilic substitution process. Both emitters showed clear TADF characteristics and emission peaks at 470 nm. With the help of the quick RISC process, a notable PLQY of 76% for P-BPCZ4 resulted in a high EQE of 18.3% in doped devices. The racemization temperature and photophysical properties of these units were influenced by the position difference of the other two carbazole units. With the help of phosphorescence and fluorescence spectra (toluene at 77 K), the energy levels of triplet, singlet and ΔE_{ST} were measured. The energy level values for ΔE_{ST} were 0.09 eV for M-BPCZ4 and 0.05 eV for P-BPCZ4. The transient PL decay curves of the doped films of M-BPCZ4/P-BPCZ4 showed prompt component of 15.4/24.3 ns and delayed component of 6.4/7.0 microseconds, respectively. It was found that as the temperature was increased, a decreased in lifetime and an increase in delayed fluorescence components were noticed. With the help of DFT calculations, the root mean squared deviation showed that there were only minor differences between the excited state geometries and ground state geometries for both developed molecules. P-BPCZ4 had a more rigid molecular structure to produce high PLQY, with a reduced root mean squared deviation of 1.461 Å. Both the molecules exhibited robust CPL in toluene, with $|g_{PL}|$ factors reaching 5.0×10^{-3} ((*R/S*)-M-BPCZ4) and 4.7×10^{-3} ((*R/S*)-P-BPCZ4). Additionally, the doped CP-OLEDs demonstrated acceptable CPEL characteristics, with $|g_{EL}|$ values of 5.5×10^{-3} (((*R/S*)-P-BPCZ4)).

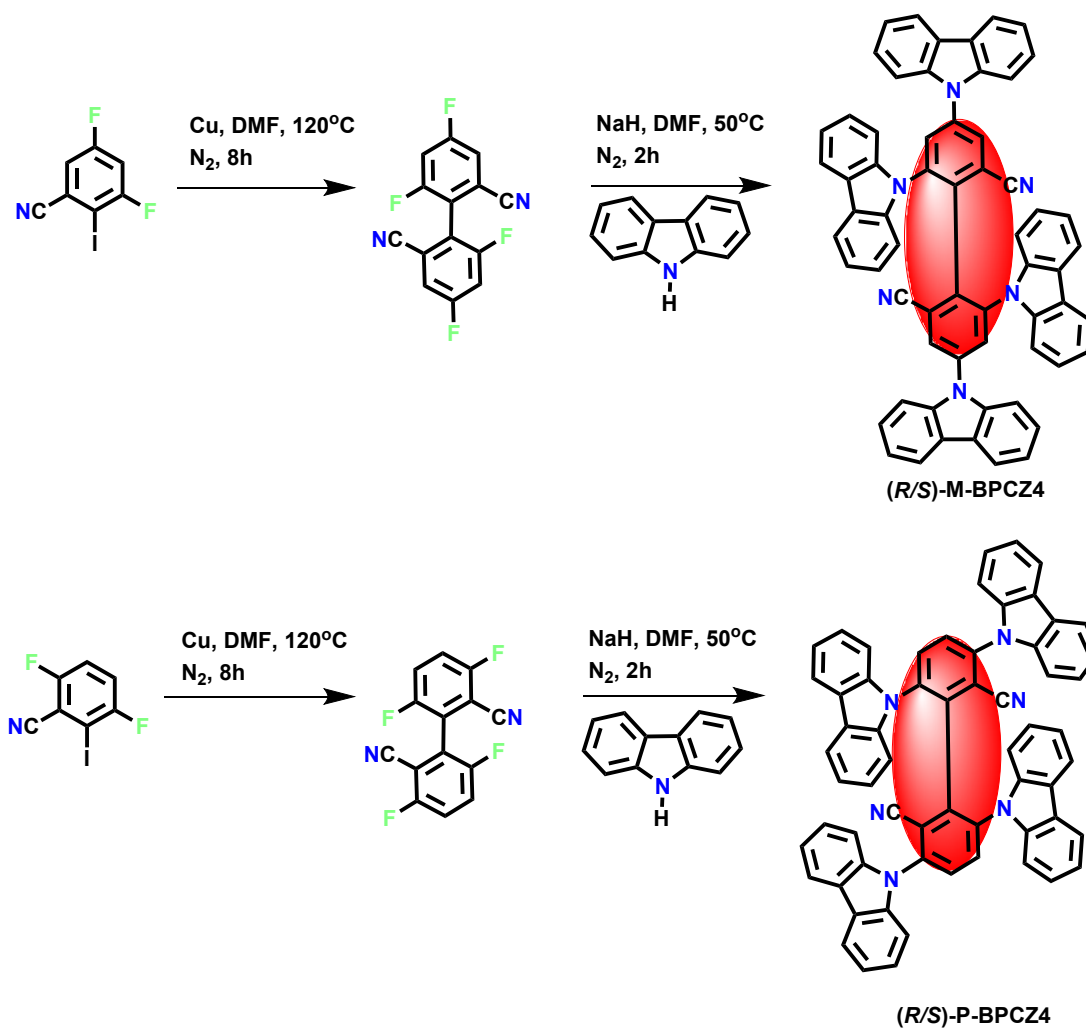


Figure 16. Synthetic scheme of some biphenyl based chiral TADF molecule.^[42]

Chen et al., in 2024, used acceptor copolymerization to create axially chiral conjugated polymers with TADF characteristics.^[43] The chiral polymers (*R*)-PAC and (*S*)-PAC were developed by copolymerizing benzophenone with axially chiral biphenyl (**Figure 17**). The polymers featured chiral conjugated main chains and visibly separated HOMO and LUMO, resulting in obvious TADF characteristics with modest ΔE_{ST} of 0.05 eV and high PLQYs of 81%. The CD and CPL spectra revealed high chiroptical activity in film states, with $|g_{lum}|$ values approaching 3×10^{-3} . The chiral conjugated polymers demonstrated a high EQEmax of 17.8% and strong CPEL signals with $|g_{EL}|$ of 3.4×10^{-3} .

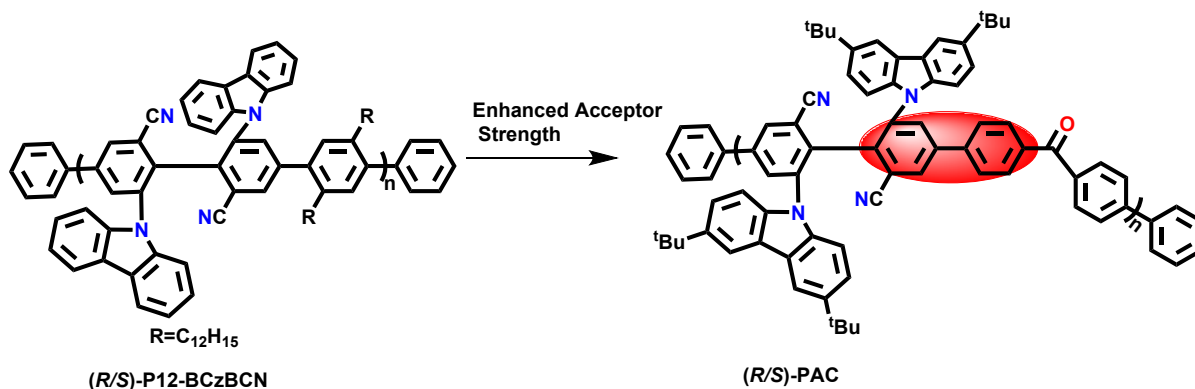


Figure 17. Chemical structure for (R/S)-PAC.^[43]

Chen et al. in 2023 developed CP-TADF enantiomers (*S/R*)-ax-DMAC through molecular engineering (**Figure 18**).^[44] They introduced two stronger electron donors into the chiral-emitting skeleton to increase the device's performance. The CP-TADF emitters had a twisted chiral skeleton that promoted HOMO and LUMO separation, resulting in a small ΔE_{ST} of 0.01 eV and excellent TADF properties with 90% PLQY. They observed that the developed enantiomers exhibited intense and opposite CD and CPL responses in toluene, accompanied by a $|g_{lum}|$ of $\sim 2.2 \times 10^{-3}$. In addition to achieving EQEmax of up to 30.1%, CP-OLEDs with CP-TADF emitters demonstrated clear CPEL signals with a $|g_{EL}|$ of 2.0×10^{-3} .

Chen et al. in 2024, proposed a π -extended acceptor method for developing chiral TADF-active materials with efficient CPEL characteristics.^[45] Three pairs of TADF-property depicting enantiomers, (*R/S*)-Ax-CN, (*R/S*)-Ax-H, and (*R/S*)-Ax-OCH₃, were developed with the help of an axially chiral biphenyl skeleton (**Figure 18**). Several para-substituted push-pull electron groups were added to the axially chiral skeleton to understand the structure-property connection. They could observe that compared to (*R/S*)-Ax-H and (*R/S*)-Ax-OCH₃, (*R/S*)-Ax-CN had a higher PLQY of 88.6% and a smaller ΔE_{ST} of 0.13 eV. This was due to the pull electron effect of the CN group, resulting in a more delocalized distribution of LUMO orbitals and less overlapping of frontier molecular orbitals. They fabricated the CP-OLEDs and found that the (*R/S*)-Ax-CN based CP-OLEDs demonstrated high EQE of 21.0% and 19.7%, as well as strong CPEL signals with g_{EL} of $+4.2 \times 10^{-3}/-4.4 \times 10^{-3}$, respectively.

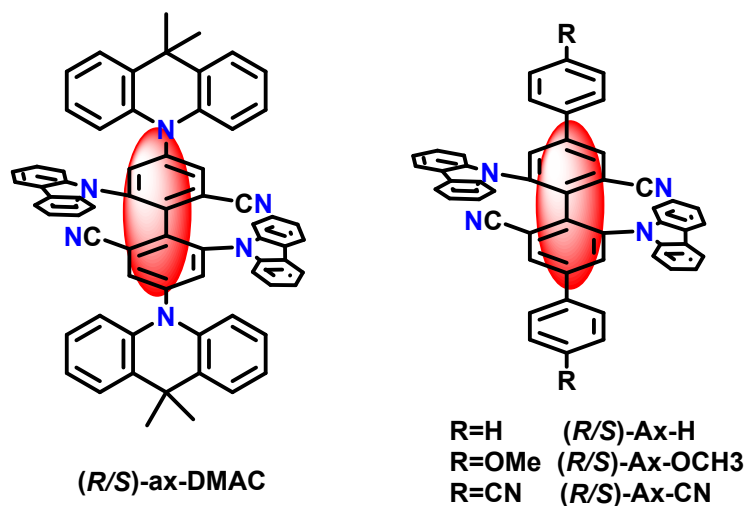
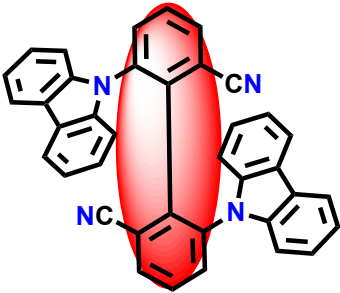
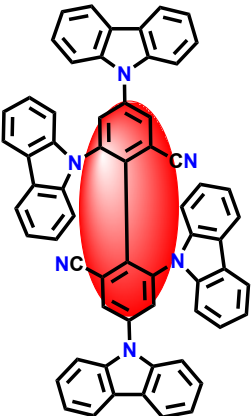
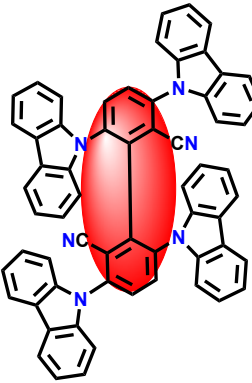
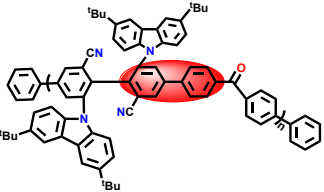
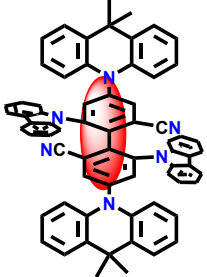
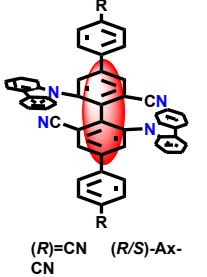
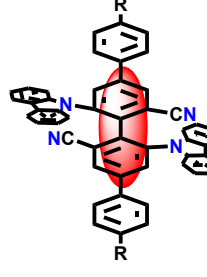
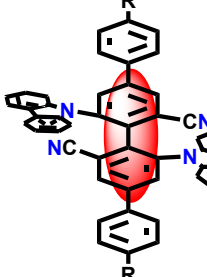


Figure. 18. Chemical structures for some biphenyl-based chiral TADF molecules.^[44-45]

Table 3. Chiroptical properties of biphenyl-based chiral TADF molecules.

Compound	$EQE_{m,ax}$ (%) (Isomer used as emitter)	Luminescence dissymmetry factor	Electroluminescence dissymmetry factor	Reference
 (rac)-BPPOACZ	17.8 (S)	$g_{PL} = -8.7 \times 10^{-3} / 9.7 \times 10^{-3}$ (R/S) (Toluene)	$g_{EL} = -2.8 \times 10^{-3} / 4.5 \times 10^{-3}$ (R/S)	[39]
 4tBuCzPN	20.8	$g_{lum} = +5.4 \times 10^{-3} / -5.0 \times 10^{-3}$ (Toluene)	-	[40]

 <p>rac-Cz-Ax-CN</p>	<p>12.7 (<i>R</i>)</p>	<p>$g_{PL} = 4.5 \times 10^{-3} / -4.8 \times 10^{-3}$ (<i>R/S</i>)</p>	<p>$g_{EL} = 1.4 \times 10^{-2} / -1.2 \times 10^{-2}$ (<i>R/S</i>)</p>	<p>[41]</p>
 <p>(<i>R/S</i>)-M-BPCZ4</p>	<p>16.7 (<i>R</i>)</p>	<p>$g_{PL} = -5.0 \times 10^{-3} / 4.9 \times 10^{-3}$ (<i>R/S</i>)</p>	<p>$g_{EL} = -3.8 \times 10^{-3} / 2.3 \times 10^{-3}$ (<i>R/S</i>)</p>	<p>[42]</p>
 <p>(<i>R/S</i>)-P-BPCZ4</p>	<p>18.3 (<i>R</i>)</p>	<p>$g_{PL} = -4.7 \times 10^{-3} / 4.7 \times 10^{-3}$ (<i>R/S</i>)</p>	<p>$g_{EL} = -5.5 \times 10^{-3} / 5.5 \times 10^{-3}$ (<i>R/S</i>)</p>	<p>[42]</p>
 <p>(<i>R/S</i>)-PAC</p>	<p>17.8 (<i>R</i>)</p>	<p>$g_{lum} = 3 \times 10^{-3}$</p>	<p>$g_{EL} = 3.4 \times 10^{-3}$</p>	<p>[43]</p>

 <p>(<i>R/S</i>)-ax-DMAC</p>	30.1 (<i>S</i>)	$ g_{lum} = 2.2 \times 10^{-3}$	$ g_{EL} = 2.0 \times 10^{-3}$	[44]
 <p>(<i>R</i>)=CN (<i>R/S</i>)-Ax-CN</p>	21 (<i>R</i>)	$g_{lum} = 3.3 \times 10^{-3} / -3.2 \times 10^{-3}$ (<i>R/S</i>)	$g_{EL} = 4.2 \times 10^{-3} / -4.4 \times 10^{-3}$ (<i>R/S</i>)	[45]
 <p><i>R</i>=H (<i>R/S</i>)-Ax-H</p>	12.3 (<i>R</i>)	$g_{lum} = 3.5 \times 10^{-3} / -3.1 \times 10^{-3}$ (<i>R/S</i>)	$g_{EL} = 3.2 \times 10^{-3} / -3.1 \times 10^{-3}$ (<i>R/S</i>)	[45]
 <p>(<i>R</i>)=OMe (<i>R/S</i>)-Ax-OCH₃</p>	10 (<i>R</i>)	$g_{lum} = 3.6 \times 10^{-3} / -3.6 \times 10^{-3}$ (<i>R/S</i>)	$g_{EL} = 3.4 \times 10^{-3} / -3.5 \times 10^{-3}$ (<i>R/S</i>)	[45]

2.4. Binaphthyl based chiral TADF molecules.

Two pairs of chiral TADF enantiomers were synthesized in 2019 by expanding the conjugated skeletons of chiral BINOL ((*R/S*)-1 and (*R/S*)-2) (**Figure 19**).^[46] The DFT calculation predict that the LUMO was found on the electron acceptor xanthenone moieties in (*S*)-1 and (*S*)-2, whereas the HOMO was attached to the phenoxazine unit. Such distinct spatial electronic distribution separation in HOMO and LUMO was advantageous to the reduction of ΔE_{ST} . The TGA/DSC experiments depicted high thermal stability of the compounds. The 5% weight loss

temperatures and glass-transition temperatures of (*R*)-1 and (*R*)-2 were above 350 °C and 200 °C, respectively. In THF and water experiment both the synthesized compounds ((*R/S*)-1 and (*R/S*)-2) exhibited AIE characteristics and displayed TADF characteristics in a doped-film condition. In the THF solution, (*R*)-1 and (*R*)-2, both displayed nearly negligible emission. The fluorescence emission enhancement could be seen for both the compounds as water was gradually added. The aggregate solution displayed typical AIE characteristics for both chiral molecules when the water percentage was raised to 99%. It was found that the emission wavelength of (*R*)-1 was 38 nm bathochromically shifted than that of (*R*)-2. This might be possible as (*R*)-1 had a stiffer conjugated skeleton. At room temperature, the transient PL spectra of both (*R*)-1 and (*R*)-2 in non-doped and doped films was measured a double-exponential functions were used to fit the transient PL spectra of the films. The prompt component of 29.1/18.5 ns and delayed component of 1.03/0.97 microseconds for (*R*)-1/(*R*)-2 in doped films was observed and found that the components of the delayed fluorescence for both emitters were amplifying with rising temperature. This phenomenon directly supported the TADF nature. The developed chiral TADF emitters provided excellent mirror-imaged CD signals. Cotton's effects in the 200-300 nm wavelength range could be attributed to chiral binaphthyl absorption. Cotton effects in the long-wavelength range (450 nm) indicated ICT absorption. However, it was found that only one molecule (*R/S*)-1 could show CPL active emission. In toluene solution and in thin neat films, the luminescence dissymmetry factors (g_{lum}) reached up to 1.6×10^{-3} and 9.2×10^{-4} , respectively. The fabricated CP-OLEDs based on the (*R/S*)-1 as the chiral emitter showed CP-EL signals with g_{EL} of $-0.9 \times 10^{-3}/+1.0 \times 10^{-3}$. **Table 4** summarizes different chiroptical properties of binaphthyl-based chiral TADF molecules.

Nine chiral binaphthyl based molecules ((*R/S*)-1–(*R/S*)-9) were developed in 2019 (**Figure 19**).^[47] Various bridged alkyl chains were added to the hydroxyl groups of BINOL to make these chiral molecules. The functionalized substituents with various steric hindrances were used at various positions of these binaphthyl based molecules. The axial chirality induced the CP-EL in these chiral compounds. The level of substituent steric hindrance and the length of the alkyl chain was significantly responsible for the CPL behaviours and molecular conformations of the chiral molecules. This alkyl chain length and steric hindrance also controlled their ability to induce chirality on the achiral fluorescent polymer F8BT in doped films. It has been observed that due to the lack of a substituent on the 3,3'-position of the binaphthyl unit, the HOMO and LUMO totally overlap for *S*-1 to *S*-5. Regarding *S*-6 to *S*-9, the HOMO electron population are mostly concentrated at the donor groups but the LUMO

electron population are present only on the chiral binaphthyl unit. The chiral inducers with superior induction were filtered out by evaluating the CD and CPL signals from annealed films. As F8BT is achiral, the F8BT film was CPL-silent before and after thermal annealing. However, no CPL signal was noticed in as-cast films before annealing for the blends F8BT + (wt% of chiral inducers). All blended films (F8BT + wt% of chiral inducers) could release a CPL signal upon annealing. The amplified CPL signals (from blended films), $|g_{PL}|$, as high as 2.36×10^{-2} ((*R/S*)-1), 2.06×10^{-2} ((*R/S*)-6), and 1.26×10^{-2} ((*R/S*)-9) were observed from the CPL spectra. The planar stiff conjugated molecular conformation could be responsible for such a high CPL signal. The achiral fluorescence F8BT (CP-OLED emissive layer) and (*R/S*)-1 to (*R/S*)-9 (chiral inducers) were used in the fabricated CP-OLEDs. The CP-OLEDs were fabricated which demonstrated a maximum $|g_{EL}|$ value of 1.86×10^{-2} (F8BT + 5% (*R/S*)-6).

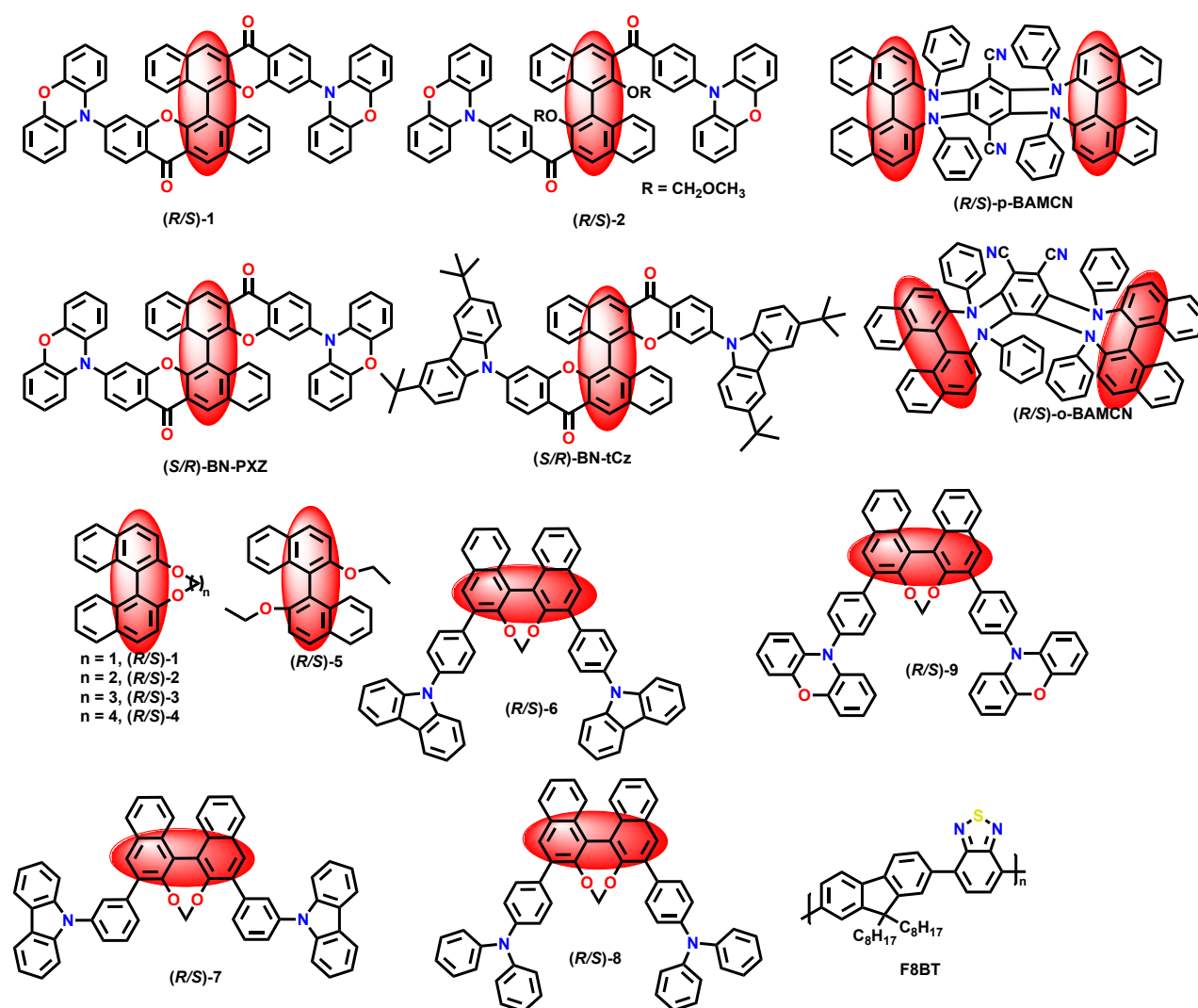


Figure 19. Binaphthyl based chiral TADF molecules.^[46-49]

Zuo's group in 2021 developed two pairs of TADF enantiomers by using binaphthalene chiral donor and cyano units as acceptor.^[48] The enantiomers with cyano units at para position of aryl group ((*R/S*)-*p*-BAMCN) were rod shaped while the cyano units at ortho position of aryl group ((*R/S*)-*o*-BAMCN) were helix-shaped (**Figure 19**). The developed materials exhibited a high PLQY of up to 0.86. These salient features could be credited to their rigid molecular structure and intramolecular arrangement. The synthesized chiral TADF materials exhibited exceptional thermal stability with decomposing temperatures above 450 °C. The electronic density population of the developed TADF emitters were clearly illustrated by the location of the highest occupied and lowest occupied natural transition orbitals. The unoccupied orbitals were present on the dicyanobenzene units of the emitters while the occupied orbitals were present on the donor moieties. There existed very small spatial overlap of these orbitals on the dicyanobenzene moieties. The phenyl core of (*R*)-*p*-BAMCN showed greater π to π^* features than those of *R*-*o*-BAMCN, which resulted in bathochromic shift. The ΔE_{ST} (0.18 eV for *R*-*p*-BAMCN and 0.15 eV for *R*-*o*-BAMCN) values were measured using the phosphorescence and fluorescence spectra at 77 K. These values indicated very quick RISC process in the emitters. Both emitters exhibited the two distinct exponential decays with prompt/delayed fluorescence lifetime of 3.2 ns/32 microseconds (*R*-*p*-BAMCN) and 3.4 ns/9.4 microseconds (*R*-*o*-BAMCN). Both the materials displayed chiroptical features very easily due to the direct electronic distributions on chiral unit. The CP-OLEDs were fabricated with maximum EQE of up to 28% ((*R/S*)-*p*-BAMCN). The helix-shaped (*R/S*)-*o*-BAMCN exhibited better CPL performances with the $|g_{PL}|$ of 5.3×10^{-3} in solution and $|g_{EL}|$ of 4.6×10^{-3} . The rod-shaped (*R/S*)-*p*-BAMCN showed better device performances with the brightness of 28402 cd/m² and maximum EQE of 27.6%.

The synthesis of two chiral D-A type emitters (*S*-/*R*-BN-tCz and *S*-/*R*-BN-PXZ) comprising of carbazole donors, 1,1'-binaphthol and benzophenone acceptors was described in 2021 (**Figure 19**).^[49] With a decomposition temperature of over 499 °C and glass transition temperature of 264 °C, thermal studies demonstrated that the developed emitters had potential to be utilized in the OLEDs. DFT calculations revealed that the acceptor benzophenone units were the primary site of the LUMO electron density, while the donor carbazole derivative units were the primary location of the HOMO electron density. The effective transport and carrier injection of the emitter were made possible by the HOMO/LUMO's distinct electrical

separation. In toluene solution and thin films, the fluorescence spectra revealed emission at 474/581 and 486/587 nm for (*S*)-BN-tCz/*S*-BN-PXZ, respectively. The PLQY of the two enantiomers in solution and films were 66.9% / 47.8% and 68.0% / 47.9% for (*S*)-BN-tCz/*S*-BN-PXZ, respectively. For (*S*)-/*(R)*-BN-tCz in thin films, the absorption dissymmetry factors, g_{abs} , at 392 nm were determined to be $+4.9 \times 10^{-4}$ / -4.4×10^{-4} , respectively. The (*S*)-/*(R)*-BN-tCz enantiomers could produce clear mirror-image CPL signals and had luminescence dissymmetry factors, g_{lum} , values of $+2.68 \times 10^{-3}$ / -2.74×10^{-3} . Based on (*S*)-/*(R)*-BN-tCz emitters, the non-doped blue CP-OLEDs could produce high efficiency CPEL with g_{EL} signals of $+2.13 \times 10^{-3}$ / -2.01×10^{-3} . The white CP-OLED with the g_{EL} values of approximately 10^{-3} was effectively fabricated using basic structure devices by coupling orange emitters (*S*)-/*(R)*-BN-PXZ) with blue (*S*)-/*(R)*-BN-tCz emitters.

Louis et al. in 2023 developed carbazole/naphthalimide TADF enantiomers with a binaphthyl chiral axis.^[50] The donor D, acceptor A, and monomer M were contrasted with the dimer molecule, DM (**Figure 20**). Calculations and photophysical tests demonstrated that dimerization was necessary to produce TADF emission, which resulted in a sharp drop in the ΔE_{ST} from 0.46 eV to 0.10 eV. In the toluene solution, the dimer showed a TADF emission with a 31% PLQY up to 40% in PMMA films. The clear mirror images of CD and CPL of enantiomers depicted absolute g_{lum} up to 6.0×10^{-3} . They could observe a ten-fold increase in CPL activity from the triplet state in MeTHF at low temperatures compared to fluorescence. Compared to the solution, the CPL value of aggregates formed by reprecipitation only showed blue-shifted emission; however, the gels organized in twisted nanowires demonstrated CPL signals with absolute intensity up to 1.3×10^{-2} .

Wang et al. in 2024 reported the synthesis and structural analysis of enantiomerically pure trigonal coordinated $\{\text{Cu}(\text{CbzR})[(\text{S}/\text{R})\text{-BINAP}]\}$ [R = H (1) or 3,6-tBu₂ (2)] complex (**Figure 20**).^[51] The ligands and surrounding molecules had strong C–H $\cdots\pi$ interactions, which significantly affected the photophysical properties. Grinding significantly improved the efficiency of the TADF process with high k_r of up to $3.1 \times 10^5 \text{ s}^{-1}$ and a bathochromic shift of the emitting 1/3LLCT states to $\lambda_{\text{max}} = 579$ (1) and 606 (2) nm. They could also observe that the impact of intermolecular hydrogen bonding on excited state energies is crucial when selecting a matrix material for device preparation. The nonpolar UGH-3 or bulky CzSi material preserved the excellent TADF properties of the copper(I) complexes at lower emission energies. Because of the chirality of the emitter molecules, the electronic transitions have a considerable rotatory strength, which leads to CPL with good dissymmetry factors g_{lum} of

$\pm 1.7 \times 10^{-2}$ (1) and $\pm 2.1 \times 10^{-2}$ (2) in the solid state and $\pm 6 \times 10^{-3}$ (1) and $\pm 5 \times 10^{-3}$ (2) in solution.

Wang et al., in 2023, used a chiral binaphthyl skeleton to develop four pairs of new thioxanthone derivative enantiomers, designated (*R/S*) - 1 to (*R/S*) - 4 (**Figure 20**).^[52] They observed that most of the reported chiral TADF materials were developed via chiral perturbation, frequently reducing CPL characteristics due to the spatial separation of the TADF luminophore from the chiral unit. Given the binaphthyl skeleton's electron-rich nature and stable axial chiral configuration, when the binaphthyl donor unit is directly coupled to a suitable acceptor, it is predicted to provide a molecule with both TADF characteristics and intrinsic chirality. Thioxanthone and its derivatives have been regarded as suitable acceptors for generating efficient TADF systems due to their high ISC rate, high QY, and narrow singlet-triplet energy gap. They developed emitter (*R/S*) - 2 and (*R/S*) - 4 by increasing intramolecular charge transfer and changing the substitution sites of thioxanthone oxide. The CD spectra of these enantiomers in diluted solutions demonstrated excellent mirror images and acceptable g_{abs} (10^{-4} - 10^{-3}). However, the CPL spectra of the (*R*) and (*S*) enantiomers showed a poor mirror symmetry connection, resulting in alternating positive and negative signals due to insufficient signals and high noise. They also fabricated the OLEDs and observed that the greatest external quantum efficiencies (EQE) were 10.9% and 8.32% based on emitter (*S*)-2 and (*S*)-4, respectively.

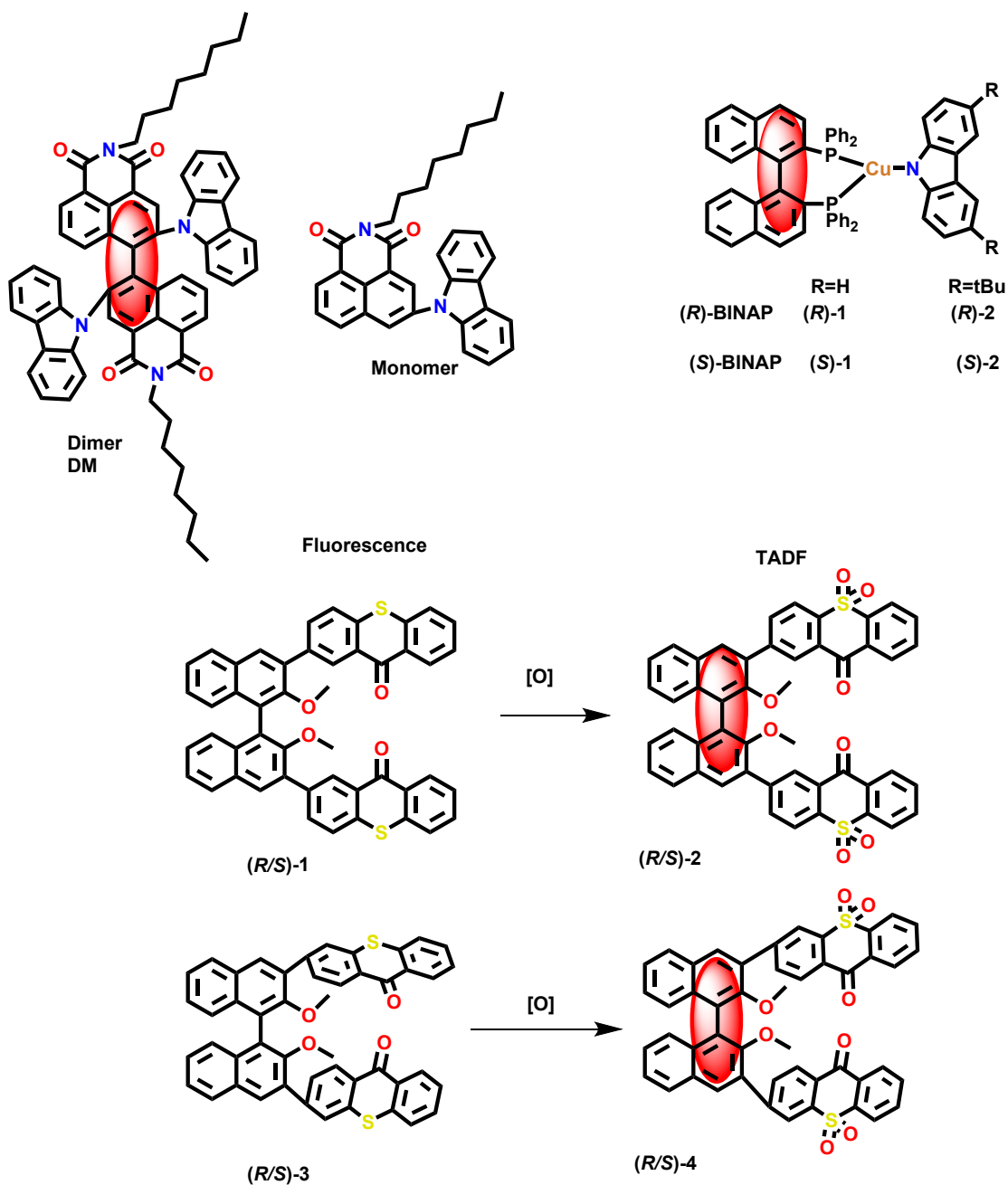


Figure 20. Chemical structures of some binaphthyl-based chiral TADF molecules.^[50-52]

A general technique for developing deep-red chiral TADF emitters remains undeveloped. Chen et al., in 2023, developed two chiral TADF polymer emitters, (*R*) and (*S*)-P (**Figure 21**).^[53] Both polymers demonstrated outstanding TADF characteristics and deep-red emission at 659 nm in TBPI and POT2T doped films. They also fabricated the solution-processed CP-PLED devices. The devices manufactured using (*R*) and (*S*)-P showed good EL performance, with maximum EQE of 6.2% and 5.8%, respectively. The devices produced strong CP-EL signals with g_{EL} of 1.6×10^{-3} and -1.7×10^{-3} at 662 nm, respectively. They demonstrated that $D \times A$

copolymerization with the chiral BINAM skeleton may provide CPEL emission at wavelengths beyond 660 nm.

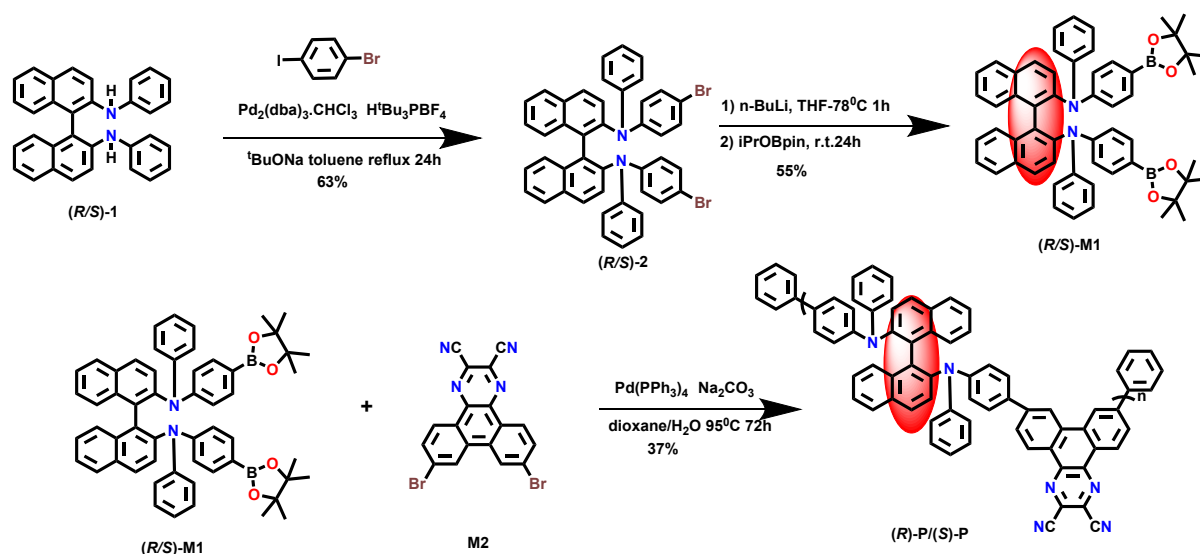


Figure 21. Synthetic scheme of binaphthyl-based chiral TADF molecule.^[53]

Chiral emitters that produce CPL with high dissymmetry factors are essential for CP-OLEDs. Zheng et al. developed three pairs of TADF enantiomers ((*R/S*)-BPSPXZ, (*R/S*)-BPSDMAC, and (*R/S*)-BPSPTCZ) with chiral (*R/S*)-sulfonyl binaphthalene units (**Figure 22**).^[54] The synthesized compounds depicted small ΔE_{ST} values of 0.11, 0.095, and 0.062 eV and high PLQYs of 69%, 74%, and 88%, respectively. They separated the enantiomers, which demonstrated excellent configuration stability, with strong mirror symmetric CD and CPL spectra and high $|g_{\text{PL}}|$ values of up to 6.0×10^{-3} in doped films. The CP-OLEDs based on the (*R/S*)-BPSPXZ, including phenoxazine electron donor, obtained high EQE of up to 28.5% and displayed strong CPEL spectra with g_{EL} values of 8.8×10^{-3} and -8.5×10^{-3} .

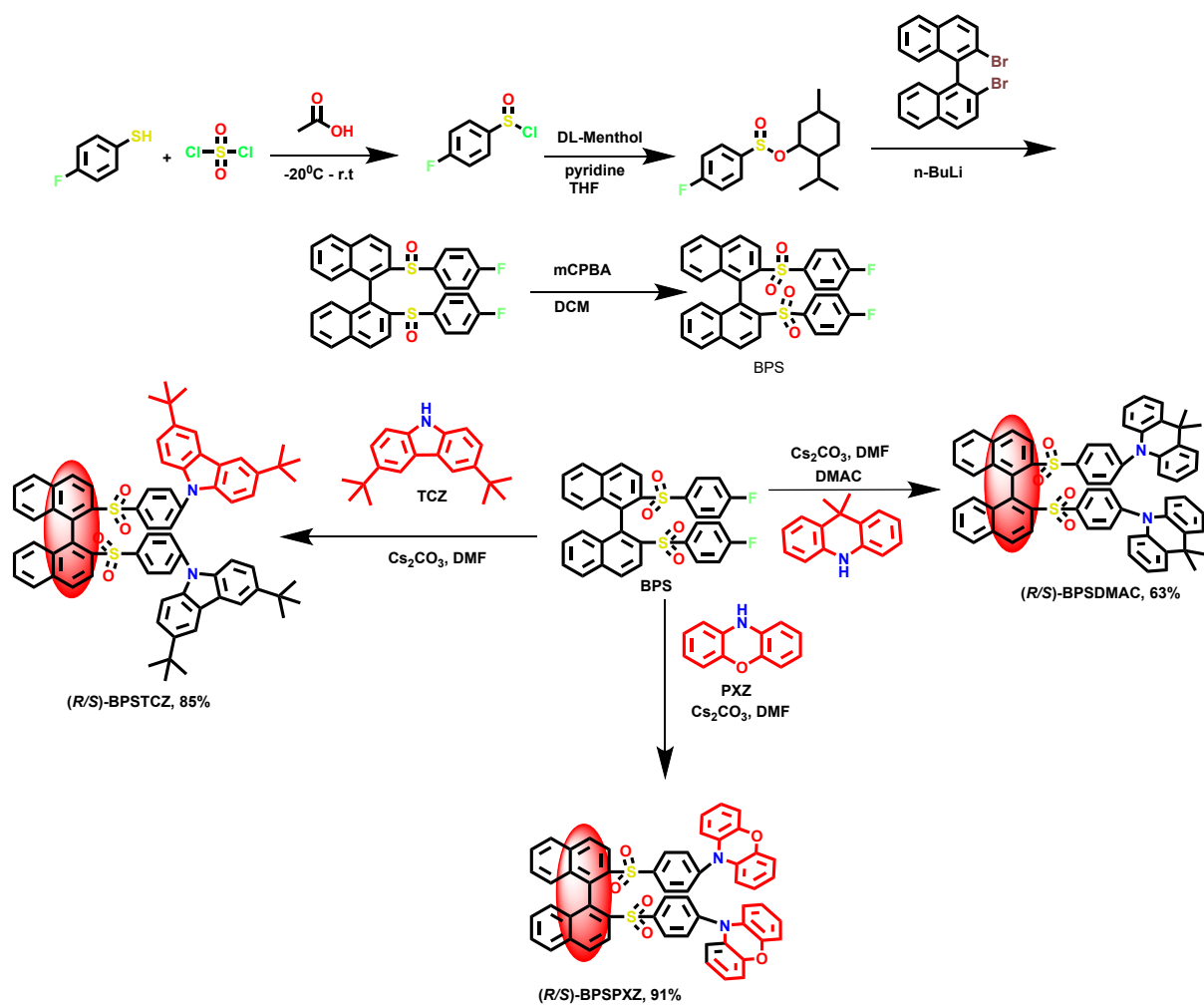
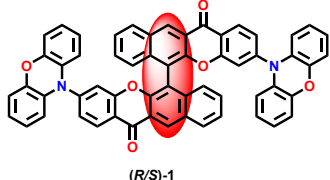
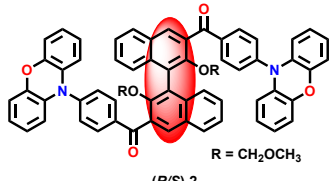
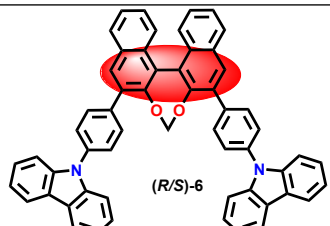
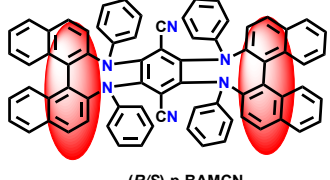
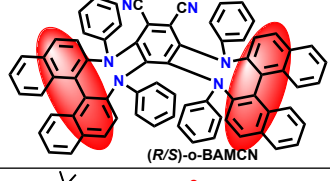
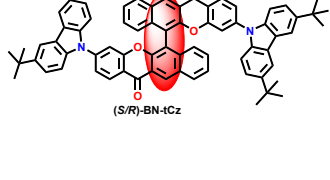
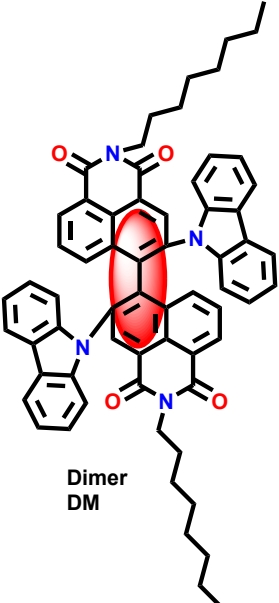
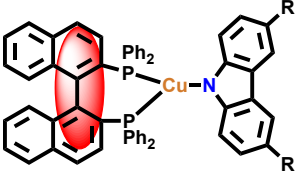
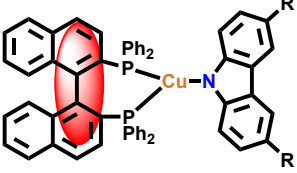
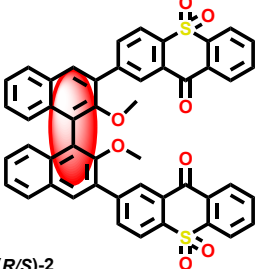
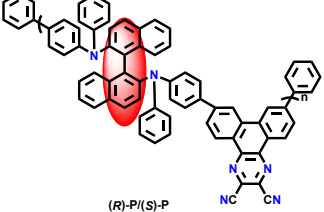
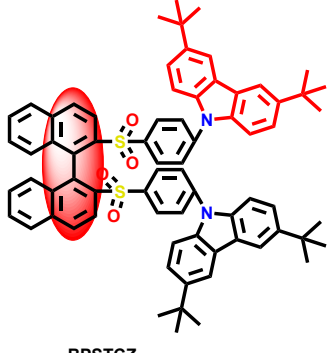
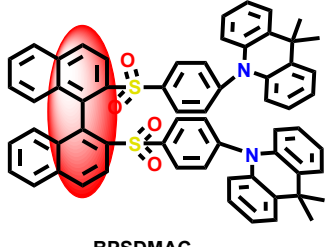
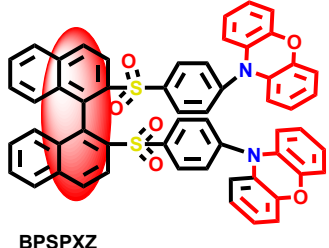


Figure 22. Synthetic scheme of some binaphthyl-based chiral TADF molecules.^[54]

Table 4. Chiroptical properties of binaphthyl-based chiral TADF molecules.

Compound	EQE _{max} (%) (Isomer used as emitter)	Luminescence dissymmetry factor	Electroluminescence dissymmetry factor	Reference
 (R/S)-1	1.8 (S) Doped	$g_{lum}^{\pm} = -1.2 \times 10^{-3} / 1.6 \times 10^{-3},$ (Toluene) $-7.1 \times 10^{-4} / 9.2 \times 10^{-4}$ (Neat films) (R/S)	$g_{EL}^{\pm} = -0.9 \times 10^{-3} / 1 \times 10^{-3}$ (R/S)	[46]
 (R/S)-2 R = CH ₂ OCH ₃	-	-	-	[46]
 (R/S)-6	0.54 (S) (Blend d films)	$ g_{PL} = 2.06 \times 10^{-2}$	$g_{EL}^{\pm} = 1.79 \times 10^{-2} / -1.86 \times 10^{-2}$ (R/S)	[47]
 (R/S)-p-BAMCN	27.6 (R)	$g_{PL}^{\pm} = -0.3 \times 10^{-3} / 0.3 \times 10^{-3}$ (Toluene)	-	[48]
 (R/S)-o-BAMCN	20.5 (R)	$g_{PL}^{\pm} = -5.3 \times 10^{-3} / 5.3 \times 10^{-3}$ (Toluene)	$ g_{EL} = 4.6 \times 10^{-3}$	[48]
 (S/R)-BN-tCz	1 (S)	$g_{lum}^{\pm} = -2.74 \times 10^{-3} / 2.68 \times 10^{-3}$ (R/S) (Films)	$g_{EL}^{\pm} = -2.01 \times 10^{-3} / 2.13 \times 10^{-3}$ (R/S)	[49]

 <p>Dimer DM</p>	-	$g_{lum} = 6 \times 10^{-3} / -4 \times 10^{-3}$ (R/S)	-	[50]
 <p>R=H (R)-BINAP (R)-1</p> <p>(S)-BINAP (S)-1</p>	-	$ g_{lum} = \pm 1.7 \times 10^{-2}$	-	[51]
 <p>R=tBu (R)-BINAP (R)-2</p> <p>(S)-BINAP (S)-2</p>	-	$ g_{lum} = \pm 2.1 \times 10^{-2}$	-	[51]
 <p>(R/S)-2</p>	10.9 (S)	-	-	[52]
 <p>(R)-P/(S)-P</p>	6.2 (R)	$g_{lum} = 1.7 \times 10^{-3} / -1.7 \times 10^{-3}$ (R/S)	$g_{EL} = 1.6 \times 10^{-3} / -1.7 \times 10^{-3}$ (R/S)	[53]

 <p>BPSTCZ</p>	3.8	$g_{PL} = -5.2 \times 10^{-3} / 6.0 \times 10^{-3}$ (R/S)	$g_{EL} = -5.5 \times 10^{-3} / 6.2 \times 10^{-3}$ (R/S)	[54]
 <p>BPSDMAC</p>	7.5	$g_{PL} = -3.0 \times 10^{-3} / 3.0 \times 10^{-3}$ (R/S)	$g_{EL} = -6.4 \times 10^{-3} / 7.1 \times 10^{-3}$ (R/S)	[54]
 <p>BPSPXZ</p>	28.5	$g_{PL} = -4.9 \times 10^{-3} / 5.1 \times 10^{-3}$ (R/S)	$g_{EL} = -8.5 \times 10^{-3} / 8.8 \times 10^{-3}$ (R/S)	[54]

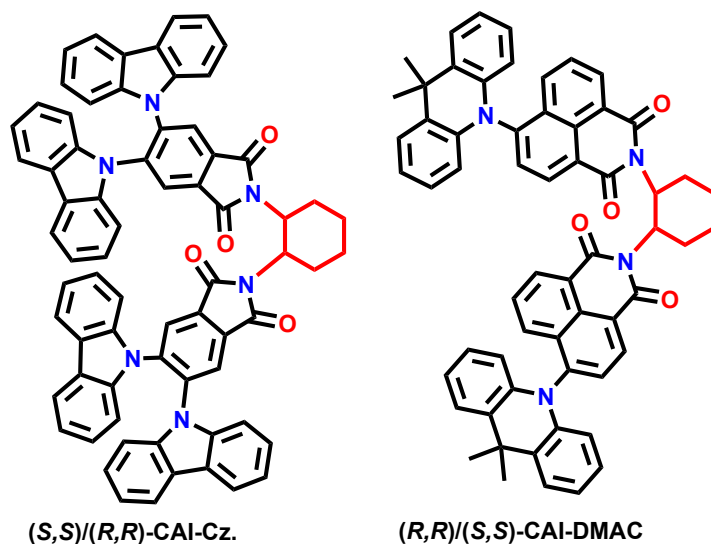


Figure 23. 1,2-diaminocyclohexane-based chiral TADF molecules.^[55-56]

2.5. 1,2-diaminocyclohexane based chiral TADF molecules

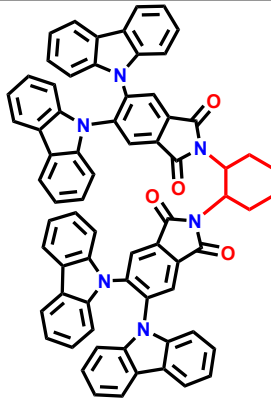
Chen's group developed a chiral TADF molecule by inducing chirality with the help of 1,2-diaminocyclohexane to the achiral TADF unit ((R,R)-CAI-Cz and (S,S)-CAI-Cz) (**Figure**

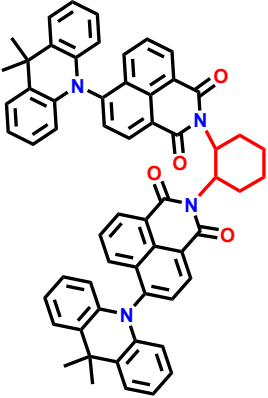
23).^[55] The synthesis of the TADF emitters was carried out by lactamization of difluorophthalic anhydride with chiral 1,2-diaminocyclohexane and a followed by substitution reaction with carbazole. No racemization of the chiral TADF emitters took place throughout their synthesis because of stable central chirality of the 1,2- diaminocyclohexane. Based on chiral-phase HPLC, significant enantiomeric excesses (>99%) of the desired TADF enantiomers were attained. The developed TADF enantiomers could achieve 98% PLQY and small ΔE_{ST} of 0.06 eV. The DFT calculations depicted that the carbazole units were containing HOMO population, while the aromatic imide units were having LUMO density. The distinct spatial electronic separation of HOMO and LUMO was observed, which was necessary for getting a low ΔE_{ST} value. One can see a little overlap of LUMO and HOMO on the aromatic imide moiety, which was important for the high luminescence efficiency. Also, the frontier molecular orbital distribution showed that the 1,2-diaminocyclohexane unit did not participate in the chiral TADF emitter, but it could still effectively cause the TADF units to exhibit CD and CPL features. The temperature dependent transient PL studies depicted that, from 150 to 300 K, the delay component of the transient PL gradually increased. This showed the presence of a thermal activation energy barrier for TADF. The more RISC of excitons from first triplet to first singlet was observed by gradual warming. The transient decay properties depicted a prompt fluorescence component of 44 ns and delayed component of 130 microseconds. The TADF enantiomers further displayed mirror-image CD and CPL activity. The CP-OLEDs were fabricated by using these enantiomers as emitters and could reach an EQE values of up to 19.8%. The mirror-image between the CD spectra of developed enantiomers confirmed that the chiral unit in enantiomers successfully introduced chirality in the ground state of the enantiomers. The CPL spectra of the enantiomers were almost mirror-image with $|g_{lum}|$ at 1.1×10^{-3} confirming their chiroptical character in the excited state. Introducing a chiral unit into the TADF molecular framework allows for the development of new TADF materials with CD and CPL capabilities, ultimately leading to high-performance CP-OLEDs with intense CPEL. The opposing dissymmetry factor (g_{EL}) signals produced by the two distinct enantiomer-based CP-OLEDs were -1.7×10^{-3} ((*S,S*)-CAI-Cz) and 2.3×10^{-3} ((*R,R*)-CAI-Cz). **Table 5** summarizes different chiroptical properties of 1,2-diaminocyclohexane-based chiral TADF molecules.

Further, they developed a pair of chiral enantiomers by adding a chiral unit to the 1,8-naphthalimide-based TADF skeleton ((-)-(*R,R*)/(+)-(*S,S*)-CAI-DMAC) (**Figure 23**).^[56] The DFT calculations depicted that the HOMO and LUMO of CAI-DMAC were mostly found on the acridine and aromatic imide moieties, respectively. The phenyl ring of the aromatic imide

unit was having a little overlap of the HOMO and LUMO. This distinct electronic separation of HOMO-LUMO was advantageous to produce very low value of ΔE_{ST} (0.01 eV). A high thermal stability of the (-)-(R,R)-CAI-DMAC was observed with a high decomposition temperature of 405 °C. The (-)-(R,R)-CAI-DMAC co-doped with CBP in film was used at 77K to examine ΔE_{ST} value. The estimated S_1 energy level was 2.08 eV from fluorescence spectra and T_1 energy level was determined to be 2.01 eV from phosphorescence spectra. As a result, the ΔE_{ST} value was estimated to be 0.07 eV. The transient PL decay for the doped film of the enantiomer was measured and it revealed a long lifetime of 37.4 microseconds, further supporting the TADF features. Additionally, due to oxygen quenching, the PL intensity in air was lower than in vacuum. The absolute PLQY of (-)-(R,R)-CAI-DMAC in the CBP host was 25.8% in the air at ambient temperature and rose dramatically to 39.9% in a vacuum environment. The CD spectra of both enantiomers clearly displayed mirror images proving the presence of chirality in the structures. The CPL spectra of the TADF enantiomers clearly showed mirror images. The developed enantiomers depicted the luminescence dissymmetry factor, g_{lum} of 9.2×10^{-4} . The CP-OLEDs were fabricated by using these enantiomers as emitters. The doped OLEDs displayed an orange-red emission band at 592 nm and had maximum EQE values around 12%.

Table 5. Chiroptical properties of 1,2-diaminocyclohexane-based chiral TADF molecules.

Compound	EQE _{max} (%) (Isomer used as emitter)	Luminescence dissymmetry factor	Electroluminescence dissymmetry factor	Reference
 (S,S)/(R,R)-CAI-Cz.	19.8 (R,R)	$g_{lum} = 1.1 \times 10^{-3} / -1.1 \times 10^{-3}$ (R/S)	$g_{EL} = 2.3 \times 10^{-3} / -1.7 \times 10^{-3}$ (R/S)	[55]

 <p>(R,R)/(S,S)-CAI-DMAC</p>	12.4 (R)	$g_{lum} = 9.2 \times 10^{-4} / -9.2 \times 10^{-4}$ (R/S)	-	[56]
---	-------------	---	---	------

2.6. Central chirality based chiral TADF molecules

In 2015, an aromatic compound with TADF and CPL properties (DPHN) was reported (**Figure 24**).^[57] Their goal was to develop a metal-free organic conjugated molecule with a chiral center, and this chiral carbon was embedded between a triphenyl amine unit and naphthalene-5 (12H)-one unit. DPHN was synthesized by utilizing *n*-BuLi as a catalyst in a nucleophilic addition process. Through TD-DFT analysis, the HOMO and LUMO of the synthesized chiral molecule were populated in the triphenylamine and naphthalene-5 (12H)-one unit of the molecule at the S_1 level. The designed molecule had a modest ΔE_{ST} and exhibited green TADF with PLQY of 26% in the host film. The TD-DFT calculations depicted that the transition responsible for the first absorption band for the optimized S_0 structure exhibited poor charge transfer characteristics. It was found that pure charge transfer character between the HOMO and LUMO for the optimized S_1 . A clear π - π^* character was seen during the shift from S_0 to T_1 . It was found that the energy of T_1 state was somewhat lower than energy of S_1 state due to the π - π^* nature of T_1 . The calculated ΔE_{ST} value was 0.07 eV. The circular phase separation and circular dichroism (CD) was noticed in the developed enantiomers. They measured circular dichroism and circular phase separation with dissymmetry values of $|1.2 \times 10^{-3}|$ and $|1.1 \times 10^{-3}|$. The substantial conformational shift was witnessed between the ground state (S_0) and the S_1 resulted in sign inversion between the CD and the CPL as well. **Table 6** summarizes different chiroptical properties of central chirality-based chiral TADF molecules.

Shi's group described a pair of aggregation induced emission active enantiomers that exhibited mechano-luminescence when subjected to external stress (*R*) and (*S*)- ImNT (**Figure 24**).^[58] A phthalimide unit could create strong intermolecular hydrogen bonds and rigidify the molecular conformation. Therefore, the phthalimide was chosen to inhibit the nonradiative decay from providing aggregation-induced emission features. The phenothiazine was selected as a

donating group since its derivatives were known to have varied conformations with varying HOMO-LUMO and single-triplet energy gaps. The THF-water experiment was performed to find out the possibility of presence of aggregation induced emission in the developed chiral compounds. When the developed enantiomers and their racemate were thoroughly dissolved in pure THF, hardly any signals were seen. It was found that at 70% water concentration in THF, a considerable emission increment and Mie scattering effect in absorption spectra were observed. These findings claimed that the nanoaggregates were responsible for the enhancement in the luminescence. These results proved that the developed enantiomers were aggregation induced emission active in nature. The chiroptical characteristics were investigated via CPL measurements. It was found that racemic mixture of both enantiomers prevented it from generating CPL when exposed to UV light. The luminescence dissymmetry factors, g_{lum} , of (*R*)-ImNT and (*S*)-ImNT yielded distinct mirror-image CPL signals with values of 3.42×10^{-3} and -3.65×10^{-3} , respectively. It was found that shearing the powders of developed enantiomers with a spatula resulted in bluish-green light emissions.

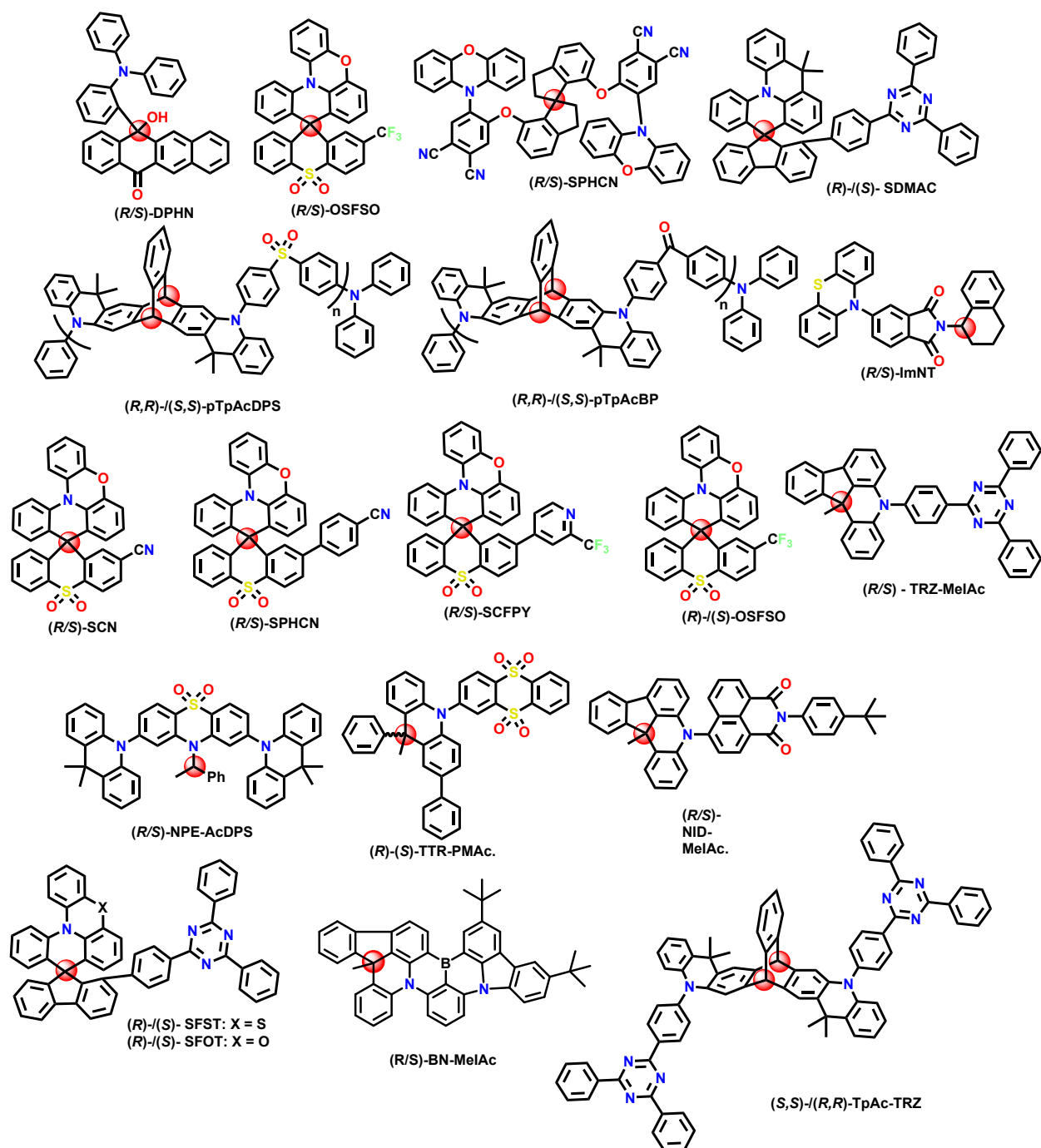


Figure 24. Molecular structures of chiral carbon based TADF molecules.^[57-69]

A central chirality based (TTR-PMac) donor-acceptor molecule with the asymmetric carbon on the donor unit was reported in 2020 (**Figure 24**).^[59] Two geometries were noticed, one in a quasi-planar conformation between the acceptor and donor with a dihedral angle of 173° and the other in a quasi-orthogonal conformation at an angle of 86° by theoretical modelling. Both enantiomers had two characteristic intramolecular charge transfer absorption bands in diluted toluene. The weak absorption band at 400 nm might be attributed to the highly twisted

orthogonal conformation. The strong absorption band at 357 nm was attributed to the almost planar conformations. The S_1 and T_1 levels were evaluated in dilute 2-MeTHF and the ΔE_{ST} was observed as 0.36 ((*R*)-TTR-PMAC) and 0.39 eV ((*S*)-TTR-PMAC). Triplet excitons could rarely be used in these conformations due to high value of ΔE_{ST} . The neat films of the enantiomers depicted significantly lower ΔE_{ST} of 0.02 and 0.05 eV, which displayed the TADF characteristics. It was found that the orange emission from almost orthogonal conformations under an air environment showed a substantial improvement after nitrogen degassing. Additionally, double exponential decays could be seen clearly in the transient decay curves from the emission from roughly orthogonal conformations with significant oxygen sensitivity. The (*R*)- and (*S*)-enantiomers exhibited very faint mirror-image signals in the CPL spectra taken from spin-coated thin sheets on a CPL spectrometer.

Two pairs of chiral molecules (SFST and SFOT) having asymmetric donor spiro structures were reported in 2020 (**Figure 24**). In these newly created CP-TADF molecules, the donor and acceptor units were cofacially held proximally.^[60] In particular, an asymmetric donor, phenothiazine derivative or phenoxazine derivative, cyclized the C9 site that formed a spirostructure. A prominent acceptor triazine derivative was appended on the C1 site of fluorene. Both emitters could experience intramolecular through-space charge transfer, which resulted in TADF characteristics. The crystal structures proved that the intramolecular steric hindrance caused deformed spiro backbones in SFST and SFOT. Solid-state structures showed proton-phenothiazine or phenoxazine interactions in the fluorene linker. SFOT had a shorter donor-acceptor distance, resulting in more efficient intramolecular charge transfer than SFST. In solid state, the dihedral angles between fluorene and phenothiazine planes were 52.34° (SFST) and 67.09° (SFOT). The intermolecular short contacts and intramolecular contacts limit intramolecular mobility, resulting in aggregation-induced emission behavior and increased PLQY in the solid state. The phenoxazine moiety in SFOT is more planar than the phenothiazine unit in SFST. The bigger distortion of phenothiazine units might be responsible for a higher g_{lum} value in SFST. The minor variations of sulphur and oxygen atoms in the donor units had a significant influence on the chiroptical, EL and photophysical characteristics. Based on their phosphorescence and fluorescence spectra at 77 K, the values of ΔE_{ST} for SFST (0.052 eV) and SFOT (0.053 eV) were very small which was essential for RISC. The transient decay curves of doped films showed two components and the first decay curve had lifetime in nanoseconds range, SFOT (10 ns) and SFST (141 ns), respectively. The delayed emission component with lifetime of 6.78 and 7.98 microseconds for SFST and SFOT, respectively, was

the second part. These findings supported the presence of the TADF feature in both materials. The temperature-dependent transient PL in the doped films depicted that as the temperature rose, the delayed emission component eventually got stronger which also confirmed the TADF property. HOMOs and LUMOs were mostly found on the donor and acceptor units, respectively. The HOMO of SFOT was greater than that of SFST, suggesting that the former possessed a more potent donor. The very low ΔE_{ST} values resulted from short HOMO/LUMO overlaps, which implied that TADF might be induced by fast RISC from T_1 to S_1 . The very small values of oscillator strengths resulted from the low overlap. The competitive vibronic couplings that facilitated nonradiative decay were greatly inhibited by the steric barrier between the donor and acceptor. With EQE of up to 23.1%, SFOT significantly improved EL performance in doped OLEDs. The comparatively bigger sulfur atom in SFST caused the molecular backbone to be distorted, which lengthened the donor-acceptor distance. Hence, SFST had a quicker nonradiative decay rate as a heavy atom effect was present. The overall effect was a significantly lower EQE value of SFST than the EQE of SFOT. The luminescence dissymmetry factor, $|g_{lum}|$, of CPL of one enantiomer of SFST was almost twice that of SFOT enantiomer because SFST had a more deformed molecular architecture than SFOT. Cotton effects in the short-wavelength region of (*R*)-SFST/(*S*)-SFST can be attributed to the $\pi-\pi^*$ and $n-\pi^*$ electronic transitions. Weak absorption bands after 325 nm indicated intramolecular charge transfer from donor to acceptor. The g_{lum} values for (*S*)-SFOT/(*R*)-SFOT had been recorded up to 2.2×10^{-3} / 2.0×10^{-3} . In comparison, the g_{lum} values for (*S*)-SFST/(*R*)-SFST were substantially higher, at 3.4×10^{-3} / 4.0×10^{-3} , respectively. The CP-OLEDs exhibited CP-EL signals with g_{EL} values for (*S*)-SFST and (*S*)-SFOT of 1.30×10^{-3} and 1.0×10^{-3} , respectively.

A central chiral electron donor was synthesized by integrating the acridine and indene subunits to construct MeIAc.^[61] The chiral unit MeIAc depicted a high-lying triplet state energy level, strong structural stiffness and an appropriate electron-donating capacity. The MeIAc-derived chiral donor-acceptor type systems, TRZ-MeIAc and NID-MeIAc, exhibited a highly inflexible molecular structure (**Figure 24**). A three-step process involving the Wittig reaction, C–N coupling (Pd-catalyzed), and intramolecular cyclization reaction was used to develop the designed MeIAc donor. MeIAc and the acceptor unit underwent C–N coupling (Pd-catalyzed) reactions to yield the target molecules. These central chirality-based molecules showed perfect quasi-equatorial conformer geometry and TADF behaviour with PLQYs >85%. The CP-OLEDs were fabricated which displayed maximum EQEs of 20.3% and 23.7% for NID-MeIAc and TRZ-MeIAc, respectively. Two components were observed in the transient PL curves in

toluene solution for the developed materials. The delayed component was completely quenched after exposure to air. For TRZ-MeIAc and NID-MeIAc, the predicted ΔE_{ST} values from the fluorescence and phosphorescence spectra of the doped films were 0.19 and 0.22 eV, respectively. The transient PL decay curves and steady state emission curves at various temperatures were measured. The TADF mechanism was supported by the rising ratios of the delayed components and the intensity of the steady-state emission with temperature. DFT studies revealed that the acceptor unit was containing the LUMOs, whereas the acridine component was the possessing HOMOs. The frontier molecular orbital distributions of the developed molecules produced small ΔE_{ST} (0.05 eV ((*R*)-TRZ-MeIAc) and 0.30 eV ((*R*)-NID-MeIAc)) which ensured an effective RISC transition. It was found that the CPPL spectra of two pairs of enantiomers were mirror-symmetric images. The CD spectra in the π - π^* transition region exhibited a bisignate Cotton effect. The absorption peak at 330 nm represents the absorption band of chiral donor. The CD spectra in the charge transfer area demonstrated a monosignate Cotton effect, suggesting successful chirality transfer from the point chiral donor to D*-A systems. The CPPL spectra of the synthesized enantiomers showed structureless mirror-symmetric pictures, indicating chirality transfer in the first excited state. The luminescence dissymmetry factors, g_{PLs} , were $+5.9 \times 10^{-4}$ ((*R*)-TRZ-MeIAc), -5.9×10^{-4} ((*S*)-TRZ-MeIAc). Similarly decent g_{PLs} , were observed for (*R*)-NID-MeIAc ($+2.0 \times 10^{-3}$) and (*S*)-NID-MeIAc (-2.0×10^{-3}). The devices based on (*R*) and (*S*)-NID-MeIAc displayed g_{EL} values of $+2.0 \times 10^{-3}$ and -2.4×10^{-3} , respectively. The OLEDs based on the TRZ-MeIAc enantiomers showed clear mirror-image CPEL signals with g_{EL} values of $+6.4 \times 10^{-4}$ (*R*) and -7.3×10^{-4} (*S*).

Two CP-TADF enantiomers with phenoxazine as the donor and a derivative of thioxanthene dioxide as the acceptor (*R* and *S*-OSFSO) were developed in 2021 (Figure 24).^[62] The developed molecule was based on a chiral spiro-axis skeleton. The thioxanthene derivative was attached to TADF molecule as an acceptor unit, resulting in a confined dispersion of the electronic cloud and a short donor-acceptor distance. DFT calculations predicted that the LUMOs and HOMOs were found on acceptor and donor units, respectively. Both HOMO and LUMO were well separated from each other. As the trifluoromethyl group had the potential to extract electrons, the LUMOs were mostly found on one side of the thioxanthene unit, with 71.7% positioned at the benzene ring where the trifluoromethyl group was attached. DFT calculation determined the ΔE_{ST} as 0.07 eV which was beneficial for the RISC process. The confined distribution of LUMOs on the electron-deficient benzene ring combined with the close proximity of the donor and acceptor units might result in HOMO-LUMO spatial overlap,

which was necessary for the efficiency of TADF molecules by the through space charge transfer process. The fluorescence and phosphorescence spectra at 77 K depicted the ΔE_{ST} of 0.022 eV which would aid RISC process. A PLQY of 30.0% was achieved in nitrogen-filled toluene solution, and after bubbling air, the efficiency fell to just 14.9%. After putting air, the delayed fluorescence component, which was measured to be 2.9 microseconds, was fully quenched. Through temperature-dependent transient PL that as temperature rose, more delayed fluorescence components appeared. The CD spectra of both enantiomers exhibited a mirror image connection. The enantiomers depicted the symmetrical CPL signals with dissymmetry factors, g_{PL} , of about -1.6×10^{-3} for (*R*)-OSFSO and 1.4×10^{-3} for (*S*)-OSFSO, respectively. The CP-OLEDs were fabricated by using the developed enantiomers as emitters. The CP-OLEDs exhibited emission centered at 472 nm with an EQEmax of 20.0%. Additionally, strong CPEL signals were detected, with g_{EL} values of -3.0×10^{-3} ((*R*)-OSFSO) and 3.1×10^{-3} ((*S*)-OSFSO).

Chen's group in 2021 described the synthesis and CP-OLED device fabrication of chiral TADF molecules ((*R,R*)-(-)-TpAc-TRZ and (*S,S*)-(+)-TpAc-TRZ) (**Figure 24**).^[63] The triptycene framework induced chirality to the designed molecule and triazine derivative as the acceptor. The developed enantiomers had high value of PLQY up to 85%. DFT calculations revealed that the two acceptor units exhibited the majority of the LUMO population owing to their electron-withdrawing ability while the HOMO was present on entire donor unit based on the triptycene scaffold. The clear spatial separation of HOMO and LUMO gave indication of small ΔE_{ST} . TD-DFT used to find the singlet (S_1) and triplet (T_1) energy levels and measured the ΔE_{ST} value as 0.06 eV which encouraged the RISC process. The crystal structure depicted that the developed molecule was possessing complete twisted geometry. The effective separation of frontier molecular orbitals and low electronic coupling was facilitated by the nearly perpendicular donor-acceptor connection. This resulted in a very small ΔE_{ST} and an efficient TADF property. The single crystal structure also evidenced the absence of π - π stacking owing to the triptycene structure. The fluorescence and phosphorescence spectra of the emitter ((*S,S*)-(+)-TpAc-TRZ) was measured at 77K and the calculated S_1 , T_1 energy level and the associated ΔE_{ST} were 2.53, 2.50, and 0.03 eV, respectively. The transient PL decay curve yielded the prompt and delayed lifetimes of 50 ns and 1.1 microseconds for the molecule. Furthermore, from 100 to 300 K, there was a considerable reduction in the delayed components of (*S,S*)-(+)-TpAc-TRZ. In THF/water mixture the PL emission study reveals that the emission intensity fell as the water concentration increased from 0 to 50%. The enhanced polarity of solution due to the addition of water led to a strongly twisted intramolecular charge transfer process and a

rise in the inter system crossing rate, which in turn caused the excitons to quench. The PL intensity rose up again as the water concentration increased from 50 to 99% which revealed the aggregation induced phenomenon in the enantiomer. The emission maxima also showed a blue-shift following the creation of aggregates indicating a restriction in intramolecular rotational motion. A mirror-image relation between the CD and CPL spectra of the synthesized enantiomers was observed. In the short wavelength range, chiral acridine unit was responsible for strong Cotton effects. The weak Cotton effects can be seen in the long wavelength due to the absorption of D- π -A electronic structures. This indicates that chirality may be transferred from the donor moiety to the complete molecular skeleton in the ground state. A mirror-image CPL signals were observed for the synthesized enantiomers with PL dissymmetry factors, g_{PL} , of 1.9×10^{-3} ((*S,S*)-(+)-TpAc-TRZ) and -1.8×10^{-3} ((*R,R*)-(-)-TpAc-TRZ). The CP-OLEDs were fabricated (non-doped) via solution-processed method using developed enantiomers as the emitters and achieved dissymmetry factors (g_{EL}) of 1.5×10^{-3} / -2.0×10^{-3} with EQE up to 25.5%.

Two sets of chiral nonconjugated polymers ((*R,R*)-/(*S,S*)-pTpAcBP and (*R,R*)-/(*S,S*)-pTpAcDPS) were synthesized through "chiral donor-acceptor copolymerization" strategy in 2021 (**Figure 24**).^[64] Benzophenone and benzophenone diphenyl sulfone were utilized as the acceptors in these polymers, while the triptycene scaffold-based acridine served as the chiral donor. Palladium catalyzed coupling was used to produce these chiral TADF polymers. The DFT calculations were performed to calculate the theoretical properties by choosing two repeating units of the polymers. It was found that, due to the homoconjugation effect, the HOMOs were concentrated across the donor units based on the triptycene scaffold. The majority of the LUMOs were found on the electron-accepting units. These DFT calculations showed the presence of charge transfer in the chiral polymers. There was very little overlap between the HOMO and LUMO wavefunctions, which led to a very small ΔE_{ST} . The TD-DFT calculations predicted the S_1/T_1 values which were 2.841/2.830 eV (pTpAcDPS) and 2.193/2.187 eV (pTpAcBP). According to these calculations, the ΔE_{ST} were 0.011 eV and 0.006 eV, respectively, suggesting the efficient RISC from T_1 to S_1 . With the help of fluorescence and phosphorescence spectra (at 77K), the energy levels of singlet (for (*R,R*)-pTpAcDPS and (*R,R*)-pTpAcBP, the S_1 energy values were 2.84 eV and 2.65 eV), triplet (2.81 eV for (*R,R*)-pTpAcDPS and 2.64 eV for (*R,R*)-pTpAcBP) and ΔE_{ST} were measured. The energy level values for ΔE_{ST} were 0.03 eV and 0.01 eV, respectively. The transient PL curve exhibited two exponential decays, which were attributed to prompt fluorescence and delayed component. The (*R,R*)-/(*S,S*)-pTpAcDPS and (*R,R*)-/(*S,S*)-pTpAcBP had delayed fluorescent

lifetimes of 1.07/1.05 microseconds and 1.75/1.58 microseconds, respectively. Both the pairs of isomers of chiral polymers exhibited mirror-image CPL spectra, with $|g_{\text{PL}}|$ values ranging from 1.0×10^{-3} to 1.4×10^{-3} . The fabricated solution-processed CP-OLEDs devices based on TADF polymers showed maximum EQE of 22.1%. The CP-OLEDs based on these enantiomers exhibited CPEL characteristics with $|g_{\text{EL}}|$ value of up to 1.6×10^{-3} .

A chiral unit, (*S*)-/(*R*)-1-phenylethylamine, was connected to the previously known TADF emitter DMAC-DPS to develop a pair of enantiomers ((*S*)/(*R*)-NPE-AcDPS) in 2022 (**Figure 24**).^[65] Both enantiomers were synthesized by two-step synthetic technique without requiring necessity for chiral resolution. These emitters exhibited a very small splitting of the energy levels (ΔE_{ST}) of 0.05 eV between the S_1 and T_1 states. The emitters also displayed deep blue emission in both the doped film and toluene solution, with peaks at 440 and 451 nm, respectively. The DFT calculations depicted that the donor unit, acridine, and acceptor unit, diphenylsulfone, were containing the HOMO and LUMO, respectively. The twisted structure of the developed molecule and huge dihedral angles between the donor and acceptor units, there was a wide separation of frontier molecular orbitals. This resulted in a small ΔE_{ST} value of 0.03 eV, which was advantageous for RISC process. The deep blue emission of the emitter was predicted by the high energy level of S_1 (3.13 eV) and the high band-gap value of 3.59 eV (theoretical value). Additionally, it was observed that the chiral phenylethylamine unit participated in the frontier molecular orbitals which gave the emitter chiroptical activity. In order to calculate the experimental first excited singlet and triplet energy level, the fluorescence and phosphorescence spectra were measured. The energy levels of the S_1 and T_1 states were calculated to be 3.08 eV and 3.03 eV, respectively. The experimentally found small ΔE_{ST} of 0.05 eV which was very much parallel to the theoretical ΔE_{ST} , 0.03 eV. The transient PL studies depicted two components, the prompt component (23 ns) and delayed component (3.4 microseconds). The temperature-dependent transient PL measurements (for (*S*)-NPE-AcDPS) displayed that the intensity of the delayed emission increased as the temperature increased. In order to prove the aggregation induced emission property of the emitter, the THF:water experiment was performed for (*S*)-NPE-AcDPS. The emitter showed a sky-blue emission of moderate intensity in pure THF. The emission was redshifted to blue with increase in water concentration. With the progressively blue-shifted PL spectra, the moderate emission intensity was regained and sustained until the water concentration was increased further to 70%. The emission intensity increased dramatically when the water concentration was above 80% due to aggregates formation. The two enantiomers showed nearly mirror-image CPL signals in

toluene and THF/water (water concentration = 99%) mixed solvent. The values of the PL dissymmetry factor $|g_{\text{PL}}|$ were around 10^{-4} . The CP-OLEDs were fabricated by using the developed molecule ((*S*)-NPE-AcDPS) as chiral emitter and observed maximum EQE of 18.5%.

Jiang's group in 2022 described the synthesis of π -stacked 9,10-dihydroacridine functionalized spiro-fluorene building block (SDMAC) (**Figure 24**).^[66] By combining the benefits of 9,10-dihydroacridine derivative and spiro-fluorene functionalities, SDMAC exhibited strong molecular rigidity, intramolecular through-space charge transfer, steric hindrance and multi-stimulus response. Triazine derivative was used as an acceptor to the fluorene's C1 site to form SDMAC, which provided through-space charge transfer and chiral characteristics to the SDMAC. The lowest triplet and singlet states was measured from the phosphorescence and fluorescence spectra and calculated the ΔE_{ST} to 0.034 eV. The low value of ΔE_{ST} suggested the effective RISC mechanism which was essential for TADF. Their transient decay curve at 300 K was separated into the delayed emission component, 4.17 microseconds, and the prompt emission decay curve, 63.8 ns. The aggregation-induced emission enhancement characteristic of the molecule was observed with the help of THF: water experiment. The emission maxima of the compound red-shifted from 507 nm to 553 nm as the water concentration was increased from 0% to 60%. The emission peak of SDMAC showed AIE based on the restriction of intramolecular rotation and emission maxima blue shifted to 497 nm when water concentration was increased further from 60% to 90%. For every molecule in the ground state, the HOMO and LUMO were mostly found on the 9,10-dihydroacridine and triazine units, respectively. The DFT calculations were carried out for the dimer and the HOMO distribution was found in the donor region and the LUMO overlap was between two acceptors for the SDMAC dimer which suggested that the dimer might carry through-space charge transfer. The values of luminescence dissymmetry factor, $|g_{\text{lum}}|$, of the SDMAC enantiomers approached up to 1.39×10^{-3} . The CP-OLEDs were fabricated by using the developed compound as an emitter and observed and EQE of 28.4% and the CP-EL signals with enantiomeric EL dissymmetry factor $|g_{\text{EL}}|$ of up to 9.80×10^{-4} were achieved.

A spiro-type TADF material having central chirality was reported in 2022, which could completely harvest both S_1 and T_1 excitons.^[67] The chiral TADF enantiomers synthesized by them ((*R/S*)-SPOCN) functioned as yellow emitters and displayed through-bond charge transfer (**Figure 24**). A nucleophilic substitution method was used to develop the (*R/S*)-SPOCN

isomers from the 4,5-difluorophthalonitrile, phenoxazine and (*R/S*)-spirobiindane-7,7'-diol. Spirobiindane-7,7'-diol was the source of the chirality of this developed molecule. The steric crowding at phenoxazine, caused by the ortho-substituent on the indane unit, resulted in high torsional angle between phenoxazine and linked benzene ring. This high torsional angle was essential for the separation of the HOMO and the LUMO. The designed molecule had two cyano groups acting as acceptors and a phenoxazine unit acting as the donor. This type of molecular architecture narrowed the band gap and produced yellow emission. It was observed that the PL spectra in different solvents displayed a clear red shift as solvent polarity was increased while no change in the absorption spectra. A through-bond charge transfer feature in the excited state was demonstrated by the shift in the Stokes shifts. The ΔE_{ST} of 0.03 eV was measured with the help of phosphorescence and fluorescence spectra at 77 K which ensured quick RISC. Further, the temperature-dependent transient PL studies found that in a nitrogen-saturated toluene solution, a microsecond-scale fluorescence lifetime was observed, which got quenched once air bubbled through the solution. This finding demonstrated that the T_1 state was involved in the emission process. A symmetrical CPL spectrum of the enantiomers at 583 nm and the PL dissymmetry factors, g_{PL} , were found to be $+1.7 \times 10^{-3}/1.6 \times 10^{-3}$ (in toluene). It also showed symmetrical CD and CPL signals in the film state, and the g_{PL} factors were $+2.3 \times 10^{-3}/-2.6 \times 10^{-3}$. The fabricated CP-OLED device showed maximum EQE of up to 15.8% (*S*-isomer) and the signal of CP-EL with a dissymmetry factor, $|g_{EL}|$, was of 1.7×10^{-3} . The best of fabricated CP-WOLEDs possessed CIE of (0.35, 0.46) and maximum EQE of up to 21.6% with maximum brightness of 15700 cd/m². The signal of CP-EL with a dissymmetry factor, $|g_{EL}|$, was of 3.0×10^{-3} .

A B/N-doped skeleton with a rigid acridan based molecular framework having asymmetric carbon was used to develop enantiomers, (*R*) and (*S*)-BN-MeIAc (**Figure 24**).^[68] A two-step process utilizing organolithium-mediated bora-Friedel-Crafts reaction and palladium-catalyzed Buchwald-Hartwig coupling was used to produce this molecule. The synthesized molecule exhibited TADF, CPL and narrowband emission along with high triplet energy and rigid structure. The sp^3 hybridized carbon in the designed molecule provided great conformational stability and acted as the stable stereocenter to induce CPL characteristics. The MeIAc fluorenyl unit lengthened the π -conjugation of the molecule which improved the oscillator strength and horizontal anisotropic orientation. With a decomposition temperature of 430 °C, the emitter demonstrated high thermal and morphological stability. DFT calculations predicted separation between the HOMO and the LUMO for the ground state. The theoretical

calculations also predicted a substantial oscillator strength of 0.3593 for the S_1 to S_0 transition due to partial HOMO/LUMO overlap which indicated efficient radiative decay. The natural transition orbitals calculations anticipated the hole/particle distributions of the S_1 and T_1 states were almost similar and delocalized over the whole molecule. The natural transition orbitals of the T_2 state were mostly localized on the fluorenyl unit. The low-temperature fluorescence and phosphorescence spectra depicted the ΔE_{ST} value as 0.11 eV which was beneficial for the efficient RISC process. The transient PL curve showed a two components decay. The delayed component depicted an increase with the enhancement in the temperature which might be attributed to TADF. The lifetimes were measured at 300 K to be 28.1 microseconds for delayed fluorescence and 8.2 ns for prompt fluorescence. The developed enantiomers depicted the mirror-image CPL spectra with the PL dissymmetry factors, g_{PL} , for were determined to be $+2.5 \times 10^{-4}$ (*(R)*-BN-MeIAc) and -2.5×10^{-4} (*(S)*-BNMeIAc) in solutions. The CP-OLEDs were fabricated and separate CPEL signals with g_{EL} values of $+2.7 \times 10^{-4}$ for the *R*-isomer and -2.9×10^{-4} for the *S*-isomer were observed. The EQE_{max} values of 37.2% (*R*) and 36.1% (*S*) indicated the excellent efficiency of the CP-OLEDs based on chiral emitters.

Three pairs of new spiro-based TADF chiral isomers, SCN, SPHCN, and SCFPY, with comparable molecular framework were reported in 2022 (**Figure 24**).^[69] The phenoxazine donors in all three pairings of these enantiomers were the identical, but their acceptors were different. The DFT calculations depicted that the HOMOs and LUMOs were well separated by the spiro-structure for all three TADF molecules, with HOMOs situated on the donor moieties and LUMOs on the acceptor units. The theoretical calculations displayed that the HOMOs were distributed evenly on the phenoxazine and linked benzene rings for the three pairs of TADF molecule. However, LUMOs were drawn to one side of the thioxanthenedioxide unit. The benzonitrile moiety was containing the LUMOs for SCN, but the extended acceptor components of SCFPY and SPHCN possessed more delocalized LUMOs. The observed twisted geometries and electron cloud distribution might minimize the gap between HOMOs and LUMOs and encouraged their spatial interactions promoting through-space charge transfer. The fluorescence quantum yield and found SPHCN, PLQY of 67.4%, whereas SCN and SCFPY displayed high PLQYs up to almost 89%. A long-delayed fluorescence lifetime was observed for SPHCN (14.6 microseconds). On the other hand, SCN and SCFPY reported short-delayed fluorescence lifetime of 2.1 and 1.6 microseconds, respectively. The structural differentiation of acceptor units might be the reason for the variances between delayed lifetime duration and PLQY. The ΔE_{ST} values was determined with the help of phosphorescence and

fluorescence spectra at 77 K, which was found to be 0.01 eV (SCN), 0.16 eV (SPHCN), and 0.04 eV (SCFPY). These values predicted rapid RISC for an efficient TADF process. The three molecules were found to have a microsecond-scale delayed lifetime when these were in nitrogen-saturated toluene solutions that could be quenched by air. The higher slopes with rising temperatures from the temperature-dependent transient PL studies were observed which indicated a higher fraction of delayed components. In case of SCN molecule with a localized cyano group, $|g_{\text{PL}}|$ was about 1.4×10^{-3} . In case of SPHCN with benzonitrile unit, $|g_{\text{PL}}|$ was approximately 3.6×10^{-3} , and when 2-(trifluoromethyl)pyridine was utilized as a prolonged acceptor unit for SCFPY, $|g_{\text{PL}}|$ was approximately 3.5×10^{-3} . The CP-OLEDs were fabricated and an EQE_{max} of 15.4% for SPHCN, 23.3% for SCFPY and 23.0% for SCN based emitter were observed. Furthermore, with $|g_{\text{EL}}|$ factors of 1.8×10^{-3} ((*R/S*)-SCN), 3.6×10^{-3} ((*R/S*)-SPHCN), and 3.7×10^{-3} ((*R/S*)-SCFPY), the CP-OLEDs also exhibited clear CP-EL.

Luo et al. in 2023 combined sulfur-substituted spirofluorene and boron-nitrogen skeletons in Spiro-BNCz (**Figure 25a**).^[70] The synthesized chiral molecule depicted green emission with CIE coordinates (0.26, 0.69). Spiro-BNCz had a high spin-orbit coupling constant of 0.36 cm^{-1} , reverse ISC rate of $2.8 \times 10^6 \text{ s}^{-1}$, and quantum yield of 92% in the doped film. The separated (*R/S*)-Spiro-BNCz enantiomers exhibited mirror-imaged CPL spectra with a $|g_{\text{PL}}|$ of 1.3×10^{-3} . The OLED based on Spiro-BNCz obtained an EQE_{max} of 32.3%. The CP-OLEDs based on (*R/S*)-Spiro-BNCz enantiomers showed symmetric CPEL spectra with an estimated $|g_{\text{EL}}|$ factor of around 10^{-3} .

Ren et al. in 2024 built a self-powered CPL photodetector by employing a sequence of chiral polyacetylenes having TADF properties ((*R*)-PADB₃Cz₇, (*R*)-PADB₁Cz₉, and (*R*)-PADB_{0.5}Cz_{9.5}) (**Figure 25b**).^[71] TADF polymers having a small energy difference between singlet and triplet states (<13 meV) promoted up-conversion from triplet to singlet states. This up-conversion made them ideal for recycling ISC and RISC processes involving singlet and triplet excitons. The authors established a new spin photovoltaic effect that efficiently separated singlet and triplet excitons. This allowed for CPL detection without external bias. The detectors had an extraordinary CPL detection responsivity of 0.18 A W^{-1} and a high dissymmetry factor of 0.08. The chiral side chains caused helical conformations in the polyacetylene backbones, leading to a high dissymmetry factor. They also observed that hydrogen bonding between amide groups enhanced the stereoregularity of polyacetylene backbones, facilitating carrier movement.

Xu et al. designed and synthesized a pair of AIE-active CP-TADF enantiomers with strong mechanoluminescence and mechanofluorochromism properties.^[72] They used phthalimide as an electron acceptor as its derivatives typically form polar and non-centrosymmetric molecular configurations in the crystalline state. Carbazole was chosen as an electron donor and bonded to the third position of phthalimide, forming a D-A molecular framework. The N atom of phthalimide was linked to the 1-position of 1,2,3,4-tetrahydronaphthalene to activate its chirality. The resultant enantiomers, (*R*)-CzTA and (*S*)-CzTA (**Figure 25c**), exhibited strong AIE and CP-TADF characteristics due to their extremely twisted structures. The CPL g_{lum} values in toluene solutions are 0.84×10^{-3} (*R*) and -1.03×10^{-3} (*S*), respectively. When subjected to mechanical strain, crystals of (*S*)-CzTA and (*R*)-CzTA produced intense blue TADF and mechanoluminescence. Their huge dipole moments, development of polar crystal formations with noncentrosymmetric configurations, and strong intermolecular interactions are thought to contribute to their mechanoluminescence activity. Grinding (*S*)-CzTA and (*R*)-CzTA yielded green powders with substantial TADF characteristics.

Using heteroatom-based core chirality might expand the design possibilities for high-performance CP-TADF emitters. Cao et al. in 2023 described the example of CP-TADF materials with heteroatomic stereocenters. Sulfoximine-based acceptor and acaridan-based donor were used to build chiral enantiomers (*R/S*)-FAC-SIC (**Figure 25a**).^[73] This type of framework was substantially twisted. The asymmetric sulfur atom acted as a chiral source, producing separate CD and CPL signals. Enantiomers emit TADF with almost unit quantum yield due to their close-lying excited-state energy levels and numerous intramolecular interactions in the film state. The OLED device demonstrated exceptional performance, with a EQEmax of 28.5%.

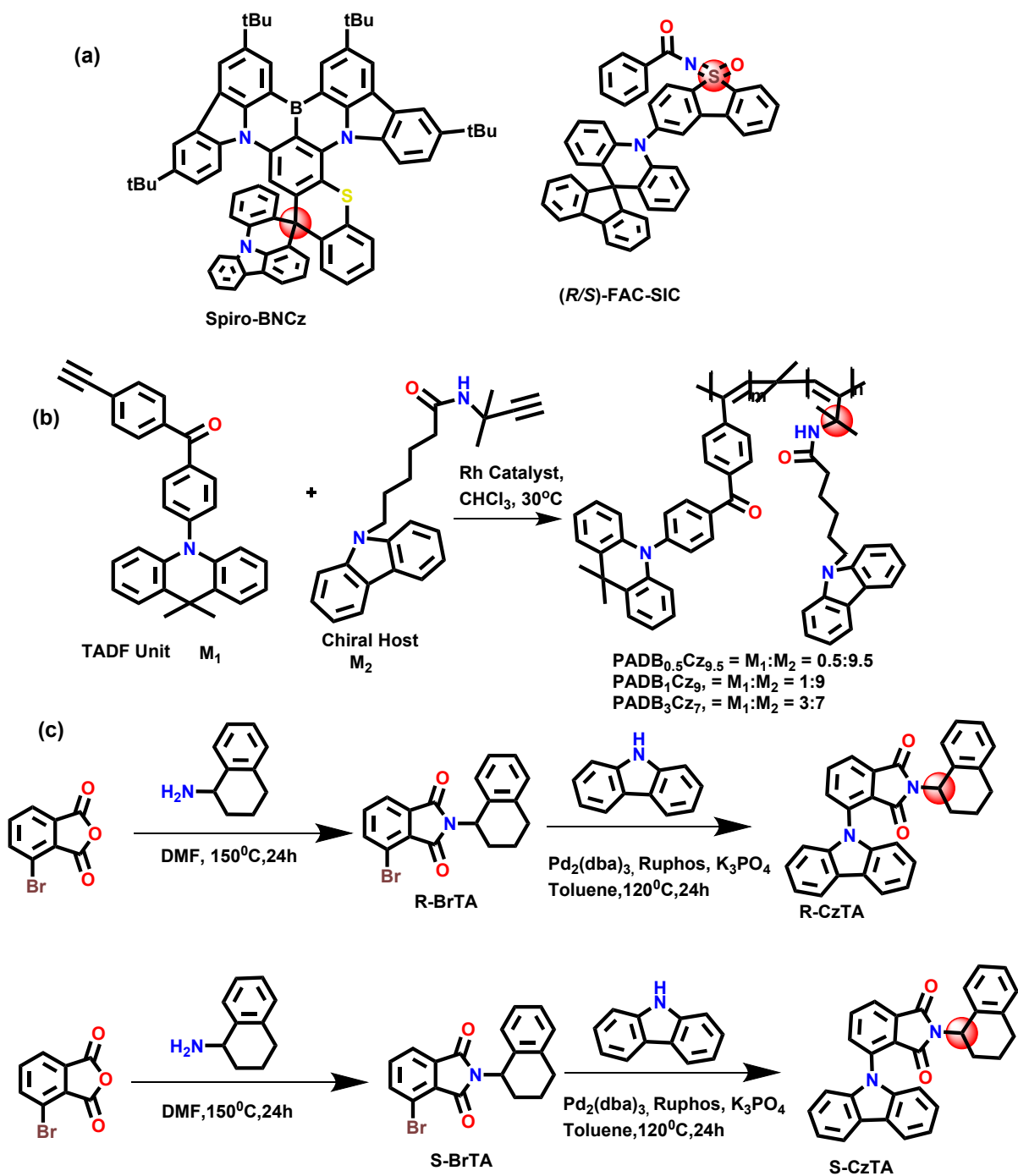
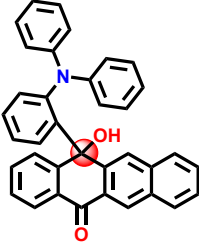
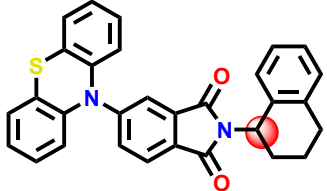
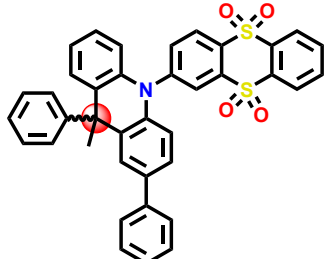
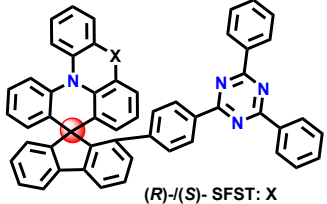
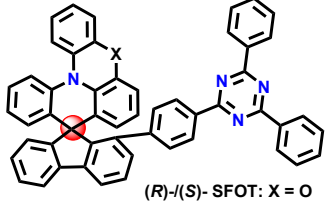
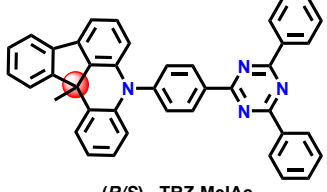
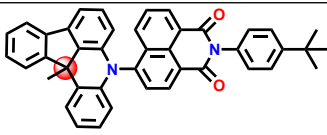
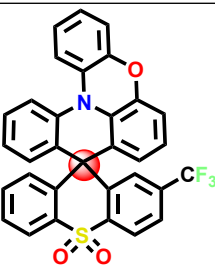
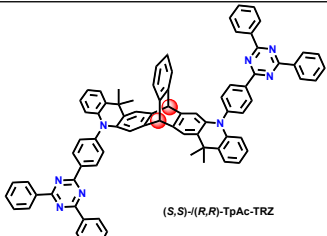
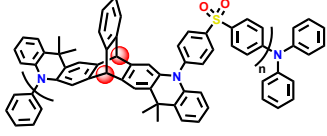
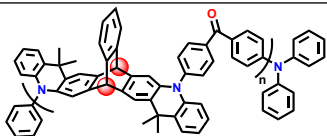
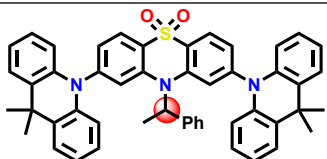
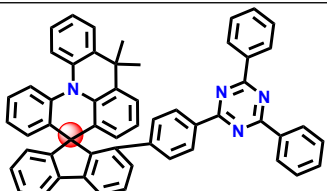
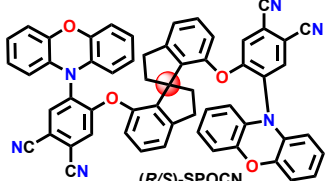
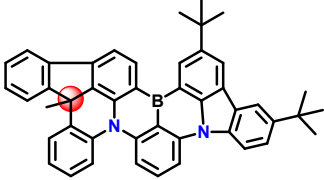
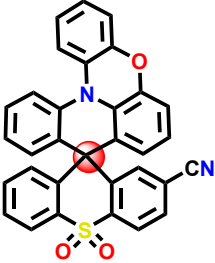
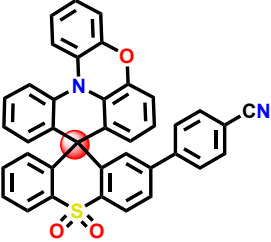
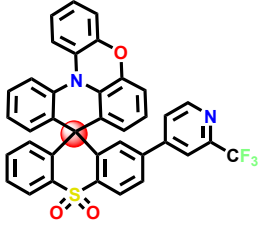
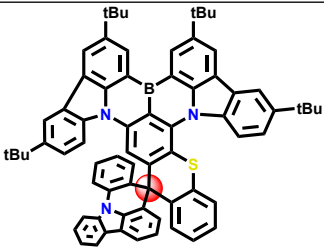
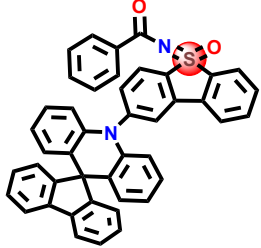


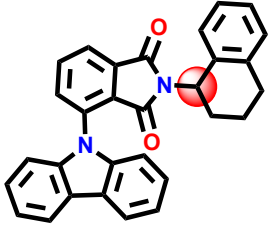
Figure 25. Chemical structures of some central chirality based TADF molecules.^[70-73]

Table 6. Chiroptical properties of central chirality-based chiral TADF molecules.

Compound	EQE _{max} (%) (Isomer used as emitter)	Luminescence dissymmetry factor	Electroluminescence dissymmetry factor	Reference
 (R/S)-DPHN	-	$ g_{PL} = 1.1 \times 10^{-3}$	-	[57]
 (R/S)-ImNT	-	$g_{lum} = 3.42 \times 10^{-3} / -3.65 \times 10^{-3}$ (R/S)	-	[58]
 (R)-(S)-TTR-PMAC.	-	-	-	[59]
 (R)-(S)-SFST: X = S	12.5	$g_{lum} = -4.0 \times 10^{-3} / 3.4 \times 10^{-3}$ (R/S)	$g_{EL} = 1.30 \times 10^{-3}$ (S)	[60]
 (R)-(S)-SFOT: X = O	23.1	$g_{lum} = -2.0 \times 10^{-3} / 2.2 \times 10^{-3}$ (R/S)	$g_{EL} = 1.0 \times 10^{-3}$ (S)	[60]
 (R/S) - TRZ-MeIAc	20.3 (R)	$g_{PL} = 5.9 \times 10^{-4} / -5.9 \times 10^{-4}$ (R/S)	$g_{EL} = 6.4 \times 10^{-4} / -7.3 \times 10^{-4}$ (R/S)	[61]

 <p>(R/S)-NID-MelAc.</p>	19.0 (R)	$g_{PL} = 2.0 \times 10^{-3} / -2.0 \times 10^{-3}$ (R/S)	$g_{EL} = 2.0 \times 10^{-3} / -2.4 \times 10^{-3}$ (R/S)	[61]
 <p>(R/S)-OSFSO</p>	20 (S)	$g_{PL} = -1.6 \times 10^{-3} / 1.4 \times 10^{-3}$ (R/S)	$g_{EL} = -3.0 \times 10^{-3} / 3.1 \times 10^{-3}$ (R/S)	[62]
 <p>(S,S)-(R,R)-TpAc-TRZ</p>	25.5 (S)	$g_{PL} = -1.8 \times 10^{-3} / 1.9 \times 10^{-3}$ (R/S) (Neat Film)	$g_{EL} = -2.0 \times 10^{-3} / 1.5 \times 10^{-3}$ (R/S)	[63]
 <p>(R,R)-(S,S)-pTpAcDPS</p>	13.9 (S)	$g_{PL} = -1.4 \times 10^{-3} / 1.3 \times 10^{-3}$ (R/S)	$g_{EL} = -1.1 \times 10^{-3} / 1.4 \times 10^{-3}$ (R/S)	[64]
 <p>(R,R)-(S,S)-pTpAcBP</p>	20.2 (S)	$g_{PL} = -1.0 \times 10^{-3} / 1.3 \times 10^{-3}$ (R/S)	$g_{EL} = -1.0 \times 10^{-3} / 1.6 \times 10^{-3}$ (R/S)	[64]
 <p>(R/S)-NPE-AcDPS</p>	18.5 (S)	$ g_{PL} = 10^{-4}$	-	[65]
 <p>(R)-(-)-SDMAC</p>	28.4	$g_{lum} = -1.19 \times 10^{-3} / 1.39 \times 10^{-3}$ (R/S)	$g_{EL} = -8.43 \times 10^{-4} / 9.84 \times 10^{-4}$ (R/S)	[66]
 <p>(R/S)-SPOCN</p>	15.8 (S)	$g_{PL} = 2.3 \times 10^{-3} / -2.6 \times 10^{-3}$ (R/S) (Thin films)	$g_{EL} = 1.7 \times 10^{-3} / -1.7 \times 10^{-3}$ (R/S)	[67]

 <p>(R/S)-BN-MeAc</p>	37.2 (R) 36.1 (S)	$g_{PL} = 2.5 \times 10^{-4} / -2.5 \times 10^{-4}$ (R/S) (In Solution)	$g_{EL} = 2.7 \times 10^{-4} / -2.9 \times 10^{-4}$ (R/S)	[68]
 <p>(R/S)-SCN</p>	23 (Racemic)	$ g_{PL} = 1.4 \times 10^{-3}$ (In Toluene)	$ g_{EL} = 1.8 \times 10^{-3}$	[69]
 <p>(R/S)-SPHCN</p>	15.4 (Racemic)	$ g_{PL} = 3.6 \times 10^{-3}$ (In Toluene)	$ g_{EL} = 3.6 \times 10^{-3}$	[69]
 <p>(R/S)-SCFPY</p>	23.3 (Racemic)	$ g_{PL} = 3.5 \times 10^{-3}$ (In Toluene)	$ g_{EL} = 3.7 \times 10^{-3}$	[69]
 <p>Spiro-BNCz</p>	34.2	$ g_{PL} = 1.3 \times 10^{-3}$	$ g_{EL} = \sim 10^{-3}$	[70]
 <p>(R/S)-FAC-SIC</p>	28.5 (R)	$g_{PL} = 2.4 \times 10^{-4} / -2.0 \times 10^{-4}$ (R/S)	-	[73]

 <p>(S)-CzTA</p>	-	$g_{lum} = 0.84 \times 10^{-3} / -1.03 \times 10^{-3}$ (R/S)	-	[72]
---	---	---	---	------

2.7. Paracyclophane based chiral TADF molecules

The design and synthesis of two [2.2]paracyclophane derivatives having planar chirality was reported by Zhao's group in 2018.^[74] The developed compounds, namely g-BNMe₂-Cp and m-BNMe₂-Cp, possessed electron-accepting BMes₂ and the electron-donating NMe₂ at the pseudo-gem and pseudo-meta locations, respectively (**Figure 26**). The nitrogen centre in g-BNMe₂-Cp is more coplanar with the amino-bonded benzene ring than it is in m-BNMe₂-Cp, which is a significant structural difference between the two molecules. The single crystals of the synthesized materials which depicted that the centroid-centroid distances of [2.2]paracyclophane's two deck benzene rings were 3.01 Å for m-BNMe₂-Cp and 3.08 Å for g-BNMe₂-Cp. These distances allowed the through-space charge-transfer transitions. The LUMO was mostly concentrated on the dimesitylborylphenyl, whereas the HOMO was primarily localized on the dimethylaminophenyl, the large separation HOMO-LUMO is beneficial for the TADF properties of the molecule. Both [2.2]-paracyclophanes based on triarylborane had oxygen sensitive fluorescence efficiency. For g-BNMe₂-Cp and m-BNMe₂-Cp in oxygen-bubbled toluene, the fluorescence QYs fell to 0.068 and 0.049, respectively. The lifetime measurement for both compounds depicted prompt and delayed fluorescence lifetimes confirming their TADF properties. Due to its intense fluorescence spectra, only g-BNMe₂-Cp was selected for chiroptical characteristics studies. The *R_p* enantiomer emits a minor positive signal at 393 nm and a strong positive signal at 313 nm. The g_{abs} at the longest wavelength (393 nm) was found to be $+1.44 \times 10^{-3}$. The CPL spectra showed mirror-image spectra with $|g_{lum}|$ values around 4.24×10^{-3} . **Table 7** summarizes the different chiroptical properties of paracyclophane-based chiral TADF molecules.

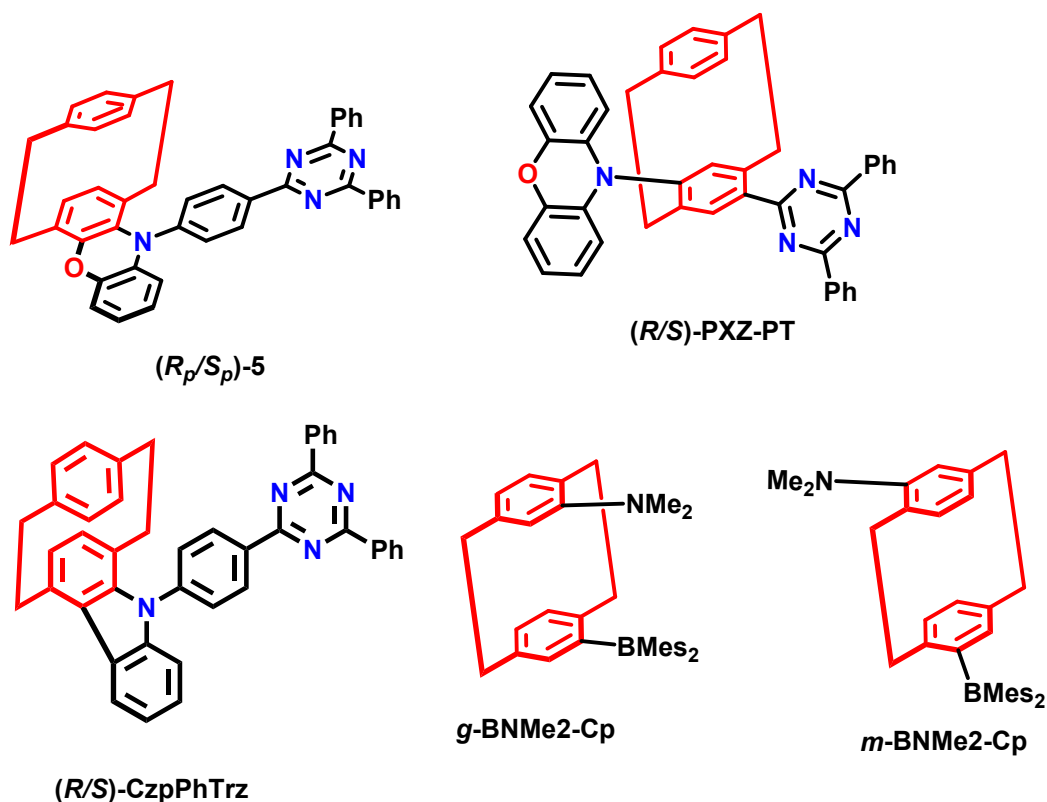


Figure 26. Paracyclophane based chiral TADF molecules^[74-77].

A planar chiral [2.2]paracyclophane-based TADF-active molecule with CP emission (*R_p*-5/*S_p*-5, **Figure 26**) was reported in 2021.^[75] Phenoxazinephane and trizine were used as a donor and as an acceptor, respectively, for the design of TADF molecule. DFT calculations were performed to study the population of the frontier molecular orbitals. It was found that the LUMO orbital was mostly located on the trizine and bridging phenyl ring while the HOMO orbital was focused on the phenoxazinephane moiety. The paracyclophane separated the HOMO/LUMO spatially by inducing a torsion between the plane of paracyclophane and the phenyl bridge. This torsion angle was responsible for minimizing the ΔE_{ST} and speeded up the RISC process. The gap between first singlet and triplet states of the molecules was as low as 0.03 eV. Thus, the DFT calculations revealed that the rate of up-conversion from the first triplet state to the first singlet state was boosted by the higher torsion of 76.9°. The time-resolved PL experiment was performed for non-doped and doped films in a nitrogen environment, which revealed delayed lifetimes of 12.1 and 6.7 microseconds, respectively. The enantiomer spectra were seen with mirror symmetry in neat films and toluene. Short-wavelength areas exhibited substantial Cotton effects, which might be attributed to ground-state absorption. It is also possible to trace

the very small Cotton effects in the 400 nm range to ICT. A yellow CP-OLEDs based on the developed enantiomer as the emitter exhibited CP-EL signal with g_{EL} factor up to 4.6×10^{-3} and EQE_{max} up to 7.8%.

Colman's group in 2019, used the carbazolophane as donor unit and triazine as an acceptor unit to develop a planar chiral TADF emitter, CzpPhTrz (**Figure 26**).^[76] The greater steric hinderance caused by the donor unit induces increased torsion between the carbazole and the aryl bridge. This increased torsion reduced the ΔE_{ST} which further enhanced the RISC property in the enantiomer. Also, the closely placed benzene and carbazole units of the paracyclophane exhibited through-space π - π interactions which enhanced the HOMO orbital's spatial occupancy. DFT calculations of the developed material revealed that the LUMO was populated over triazine and the HOMO was over carbazole with significant extension on paracyclophane. This molecule had a 70% quantum yield in degassed solution and emitted in sky blue region in toluene. The ΔE_{ST} was measured at low temperatures in doped films which came around 0.16 eV. The chiroptical properties of the developed (*R*, *S*)-CzpPhTrz in toluene displayed the mirror image spectra (**Figure 27**). The CPL dissymmetry factor for the R_p and S_p enantiomers were -1.2×10^{-3} and 1.3×10^{-3} , respectively. The CP-OLEDs were fabricated by using these enantiomers as emitters and associated EL was similar to PL with maximum EQE of 17%.

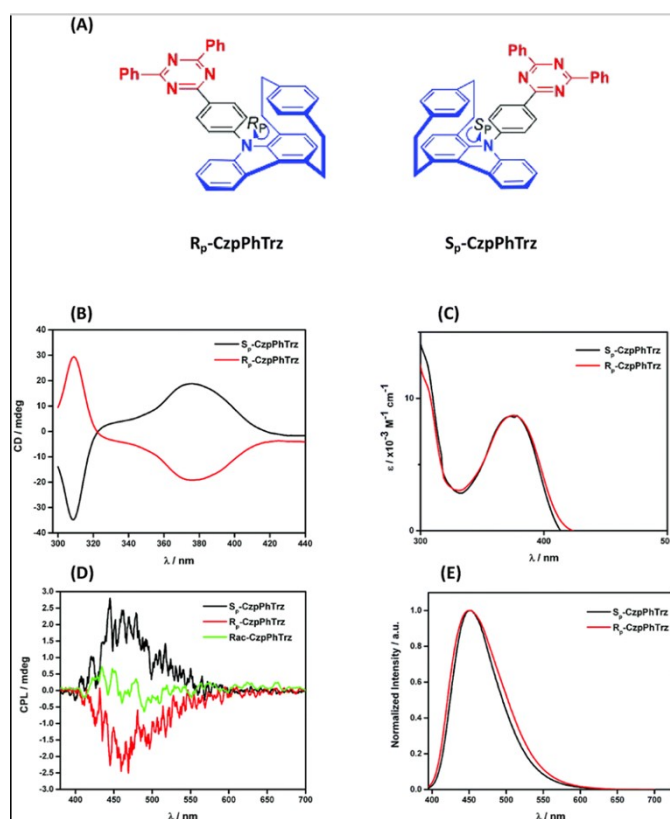


Figure 27. (A) Chemical structures (B) CD (C) UV-vis (D) CPL and (E) PL spectra of (*R_p*)-CzpPhTrz and (*S_p*)-CzpPhTrz in degassed PhMe ($\lambda_{exc} = 375$ nm).^[76]

Two novel enantiomers (*R/S*-PXZ-PT) having donor-chiral acceptor type molecular framework with TADF characteristics were synthesized in 2021 (**Figure 26**).^[77] The phenoxazine was used as donor, trizine as acceptor and paracyclophane as chirality inducer. This type of architecture could entirely suppress the racemization of the planar chirality which encouraged its use in the vacuum deposition CP-OLEDs. The HOMO/LUMO distribution was analysed with the help of DFT studies and it was found that the single crystals of *S*-PXZ-PT and their modelled ground state structures were in agreement. It was found that the emitter displayed significant dihedral angles between the donor and the acceptor in optimized geometry. The HOMO was exclusively localized on donor whereas the LUMO was mostly focused on the acceptor. There was a little overlap of HOMO and LUMO orbitals on the paracyclophane unit. It was found that the radiative decay of the first singlet state got benefited from the enhanced HOMO and LUMO overlaps. The rac-PXZ-PT was used for investigating the TADF characteristics and it was found that in inert environment, the emission intensity of rac-PXZ-PT in diluted toluene depicted an increase. This demonstrated that oxygen might hinder the luminescence process which further supported the potential TADF luminescence mechanism. The lifetime experiments of the rac-PXZ-PT doped film in CBP depicted a clear delayed fluorescence resulting from its small ΔE_{ST} value of 0.19 eV. The transient decay PL experiments of doped films depicted, both, the short lifetime signals with nanosecond lifetimes (15 ns) and the long lifetime signals (75 microseconds) with microsecond lifetimes (**Figure 28**). The enantiomeric emitters displayed excellent mirror-image CD spectra in diluted toluene solution (**Figure 28**). The CD signal was found in the 350–500 nm absorption regions, where the ICT absorption was thought to be responsible for the cotton effect. Moreover, at around 450–750 nm emission wavelength, the CPL spectra of the two chiral enantiomers showed a perfect mirror-image correspondence. It was found that the chiral moiety and luminescent moiety were precisely integrated in their design which provided high CPL activity with $|g_{lum}|$ of 1.9×10^{-3} . The CP-OLEDs were fabricated using these enantiomers as emitters. It was found that the enantiomer-based OLEDs displayed mirror-image CPEL signals with EL dissymmetry factors g_{EL} of $+1.5 \times 10^{-3}/-1.3 \times 10^{-3}$ and yellow-colored emission with a EQE_{max} of 20.1%.

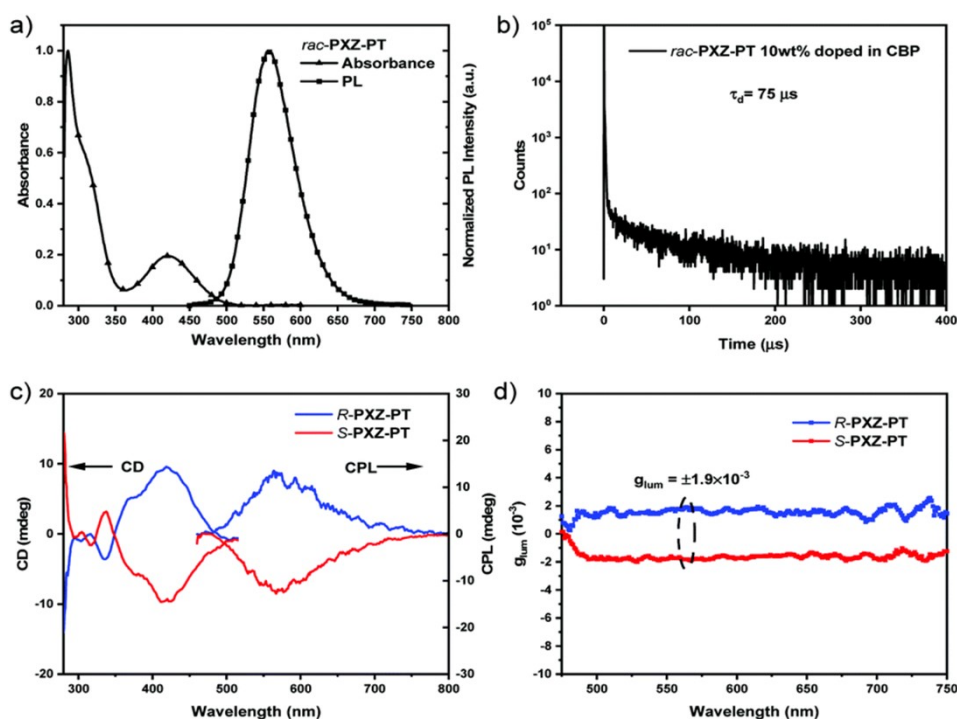


Figure 28. (a) Normalized UV-vis absorption and PL spectra in toluene (10^{-5} M) of *rac*-PXZ-PT. (b) Transient decay curve of *rac*-PXZ-PT in 10 wt% CBP film ($\lambda_{exc} = 377.3$ nm). (c) The CD and CPL spectra of *R/S*-PXZ-PT in toluene ($\lambda_{exc} = 390$ nm). (d) The g_{lum} wavelength characteristics of *R/S*-PXZ-PT.^[77]

Brase et al. in 2024 compared the photophysical and optoelectronic characteristics of the cyclophane emitters (1,7)tBuCzpPhTrz with its isomer (1,4)tBuCzpPhTrz (**Figure 29**).^[78] The (1,7) isomer of carbazophane-triazine molecule is a planar chiral TADF emitter that deviates from the paracyclophane scaffold. They could synthesize it through intra-molecular charge transfer process. The attached carbazole in (1,7) isomer underwent a significant geometric shift, decreasing donor strength. However, stiffness and steric bulk remained intact. They could observe that the full-width half maxima of the photoluminescence spectra in the toluene of the (1,7) isomer were 34% lower and 20 nm bluer than that of the (1,4) isomer. Their doped films have high quantum yields of 91 and 81%, respectively. These developed enantiomers could show mirror-image CPL behavior, with a $|g_{PL}|$ of 5×10^{-4} . They also fabricated the blue OLEDs with (1,4) and (1,7) isomers which showed similar EQEmax values of 19 and 18%, respectively. The efficiency roll-off at high brightness (100 to 1000 cd/m^2) was reduced from 73% to 57% for OLEDs with (1,4) isomer and from 77% to 35% for those with (1,7) isomer.

Zheng et al. used di[2.2]paracyclophane amine derivatives as electron donors and triazine derivatives as an electron acceptor to synthesize four TADF molecules.^[79] The C₂ symmetric molecules (DpCpCz-Trz and DpCpN-Trz) (**Figure 29**), with a chair-like planar chiral di[2.2]paracyclophane moiety, are optically pure enantiomers. B-DpCpN-Trz and B-DpCpCz-Trz have a bridge-like di[2.2]paracyclophane structure and are meso-compounds that lack optical activity. All emitters have strong quantum efficiency (up to 93%) with blue emissions at 464-485 nm. These enantiomers had symmetric CPPL spectra with $|g_{PL}|$ ranging from 3.8×10^{-4} to 6.7×10^{-4} in toluene and films. Mirror image CPL spectra of enantiomers in toluene and doped films revealed positive *S*-configuration and negative *R*-configuration signals. In toluene, the g_{PL} values were 6.4×10^{-4} and -4.5×10^{-4} ((*R/S*)-C-DpCpN-Trz), 5.9×10^{-4} and -4.0×10^{-4} ((*R/S*)-C-DpCpCz-Trz), respectively. They fabricated the OLEDs using these compounds as dopants and could attain up to 19.5% EQE (B-DpCpCz-Trz). The CP-OLEDs with these developed emitters exhibited $|g_{EL}|$ factors of up to 7.6×10^{-4} .

Zheng et al. developed two high-performance CP-MR-TADF materials for CP-OLEDs using planar chiral Czp units.^[80] The designed framework included planar chirality and a rigid structure with carbazole, phenoxazine, and other groups arranged in a specific pattern. A boron atom on the phenyl group resulted in narrow emission and a small band gap between S₁ and T₁. The (*R/S*)-Czp-tBuCzB and (*R/S*)-Czp-POAB (**Figure 29**) emitted at 478 and 497 nm, with quantum yields of 98% and 93% in doped films, respectively. They fabricated the CP-OLEDs using these sky-blue enantiomers and reached a high EQEmax of 32.1% and only 3.7% efficiency roll-off at 1000 cd/m² brightness. The developed enantiomers exhibited almost symmetric CPL signals in solutions, doped films, and devices. The g_{EL} factors in CP-OLEDs were $1.54 \times 10^{-3} / -1.48 \times 10^{-3}$ ((*R/S*)-Czp-tBuCzB), $1.30 \times 10^{-3} / -1.25 \times 10^{-3}$ ((*R/S*)-Czp-POAB)).

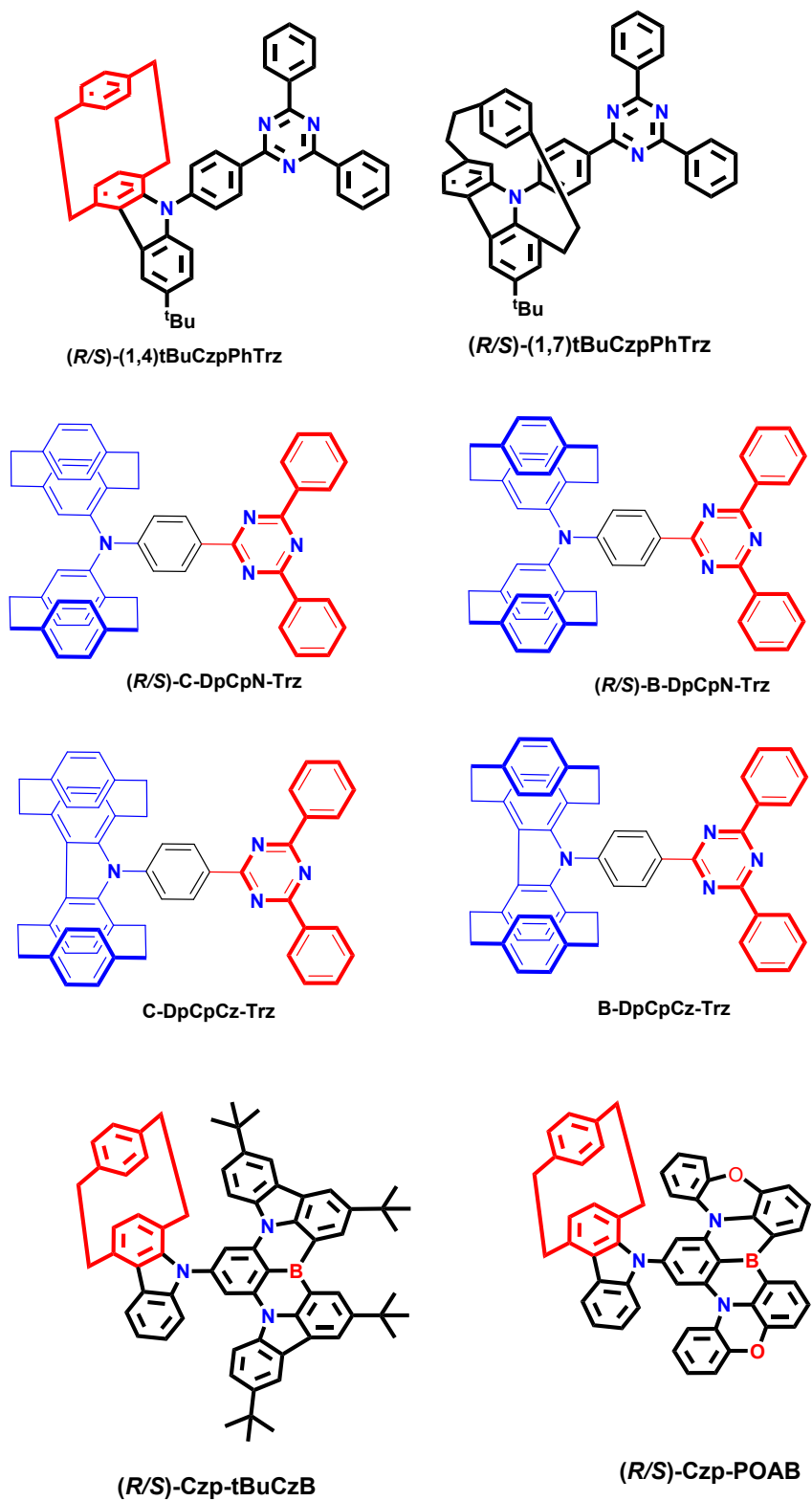
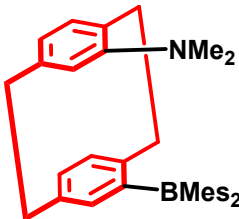
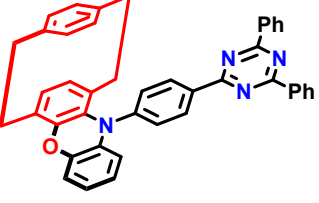
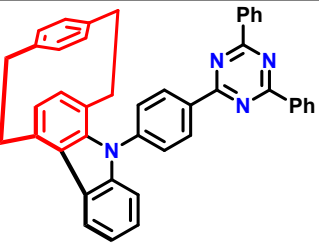
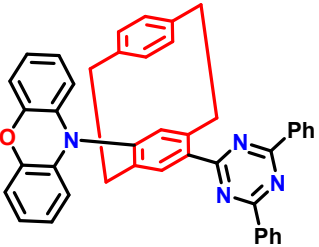
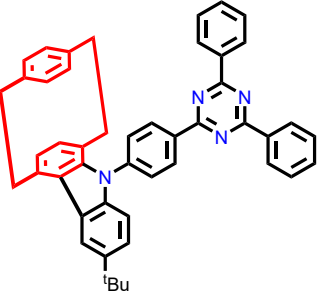
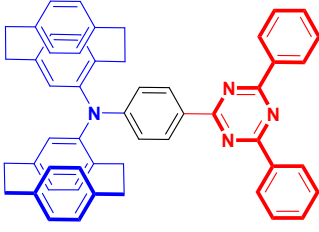
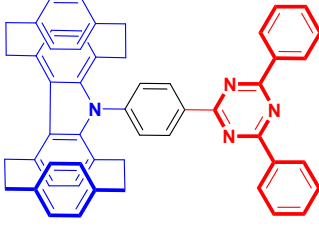
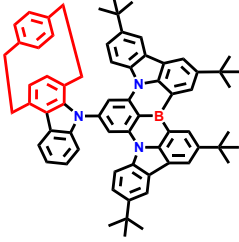
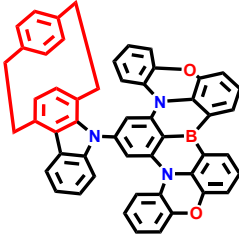


Figure. 29. Chemical structures of some planar chirality based TADF molecules.^[78-80]

Table 7. Chiroptical properties of paracyclophane-based chiral TADF molecules.

Compound	EQE_{max} (%) (Isomer used as emitter)	Luminescence dissymmetry factor	Electroluminescence dissymmetry factor	Reference
 g-BNMe2-Cp	-	$ g_{\text{lum}} = 4.24 \times 10^{-3}$	-	[74]
 (<i>R_p/S_p</i>)-5	7.8 (<i>S</i>)	$g_{\text{lum}} = -2.3 \times 10^{-3} / 2.7 \times 10^{-3}$ (<i>R/S</i>)	$g_{\text{EL}} = -4.6 \times 10^{-3} / 4.3 \times 10^{-3}$ (<i>R/S</i>)	[75]
 (<i>R/S</i>)-CzpPhTrz	17.0 (rac)	$g_{\text{lum}} = -1.2 \times 10^{-3} / 1.3 \times 10^{-3}$ (<i>R/S</i>)	-	[76]
 (<i>R/S</i>)-PXZ-PT	20.1 (<i>R</i>)	$ g_{\text{lum}} = 1.9 \times 10^{-3}$	$g_{\text{EL}} = 1.5 \times 10^{-3} / -1.3 \times 10^{-3}$ (<i>R/S</i>)	[77]
 (<i>R/S</i>)-(1,4)tBuCzpPhTrz	19	$ g_{\text{PL}} = 5 \times 10^{-4}$	-	[78]

 <p>(R/S)-C-DpCpN-Trz</p>	11.3	$g_{PL} = 6.4 \times 10^{-4} / -4.5 \times 10^{-4}$ (S/R)	$g_{EL} = 7.6 \times 10^{-4} / -6.9 \times 10^{-4}$ (S/R)	[79]
 <p>(R/S)-C-DpCpCz-Trz</p>	10	$g_{PL} = 5.9 \times 10^{-4} / -4.0 \times 10^{-4}$ (S/R)	$g_{EL} = 5.30 \times 10^{-4} / -7.2 \times 10^{-4}$ (S/R)	[79]
 <p>(R/S)-Czp-tBuCzB</p>	32.1 (R)	$g_{PL} = 0.54 \times 10^{-3} / -0.51 \times 10^{-3}$ (R/S)	$g_{EL} = 1.54 \times 10^{-3} / -1.48 \times 10^{-3}$ (R/S)	[80]
 <p>(R/S)-Czp-POAB</p>	28.7 (R)	$g_{PL} = 0.48 \times 10^{-3} / -0.46 \times 10^{-3}$ (R/S)	$g_{EL} = 1.3 \times 10^{-3} / -1.25 \times 10^{-3}$ (R/S)	[80]

2.8. Helical chirality based chiral TADF molecules

A rigid hetero-helicene-based blue CP-TADF emitter (QAO-PhCz) was developed in 2021 (**Figure 30**).^[81] The helical structure of the molecule was responsible for molecular chirality. The single crystal geometries depicted that QAO has a twisted form with a dihedral angle of 47.231. The addition of functional groups at the central nitrogen's ortho position increased the dihedral angle. The addition of functional groups at the central nitrogen's para position had no impact. It was found that the rising steric barrier between the QAO and PhCz groups and the growing overlap between the terminal aryl rings induced the helical twist of QAO-PhCz. Through single crystal X-ray diffractions of the developed molecules that racemic mixes of atropisomers were found in them. It was also observed that, due to the low enantiomeric stability, the racemic QAO could not be separated by chiral HPLC at room temperature. In

contrast, because of the larger helical overlap brought about by the PhCz unit and the resultant enhanced enantiomeric stability, the racemic QAO-PhCz might be separated by chiral HPLC at ambient temperature. Due to its rigid molecular structure and higher molecular weight, QAO-PhCz demonstrated improved thermal stability with a decomposition temperature of 418 °C. The CP-OLEDs were fabricated by using the developed molecule as chiral emitter. The EL performance of the synthesized emitter was good with EQE of 14.0%. The enantiomeric emitters displayed excellent mirror-image CD spectra as depicted in Figure 31. The enantiomers of the molecule depicted $|g_{lum}|$ and $|g_{EL}|$ up to 1.1×10^{-3} and 1.5×10^{-3} , respectively. Table 8 summarizes different chiroptical properties of helix chirality-based chiral TADF molecules.

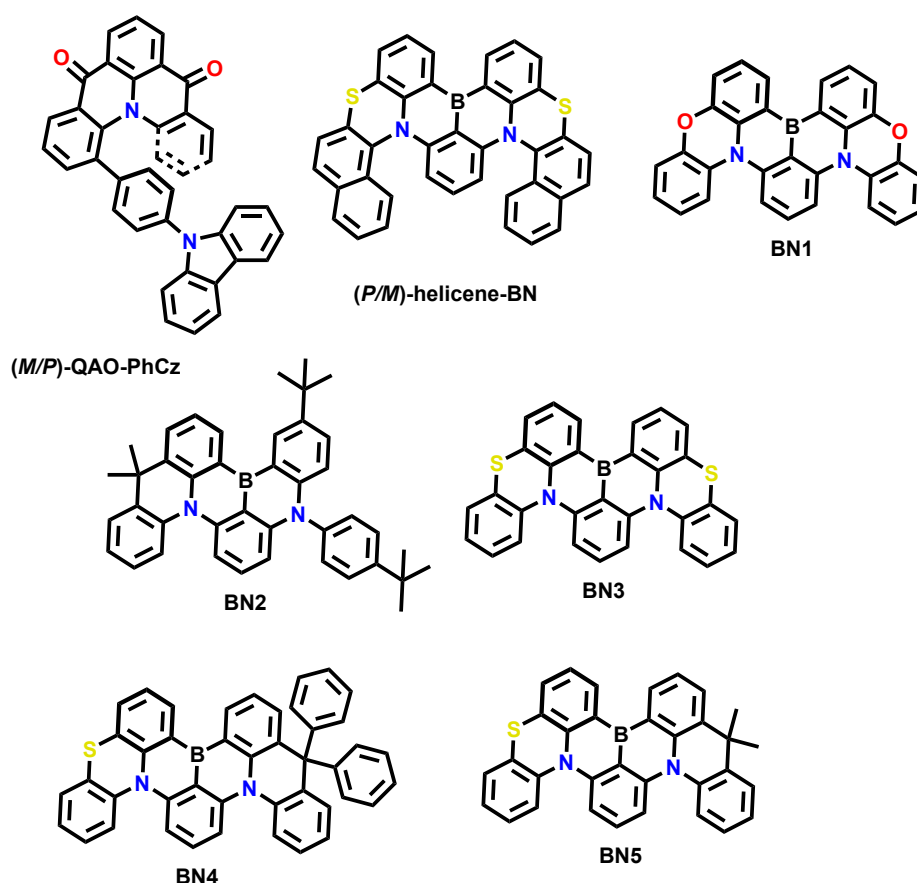


Figure 30. Helical chirality based chiral TADF molecules.^[81-83]

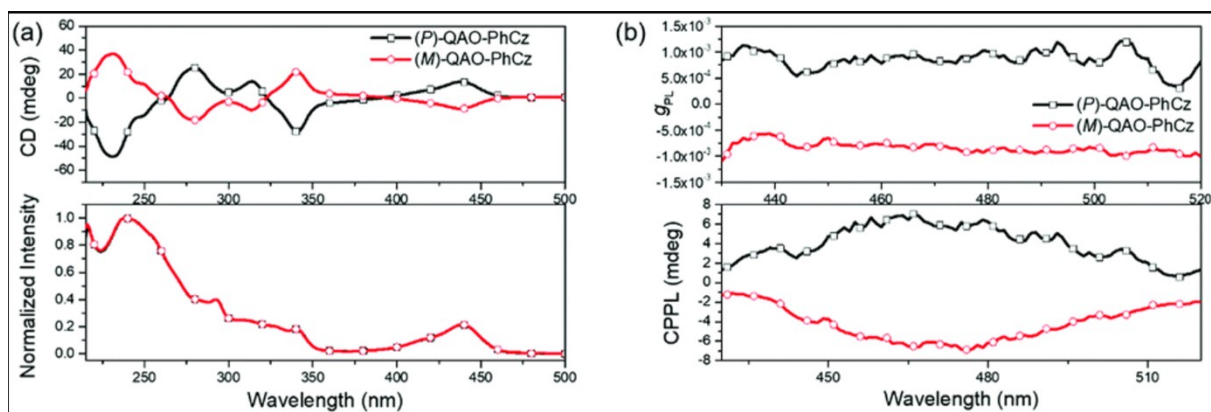


Figure 31. (a) CD spectra (top) and absorption spectrum (bottom) of (*M*)-QAO-PhCz and (*P*)-QAO-PhCz; (b) CPPL spectra of (*M*)-QAO-PhCz and (*P*)-QAO-PhCz.^[81]

In 2022 two helicene-framework containing enantiomers, (*P*)/(*M*)-helicene-BN was synthesized and studied their optical properties (**Figure 30**).^[82] Their design combined helical chirality with a polycyclic aromatic structure that had a boron, nitrogen and sulphur inserted to it. This molecule displayed CPL and narrow TADF properties. The synthetic procedure involved the Buchwald-Hartwig coupling process that is palladium-catalyzed. High-performance liquid chromatography column was used to separate the optically pure enantiomers of (*P/M*)-helicene-BN and could achieve an enantiomeric excess >98%. The molecular electronic characteristics of (*M*)-helicene-BN was calculated and found that the ortho/para locations of the triphenyl boron core and the boron atom were home to the LUMO population. The HOMO was scattered throughout a number of segments that included sulfur atoms, nitrogen atoms and meta positions of boron atoms. This distribution suggested that the double hetero[5]helicene emission core was involved in electron density distribution and it had a significant effect on the helically-chiral CPL activity. The natural transition orbital (NTO) calculations for S_1 that the multi resonance-type transition was clearly preserved. This multi resonance-type transition helped to maintain a tight FWHM. Additionally, a high 317.16 kcal mol⁻¹ estimated energy barrier for the isomerization process from one isomer (*M*) to another (*P*) configuration indicated remarkable chiral stability. It was found that the 1 wt% (*M*)-helicene-BN displayed narrowband green emission with a peak at 525 nm. The developed material depicted effective RISC transition from T_1 to S_1 state. This was possible because of small ΔE_{ST} value, 0.15 eV, which was calculated from the fluorescence and phosphorescence spectra of the doped material. The CP-OLEDs were fabricated by using the developed molecule as chiral emitter. The narrowband green CP-OLEDs based on enantiomers obtained maximum EQE of up to 31.5% and dissymmetry factor, $|g_{EL}|$, of 2.2×10^{-3} .

An asymmetrical peripheral lock was used to strengthen the helical structure of B/N doped nanographene (DABNA-1) in 2022.^[83] The sulfur atom was used as the bridge element to form a hard, locked ring. As sulfur atom was heavier than B, N, and O atoms, this might improve spin-orbit coupling and the intersystem crossover, particularly the RISC. Owing to its huge atomic size and enhanced helical curvature upon insertion, elemental sulfur made chiral separation easier. To improve the solubility, the methylene or phenyl substituents were used as intramolecular flexible lockers. The insertion of a peripheral lock broke down molecular symmetry which raised the barrier to racemization and enabled chiral separation. Two classes of B/N-doped nanographenes, designated as BN4 and BN5 as CPMR-TADF molecules and their symmetric counterparts BN1 and BN3 containing sulfur or oxygen were developed (**Figure 30**). A molecular design without an intramolecular lock was also developed, BN2 molecule (**Figure 30**). The asymmetrical BN4 and BN5 had enough racemization barriers, making it possible to separate enantiomers. The single crystals structures found that each crystal cell contained connected mirror-symmetric molecules with a 1:1 stoichiometric ratio. In the degassed toluene solutions, the sulfur-atom-inserted B/N nanographenes (BN3, BN4, and BN5), displayed TADF properties. They observed that the PLQY of BN3, BN4, and BN5 in the toluene solution increased to 0.72, 0.88, and 0.87, respectively, after degassing. This indicated the triplet state's and TADF's contribution to the fluorescence emission. The transient PL of BN3, BN4, and BN5 displayed delayed component of fluorescence in the degassed solution, with decay times of 16.2, 8.3, and 23.1 microseconds, respectively. It was found that the spectral patterns of circular dichroism were mirrored in the absolute configuration of BN4 and BN5. Their findings demonstrated that the helical moieties also took part in the FMOs. The enantiomers of BN4 and BN5 displayed significant variations in the spectral patterns of the CPL signals, exhibiting mirror-imaged PL dissymmetry factors ($|g_{PL}|$) of $(1.0-2.0) \times 10^{-3}$. The DFT calculations predicted that the degenerate HOMOs and LUMOs were present in all B/N nanographenes. This finding suggested that many LUMO gaps were filled by the HOMOs and vice versa. The narrow mission was explained by a short-range spatial separation distribution of frontier molecular orbitals for the stiff B/N nanographenes. A small intramolecular charge transfer with a strong oscillator strength was demonstrated by all of the B/N nanographenes. The CP-OLEDs were fabricated and obtained maximum EQEs of 20.6%/19.0% ((+)(-)/BN4 enantiomers) and 22.0%/26.5%, ((+)(-)/BN5 enantiomers). Their corresponding g_{EL} values were $+3.7 \times 10^{-3}/-3.1 \times 10^{-3}$ ((+)(-)/BN4 enantiomers) and $+1.9 \times 10^{-3}/-1.6 \times 10^{-3}$ ((+)(-)/BN5 enantiomers).

The CP-MR-TADF materials combine CPL, narrowband emission, and TADF to create efficient CP-OLEDs. Wang et al. in 2023 used an edge-topology molecular-engineering technique to develop high-performance CP-MR-TADF enantiomers (*P* and *M*)-BN-Py (**Figure 32b**).^[84] These enantiomers possessed inherent helical chirality into the multi-resonance framework. They fabricated the CP-OLEDs with the synthesized (*P* and *M*)-BN-Py emitters and used ambipolar transport host PhCbBCz, which produced pure green emission at 532 nm with full width at half maxima of 37 nm. They could reach maximum EQEs of 30.6% and 29.2%, as well as CPEL signals with g_{EL} of -4.37×10^{-4} and 4.35×10^{-4} for (*P*) and (*M*)-BN-Py, respectively. The CPL spectra of enantiomers (*P* and *M*)-BN-Py depicted green light emission with g_{PL} of -3.81×10^{-4} (*P*) for and $+5.19 \times 10^{-4}$ (*M*).

Qu et al. in 2023 designed a helically chiral CP-TADF hetero-helicenes with a fused D-A core skeleton.^[85] This heterohelicene skeleton had a large relative twist between the D and A groups. Spatial congestion in molecular framework facilitated HOMO-LUMO separation and the TADF feature in fused-ring systems. The synthesized hetero[4]helicenes CNSPZ and CNSOPZ (**Figure 32a**) had a merged donor-acceptor (D-A) core skeleton. The authors separated the (*P,P*)- and (*M,M*)-enantiomers with helical chirality which had higher configurational stability than hetero[4]helicenes. The designed compounds had exceptional configurational stability, making them ideal for chiroptical studies and OLED device fabrication by thermal vacuum deposition. The synthesized helical enantiomers possessed good configurational stability and effectively emitted CP light in doped sheets, with dissymmetry values up to 3.1×10^{-3} . They also fabricated the CP-OLEDs and achieved the EQE up to 20.0% with g_{EL} value of 2.9×10^{-3} .

The natural helical π -conjugated skeleton of helicene makes them ideal for CPEL. It has been observed that carbon helicenes typically have low EQE. However, adding a multi-resonance TADF BN structure to the helicenes has improved the EQE. Chen et al. in 2024 synthesized B,N-embedded hetero[9]helicenes (BN[9]H) (**Figure 32c**), which emitted a brilliant fluorescence at 578 nm and had a high g_{lum} of up to 5.8×10^{-3} .^[86] They also fabricated the CP-OLEDs with BN[9]H emitter, which exhibited a maximum EQE of 35.5% with narrow emission. The calculated g_{lum} values for *P* and *M*- isomers were -5.5×10^{-3} and 5.8×10^{-3} , respectively. The CP-OLEDs possessed a high g_{EL} value of 6.2×10^{-3} . The fabricated CP-OLEDs had the highest Q-factor ($|EQE \times g_{EL}|$) among helicene analogues, measuring at 2.2×10^{-3} .

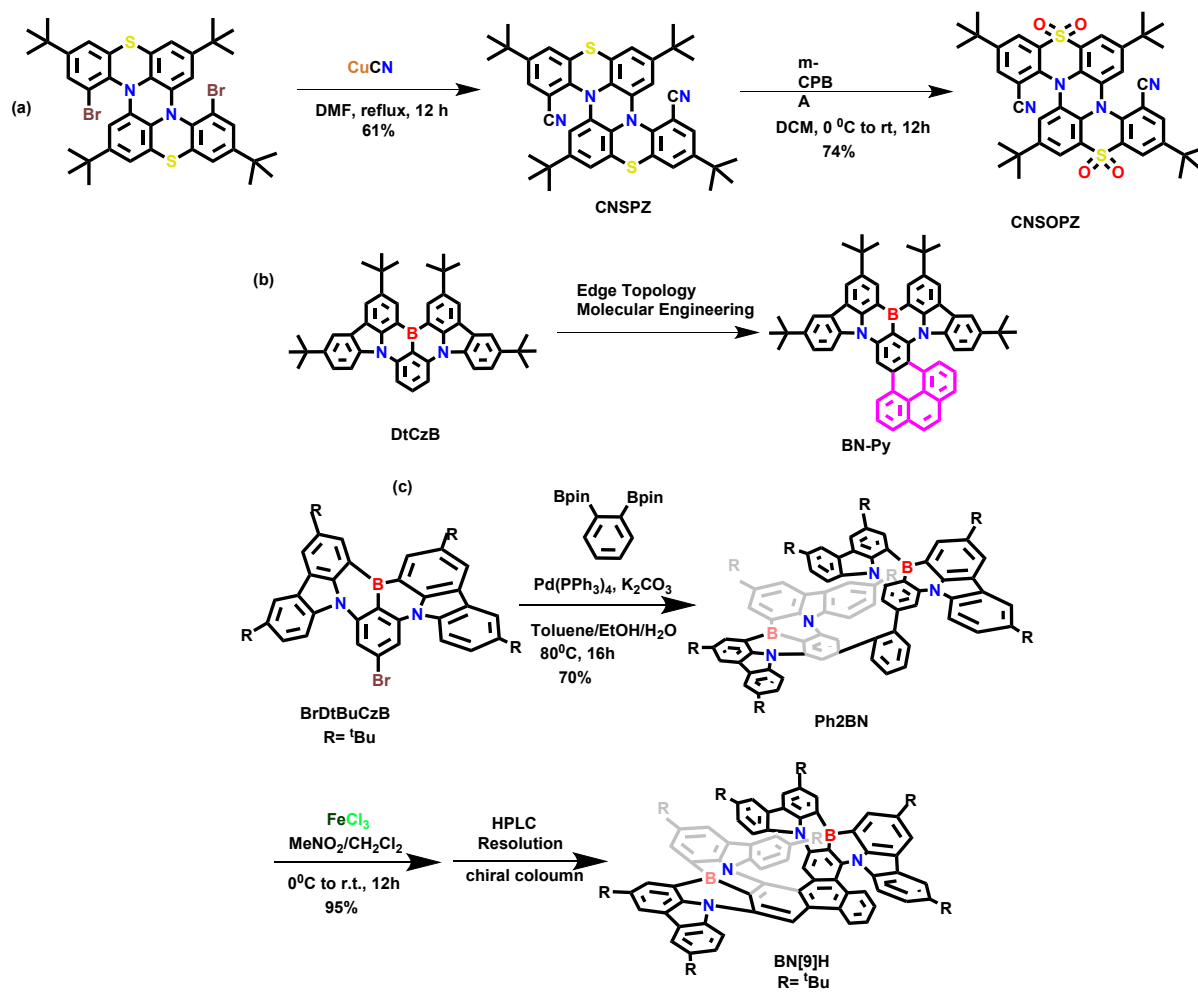
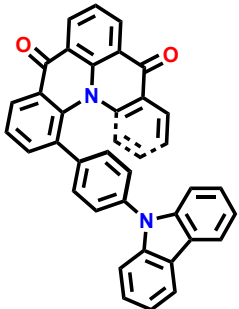
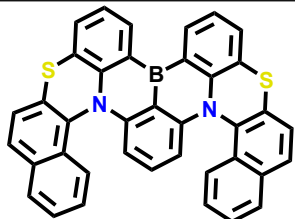
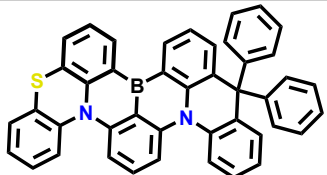
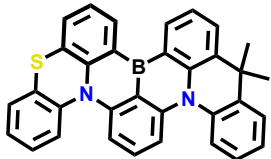
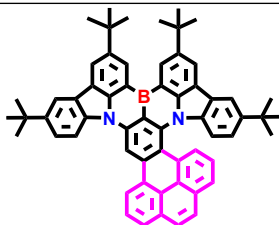
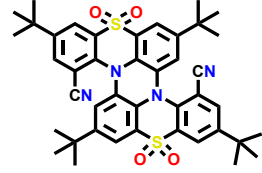
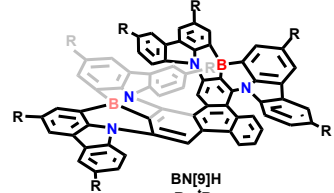


Figure. 32. Chemical structures of some helical chirality-based molecules.^[84-86]

Table 8. Chiroptical properties of helical chirality-based chiral TADF molecules.

Compound	EQE_{\max} (%) (Isomer used as emitter)	Luminescence dissymmetry factor	Electroluminescence dissymmetry factor	Reference
 <p>(M/P)-QAO-PhCz</p>	14	$g_{\text{lum}} = -9.2 \times 10^{-4} / 1.1 \times 10^{-3}$ (M/P)	$ g_{\text{EL}} = 1.5 \times 10^{-3}$ (M/P)	[81]
 <p>(P/M)-helicene-BN</p>	31.5 (P)	$g_{\text{lum}} = -2.1 \times 10^{-3} / 2 \times 10^{-3}$ (M/P) (Toluene)	$g_{\text{EL}} = -2.2 \times 10^{-3} / 1.2 \times 10^{-3}$ (M/P)	[82]
 <p>BN4</p>	20.6/19.0 (+)/(-)	$g_{\text{PL}} = 1.1 \times 10^{-3} / -1.0 \times 10^{-3}$ (films) (P/M)	$g_{\text{EL}} = 3.7 \times 10^{-3} / -3.1 \times 10^{-3}$ (P/M)	[83]
 <p>BN5</p>	22.0/26.50 (+)/(-)	$g_{\text{PL}} = 1.3 \times 10^{-3} / -1.0 \times 10^{-3}$ (films) (P/M)	$g_{\text{EL}} = 1.9 \times 10^{-3} / -1.6 \times 10^{-3}$ (P/M)	[83]
 <p>BN-Py</p>	30.6 (P)	$g_{\text{PL}} = -3.81 \times 10^{-4} / 5.19 \times 10^{-4}$ (P/M)	$g_{\text{EL}} = -4.37 \times 10^{-4} / 4.35 \times 10^{-4}$ (P/M)	[84]

 <p>CNSOPZ</p>	20.0 (<i>M,M</i>)	$g_{PL} = -3.1 \times 10^{-3} / 2.5 \times 10^{-3}$ (<i>PP/MM</i>)	$g_{EL} = 2.9 \times 10^{-3}$ (<i>M,M</i>)	[85]
 <p>BN[9]H R = ^tBu</p>	35.5 (<i>M</i>)	$g_{PL} = -5.5 \times 10^{-3} / 5.8 \times 10^{-3}$ (<i>P/M</i>)	$g_{EL} = -6.2 \times 10^{-3} / 4.9 \times 10^{-3}$ (<i>P/M</i>)	[86]

4. Conclusion and Perspective

CP-OLEDs are a highly efficient source of CP light, which opens up new possibilities for CP-EL display and technology in the future. Numerous kinds of metal complexes, macromolecules, and small- and large-sized chiral organic compounds have been synthesized with high efficiency.^[87] These days TADF technology is promising method because of its precious metal-free production and 100% internal quantum efficiency. The efficient radiative decay and the EQE from the emissive layer of the OLED increases drastically when TADF molecules are used as emitter or host. The ability to collect both electro-generated singlet and triplet excitons make TADF materials to have a high efficiency. For this reason, one of the efficient methods for developing CP-OLEDs is to induce chirality in the TADF molecules which produce CPL. Our review article summarizes different approaches used to induce chirality in small organic TADF molecules. We have discussed different types of molecular frameworks for TADF property and the organic units that induce chirality to these TADF molecules. Generally, methods of inducing chirality to the organic molecule can be broadly categorized into two classes, one of which is chiral perturbation, and the other is intrinsic or inherent chirality. Our review classifies different types of chiral organic units that impart chirality to organic TADF molecules through perturbation and intrinsically. These organic moieties include binaphthol, octahydrobinaphthol, 1,2-diaminocyclohexane, paracyclophane, biphenyl, helicene and asymmetric carbon. Additionally, we have provided an overview of their photo-physics, chiroptical characteristics, theoretical analysis, and chiral-EL efficiencies.

By reviewing the literature, we find that the research and development on the chiral TADF materials is escalating at very fast rate, but still, the value of EL dissymmetry factor (CPEL), g_{EL} , is very low. This very low value of the g_{EL} restricts these chiral materials from being

utilized in commercial applications. Therefore, improving the EL dissymmetry factor remains a significant challenge and still bottleneck for the 3D displays technology. We agree that the TADF enjoys its position as the very efficient method for improving the device efficiency but it becomes very difficult to achieve pure blue colour coordinates with the help of TADF materials. The design strategy of the TADF molecules include the strong donor and acceptor units with high dihedral angle between them. This type of molecular arrangement will lead to the separated HOMO/LUMO energy levels leading to small ΔE_{ST} , which is the pre-requisite condition for TADF compounds. However, this type of strong donor and acceptor framework also results in the appearance of high charge transfer character in the compound, leading to the red-shifted emission. We should consider each parameter while designing the ideal TADF molecular structures, including stability, color purity, and high quantum yields or efficiencies. The stability can be enhanced by choosing the rigid molecular framework and stable donor/acceptor moieties connected by phenyl linker. The strength of the donor can be enhanced by choosing multiple donor systems or connecting electron-donating chromophoric units to it. Similarly, the strength of the acceptor also influences the singlet-triplet energy gap. The small singlet-triplet energy gap can be achieved by the separation of HOMO and LUMO, while the high radiation efficiency requires overlap of the frontier molecular orbitals. Therefore, a judicious approach that can solve this trade-off must be chosen. As mentioned, the CP-TADF can be generated by perturbing the TADF molecule with some chiral unit or using the intrinsically chiral molecular design. We only need to design an ideal TADF unit that can be perturbed by the chiral structure.

It has been observed that the strong donors and acceptors populate the frontier molecular orbitals on the donor (HOMO) and acceptor (LUMO) units. Selecting this type of moieties decreases the singlet energy of TADF emitters due to the spatial separation of the HOMO and LUMOs. Whereas, the weak electron-donating units reduce the HOMO/LUMO localization, which results in a mild drop in singlet energy. Therefore, while designing the TADF molecules, strong donor units such as carbazole, acridine, etc., should be the choice. The TADF fluorophores possess a lifetime (both fluorescence and delayed fluorescence) in the nanoseconds and microseconds range. The non-radiative transitions are lesser in the case of fast-decaying fluorescence relative to slow-decaying delayed fluorescence. Therefore, the design strategy of the TADF molecules should consider the reduction of the delayed fluorescence lifetime. The design strategy to shorten the lifetime of delayed fluorescence is the same as that for minimizing the singlet-triplet energy gap. The small singlet-triplet energy gap

increases the RISC process which further controls the delayed lifetime. Thus, increasing the strength of the donor and acceptor in a molecule and distortion of the donor/acceptor from a linker are two methods available for lowering the singlet-triplet energy gap and shortening the delayed lifetime. A distorted molecular structure may be effectively designed by connecting the donor and acceptor via an ortho-position of a phenyl linker as it helps to increase the dihedral angle between donor and acceptor.

The design approaches for high PLQY might include phenyl linker, HOMO dispersing, and dual-emitting core methods. The use of a phenyl linker in molecular structures is encouraged to achieve high PLQY due to significant HOMO and LUMO overlap. The HOMO/LUMO separation is necessary for a small singlet-triplet energy gap. However, the complete separation of the frontier molecular orbitals also results in low oscillator strength. Therefore, a phenyl linker design was proposed to optimize HOMO and LUMO separation and achieve high PLQY. The phenyl linking unit aims to minimize HOMO and LUMO separation by extending both to the aromatic phenyl linker. The small extent of overlap of frontier molecular orbitals on the phenyl linker improves oscillator strength and light absorption, resulting in higher PLQY in the TADF emitter. The HOMO dispersing design aims to enhance HOMO/LUMO overlap between donors and acceptors in the backbone structure by distributing them uniformly. Increased HOMO/LUMO overlap strengthens oscillator strength and improves PLQY. In a dual-emitting core design, two TADF emitter units are connected in a single molecule. It can be anticipated that the two connected emitters aim to improve light absorption and emission. The HLCT method is a widely accepted approach for developing pure blue materials with high-efficiency values. Therefore, there should be an approach for developing the chiral-HLCT materials along with the chiral TADF molecules. The CP-OLEDs are advancing tremendously since recently; however, the stability of CP-OLEDs remains largely unexplored. The stability of the emitter is one of the main elements influencing the device lifetime of OLEDs. It is necessary to investigate the OLED lifetime of TADF-based compounds with a chiral unit. It would be beneficial to study how charge mobility, glass transition temperatures, and intramolecular hydrogen bonding affect the stability of CP-OLED molecules and the lifetime of the device.

The EQE of the OLEDs can be linked to the orientation parameter of the emitters. This orientation parameter affects the out-coupling efficiency of the device. The stable and planar geometry of the TADF emitters is one of the reasons for their suitable orientation parameter.

The area of CP-OLEDs still needs to explore about the orientation parameters of the CP-OLED emitters.^[88]

Ink-jet printing is a solution-process technology for generating large-area OLEDs. The thermal evaporation technique for fabricating OLEDs is still difficult and expensive. The synthesis of simple dendrimers and polymers as emitters for solution-processed OLEDs has received an increasing amount of attention. The development of CP-TADF-based polymers and small molecules for solution-process techniques is still lagging behind. Therefore, this field of research needs adequate attention.

It has also been observed that different types of the TADF emitters lack novel design factors. Moreover, it has been found that the majority of the TADF emitters have broad emission spectra. This red shifted and broad emission spectra also confirms the lack of deep blue emitters. Most of the CP-TADF compounds reported in the literature have green or yellow light emissions. The efficient blue and red or NIR chiral emitters with high PLQY are hard to find.^[12] The fusion of chiral units with conventional blue or NIR or red TADF/MR-TADF molecules can certainly result in the development of these types of molecules. Therefore, the new design principles with deep blue emissions of CP-TADF emitters are the need of the hour. Most of the reported CP-TADF materials have low asymmetry factors. In the future direction, a novel strategy to solve the problem of trade-off between EQE and the intensity of CP emission should be developed.

We are confident that our review will be invaluable to the researchers within large domain of scientific and display engineering field. We are also hopeful that this piece of work will make a heavy share of contribution to the progression of display technology in the future. Therefore, it is apparent that establishing a new technology or expanding the current state of the art will have an enormous impact on these sectors.

List of abbreviations

AIE	aggregation induced emission
CT	charge Transfer
CPL	circularly polarized luminescence
CE	current efficiency
CP	circularly polarized

CD	circular dichroism
EML	emissive layer
EL	electroluminescence
EM	electromagnetic
EQE	external quantum efficiency
EUE	exciton utilization efficiency
ETL	electron transport layer
HTM	hole-transport material
HIL	hole-injection layer
HTL	hole transport layer
HLCT	hybrid local and charge transfer
HOMO	high occupied molecular orbital
IC	internal conversion
ISC	intersystem crossing
IQE	internal quantum efficiency
ITO	Indium tin oxide
LUMO	lowest unoccupied molecular orbital
LCP	left-handed circularly polarized
OLEDs	Organic light-emitting diodes
PE	Power efficiency
PhOLEDs	Phosphorescent organic light-emitting diodes
PLQY	photoluminescence quantum yields
PL	photoluminescence
RISC	reverse intersystem crossing
RCP	right-handed circularly polarized
S ₁	first excited singlet state
T ₁	first triplet excited state
TADF	Thermally active delayed Fluorescence
T _g	Glass transition temperature

Conflicts of interest

The authors have no conflicts of interest.

Acknowledgements

The author DT acknowledges NPDF, SERB, Department of Science and Technology (DST), India (PDF/2023/000022) and VS acknowledges Indian Institute of Technology Hyderabad, India (SG/IITH/F324/2022-23/SG-138) for financial support.

Author Information

Corresponding Author

Sivakumar Vaidyanathan - Department of Chemistry, Indian Institute of Technology, Hyderabad, Sangareddy 502285 Telangana, India; orcid.org/0000-0002-2104-2627;

Email: vsiva@chy.iith.ac.in

Diksha Thakur

Department of Chemistry, Indian Institute of Technology, Hyderabad, Sangareddy 502285 Telangana, India; orcid: 0009-0006-9908-5316

References

- [1] C. W. Tang, S. A. VanSlyke, *Appl. Phys. Lett.* **1987**, *51*, 913.
- [2] M. Y. Wong, E. Zysman-Colman, *Adv. Mater.* **2017**, *29*, 1605444.
- [3] Y. Im, M. Kim, Y. J. Cho, J.-A. Seo, K. S. Yook, J. Y. Lee, *Chem. Mater.* **2017**, *29*, 1946.
- [4] M. A. Baldo, D. F. O'Brien, Y. You, A. Shoustikov, S. Sibley, M. E. Thompson, S. R. Forrest, *Nature* **1998**, *395*, 151.
- [5] Y. Ma, H. Zhang, J. Shen, C. Che, *Synth. Met.* **1998**, *94*, 245.
- [6] K. S. Yook, J. Y. Lee, *Adv. Mater.* **2014**, *26*, 4218.
- [7] B. Wex, B. R. Kaafarani, *J. Mater. Chem. C* **2017**, *5*, 8622.

- [8] J. R. Brandt, F. Salerno, M. J. Fuchter, *Nat. Rev. Chem.* **2017**, *1*, 1.
- [9] D.-Y. Kim, *J. Korean Phys. Soc.* **2006**, *49*, 505.
- [10] L. Frédéric, A. Desmarchelier, L. Favereau, G. Pieters, *Adv. Funct. Mater.* **2021**, *31*, 2010281.
- [11] D.-W. Zhang, M. Li, C.-F. Chen, *Chem. Soc. Rev.* **2020**, *49*, 1331.
- [12] X. Li, Y. Xie, Z. Li, *Adv. Photonics Res.* **2021**, *2*, 2000136.
- [13] Z.-L. Gong, Z.-Q. Li, Y.-W. Zhong, *Aggregate* **2022**, *3*, e177.
- [14] J. L. Lunkley, D. Shirotnani, K. Yamanari, S. Kaizaki, G. Muller, *J. Am. Chem. Soc.* **2008**, *130*, 13814.
- [15] J. L. Greenfield, J. Wade, J. R. Brandt, X. Shi, T. J. Penfold, M. J. Fuchter, *Chem. Sci.* **2021**, *12*, 8589.
- [16] K. Ma, W. Chen, T. Jiao, X. Jin, Y. Sang, D. Yang, J. Zhou, M. Liu, P. Duan, *Chem. Sci.* **2019**, *10*, 6821.
- [17] E. Samu, P. Huszthy, L. Somogyi, M. Hollósi, *Tetrahedron Asymmetry* **1999**, *10*, 2775.
- [18] J. L. Greenfield, E. W. Evans, D. Di Nuzzo, M. Di Antonio, R. H. Friend, J. R. Nitschke, *J. Am. Chem. Soc.* **2018**, *140*, 10344.
- [19] S. Feuillastre, M. Pauton, L. Gao, A. Desmarchelier, A. J. Riives, D. Prim, D. Tondelier, B. Geffroy, G. Muller, G. Clavier, G. Pieters, *J. Am. Chem. Soc.* **2016**, *138*, 3990.
- [20] F. Song, Z. Xu, Q. Zhang, Z. Zhao, H. Zhang, W. Zhao, Z. Qiu, C. Qi, H. Zhang, H. H. Y. Sung, I. D. Williams, J. W. Y. Lam, Z. Zhao, A. Qin, D. Ma, B. Z. Tang, *Adv. Funct. Mater.* **2018**, *28*, 1800051.
- [21] S. Sun, J. Wang, L. Chen, R. Chen, J. Jin, C. Chen, S. Chen, G. Xie, C. Zheng, W. Huang, *J. Mater. Chem. C* **2019**, *7*, 14511.

- [22] L. Frédéric, A. Desmarchelier, R. Plais, L. Lavnech, G. Muller, C. Villafuerte, G. Clavier, E. Quesnel, B. Racine, S. Meunier-Della-Gatta, J.-P. Dognon, P. Thuéry, J. Crassous, L. Favereau, G. Pieters, *Adv. Funct. Mater.* **2020**, *30*, 2004838.
- [23] B. He, Q. Zhong, Q. Dong, X. Yang, S. J. Cowling, W. Qiao, D. W. Bruce, W. Zhu, P. Duan, Y. Wang, *Mater. Horiz.* **2024**, *11*, 1251.
- [24] Z.-G. Wu, H.-B. Han, Z.-P. Yan, X.-F. Luo, Y. Wang, Y.-X. Zheng, J.-L. Zuo, Y. Pan, *Adv. Mater.* **2019**, *31*, 1900524.
- [25] Z.-G. Wu, Z.-P. Yan, X.-F. Luo, L. Yuan, W.-Q. Liang, Y. Wang, Y.-X. Zheng, J.-L. Zuo, Y. Pan, *J. Mater. Chem. C* **2019**, *7*, 7045.
- [26] Z.-P. Liang, R. Tang, Y.-C. Qiu, Y. Wang, H. Lu, Z.-G. Wu, *Acta Chim. Sin.* **2021**, *79*, 1401.
- [27] T.-T. Liu, Z.-P. Yan, J.-J. Hu, L. Yuan, X.-F. Luo, Z.-L. Tu, Y.-X. Zheng, *ACS Appl. Mater. Interfaces* **2021**, *13*, 56413.
- [28] Y. Xu, Q. Wang, X. Cai, C. Li, Y. Wang, *Adv. Mater.* **2021**, *33*, 2100652.
- [29] F.-M. Xie, J.-X. Zhou, X.-Y. Zeng, Z.-D. An, Y.-Q. Li, D.-X. Han, P.-F. Duan, Z.-G. Wu, Y.-X. Zheng, J.-X. Tang, *Adv. Opt. Mater.* **2021**, *9*, 2100017.
- [30] Y.-F. Wang, X. Liu, Y. Zhu, M. Li, C.-F. Chen, *J. Mater. Chem. C* **2022**, *10*, 4805.
- [31] J.-M. Teng, D.-W. Zhang, Y.-F. Wang, C.-F. Chen, *ACS Appl. Mater. Interfaces* **2022**, *14*, 1578.
- [32] W.-L. Zhao, Y.-F. Wang, S.-P. Wan, H.-Y. Lu, M. Li, C.-F. Chen, *CCS Chem.* **2022**, *4*, 3540.
- [33] Z.-P. Yan, L. Yuan, Y. Zhang, M.-X. Mao, X.-J. Liao, H.-X. Ni, Z.-H. Wang, Z. An, Y.-X. Zheng, J.-L. Zuo, *Adv. Mater.* **2022**, *34*, 2204253.
- [34] L. Qu, H. Xiao, B. Zhang, Q. Yang, J. Song, X. Zhou, Z.-X. Xu, H. Xiang, *Chem. Eng. J.* **2023**, *471*, 144709.

- [35] X. Yin, H. Huang, N. Li, W. Li, X. Mo, M. Huang, G. Chen, J. Miao, C. Yang, *Mater. Horiz.* **2024**, *11*, 1752.
- [36] J.-M. Teng, C.-F. Chen, *ChemPhotoChem* **2024**, *8*, e202300253.
- [37] J. Lei, T.-A. Lou, C.-R. Chen, C.-H. Chuang, H.-Y. Liu, L.-Y. Hsu, Y.-C. Chao, T.-L. Wu, *Chem. – Asian J.* **2024**, *19*, e202300940.
- [38] L. Chen, C. Li, Z.-F. Liu, Y. Kuboi, E. Fu, L. S. Vargas, C. Adachi, F. Mathevet, S. Zhang, *Chem. Commun.* **2024**, *60*, 1758.
- [39] Z.-L. Tu, Z.-P. Yan, X. Liang, L. Chen, Z.-G. Wu, Y. Wang, Y.-X. Zheng, J.-L. Zuo, Y. Pan, *Adv. Sci.* **2020**, *7*, 2000804.
- [40] Y.-F. Wang, M. Li, W.-L. Zhao, Y.-F. Shen, H.-Y. Lu, C.-F. Chen, *Chem. Commun.* **2020**, *56*, 9380.
- [41] M. Li, Y.-F. Wang, D. Zhang, L. Duan, C.-F. Chen, *Angew. Chem. Int. Ed.* **2020**, *59*, 3500.
- [42] Z.-L. Tu, J.-J. Lu, X.-F. Luo, J.-J. Hu, S. Li, Y. Wang, Y.-X. Zheng, J.-L. Zuo, Y. Pan, *Adv. Opt. Mater.* **2021**, *9*, 2100596.
- [43] W.-L. Zhao, K.-K. Tan, W.-C. Guo, C.-H. Guo, M. Li, C.-F. Chen, *Adv. Sci.* **n.d.**, *n/a*, 2309031.
- [44] S.-P. Wan, W.-L. Zhao, K.-K. Tan, H.-Y. Lu, M. Li, C.-F. Chen, *Chem. Eng. J.* **2023**, *468*, 143508.
- [45] K.-K. Tan, D.-W. Zhang, W.-L. Zhao, M. Li, C.-F. Chen, *Chem. Eng. J.* **2023**, *462*, 142123.
- [46] Y. Wang, Y. Zhang, W. Hu, Y. Quan, Y. Li, Y. Cheng, *ACS Appl. Mater. Interfaces* **2019**, *11*, 26165.
- [47] X. Zhang, Z. Xu, Y. Zhang, Y. Quan, Y. Cheng, *ACS Appl. Mater. Interfaces* **2021**, *13*, 55420.

- [48] Z.-P. Yan, T.-T. Liu, R. Wu, X. Liang, Z.-Q. Li, L. Zhou, Y.-X. Zheng, J.-L. Zuo, *Adv. Funct. Mater.* **2021**, *31*, 2103875.
- [49] Y. Zhang, J. Li, Y. Quan, S. Ye, Y. Cheng, *Chem. – Eur. J.* **2021**, *27*, 589.
- [50] Y. Tsuji, N. Kanno, C. Goto, S. Katao, Y. Okajima, P. Reine, P. Imbrasas, S. Reineke, K. Shizu, T. Nakashima, H. Kaji, T. Kawai, M. Louis, *J. Mater. Chem. C* **2023**, *11*, 5968.
- [51] A. M. T. Muthig, O. Mrózek, T. Ferschke, M. Rödel, B. Ewald, J. Kuhnt, C. Lenczyk, J. Pflaum, A. Steffen, *J. Am. Chem. Soc.* **2023**, *145*, 4438.
- [52] X. Dong, S. Shen, Y. Qin, X. Hu, H. Gao, G. Liu, T. Gao, Z. Pang, P. Wang, Y. Wang, *Chin. Chem. Lett.* **2023**, *34*, 108311.
- [53] J.-M. Teng, C.-F. Chen, *Adv. Opt. Mater.* **2023**, *11*, 2300550.
- [54] J. Tong, P. Wang, X.-J. Liao, Y. Wang, Y.-X. Zheng, Y. Pan, *Adv. Opt. Mater.* **n.d.**, *n/a*, 2302730.
- [55] M. Li, S.-H. Li, D. Zhang, M. Cai, L. Duan, M.-K. Fung, C.-F. Chen, *Angew. Chem. Int. Ed.* **2018**, *57*, 2889.
- [56] Y.-F. Wang, H.-Y. Lu, C. Chen, M. Li, C.-F. Chen, *Org. Electron.* **2019**, *70*, 71.
- [57] T. Imagawa, S. Hirata, K. Totani, T. Watanabe, M. Vacha, *Chem. Commun.* **2015**, *51*, 13268.
- [58] Y. Chen, C. Xu, B. Xu, Z. Mao, J.-A. Li, Z. Yang, N. R. Peethani, C. Liu, G. Shi, F. L. Gu, Y. Zhang, Z. Chi, *Mater. Chem. Front.* **2019**, *3*, 1800.
- [59] F.-Y. Hao, Y.-Z. Shi, K. Wang, S.-Y. Xiong, X.-C. Fan, L. Wu, C.-J. Zheng, Y.-Q. Li, X.-M. Ou, X.-H. Zhang, *Dyes Pigments* **2020**, *178*, 108336.
- [60] S.-Y. Yang, Y.-K. Wang, C.-C. Peng, Z.-G. Wu, S. Yuan, Y.-J. Yu, H. Li, T.-T. Wang, H.-C. Li, Y.-X. Zheng, Z.-Q. Jiang, L.-S. Liao, *J. Am. Chem. Soc.* **2020**, *142*, 17756.

- [61] F. Ni, C.-W. Huang, Y. Tang, Z. Chen, Y. Wu, S. Xia, X. Cao, J.-H. Hsu, W.-K. Lee, K. Zheng, Z. Huang, C.-C. Wu, C. Yang, *Mater. Horiz.* **2021**, *8*, 547.
- [62] Y.-P. Zhang, X. Liang, X.-F. Luo, S.-Q. Song, S. Li, Y. Wang, Z.-P. Mao, W.-Y. Xu, Y.-X. Zheng, J.-L. Zuo, Y. Pan, *Angew. Chem. Int. Ed.* **2021**, *60*, 8435.
- [63] Y.-F. Wang, M. Li, J.-M. Teng, H.-Y. Zhou, C.-F. Chen, *Adv. Funct. Mater.* **2021**, *31*, 2106418.
- [64] Y.-F. Wang, M. Li, J.-M. Teng, H.-Y. Zhou, W.-L. Zhao, C.-F. Chen, *Angew. Chem. Int. Ed.* **2021**, *60*, 23619.
- [65] Z. Huang, C.-W. Huang, Y.-K. Tang, Z. Xiao, N. Li, T. Hua, X. Cao, C. Zhou, C.-C. Wu, C. Yang, *Dyes Pigments* **2022**, *197*, 109860.
- [66] S.-Y. Yang, Z.-Q. Feng, Z. Fu, K. Zhang, S. Chen, Y.-J. Yu, B. Zou, K. Wang, L.-S. Liao, Z.-Q. Jiang, *Angew. Chem.* **2022**, *134*, e202206861.
- [67] Y.-P. Zhang, M.-X. Mao, S.-Q. Song, Y. Wang, Y.-X. Zheng, J.-L. Zuo, Y. Pan, *Angew. Chem. Int. Ed.* **2022**, *61*, e202200290.
- [68] Y. Yang, N. Li, J. Miao, X. Cao, A. Ying, K. Pan, X. Lv, F. Ni, Z. Huang, S. Gong, C. Yang, *Angew. Chem.* **2022**, *134*, e202202227.
- [69] Y.-P. Zhang, S.-Q. Song, M.-X. Mao, C.-H. Li, Y.-X. Zheng, J.-L. Zuo, *Sci. China Chem.* **2022**, *65*, 1347.
- [70] X.-F. Luo, S.-Q. Song, X. Wu, C.-F. Yip, S. Cai, Y.-X. Zheng, *Aggregate* **2024**, *5*, e445.
- [71] Y. Zhang, M. Chen, H. Li, L. Hua, Z. Zhao, H. Zhao, L. Kan, X. Chu, K. Wang, S. Yan, Z. Ren, *Chem. Mater.* **2024**, *36*, 3369.
- [72] Y. Zheng, L. Zhang, Z. Huang, S. Li, L. Zuo, Y. Liang, C. Liu, S. Luo, G. Shi, Z. Zhao, F. Sun, B. Xu, *Chem. – Eur. J.* **2023**, *29*, e202202594.
- [73] Z. Hao, N. Li, J. Miao, Z. Huang, X. Lv, X. Cao, *Chem. Eng. J.* **2023**, *454*, 140070.

- [74] M.-Y. Zhang, Z.-Y. Li, B. Lu, Y. Wang, Y.-D. Ma, C.-H. Zhao, *Org. Lett.* **2018**, *20*, 6868.
- [75] C. Liao, Y. Zhang, S.-H. Ye, W.-H. Zheng, *ACS Appl. Mater. Interfaces* **2021**, *13*, 25186.
- [76] N. Sharma, E. Spuling, C. M. Mattern, W. Li, O. Fuhr, Y. Tsuchiya, C. Adachi, S. Bräse, I. D. W. Samuel, E. Zysman-Colman, *Chem. Sci.* **2019**, *10*, 6689.
- [77] D.-W. Zhang, J.-M. Teng, Y.-F. Wang, X.-N. Han, M. Li, C.-F. Chen, *Mater. Horiz.* **2021**, *8*, 3417.
- [78] J. Seibert, Y. Xu, H. Hafeez, J. Podlech, L. Favereau, E. Spuling, C. Waldhelm, M. Nieger, O. Fuhr, Z. Hassan, J. Crassous, I. D. W. Samuel, E. Zysman-Colman, S. Bräse, *Adv. Funct. Mater.* **n.d.**, *n/a*, 2401956.
- [79] M. Gong, L. Yuan, Y.-X. Zheng, W.-H. Zheng, *Adv. Funct. Mater.* **n.d.**, *n/a*, 2314205.
- [80] X.-J. Liao, D. Pu, L. Yuan, J. Tong, S. Xing, Z.-L. Tu, J.-L. Zuo, W.-H. Zheng, Y.-X. Zheng, *Angew. Chem.* **2023**, *135*, e202217045.
- [81] S.-Y. Yang, S.-N. Zou, F.-C. Kong, X.-J. Liao, Y.-K. Qu, Z.-Q. Feng, Y.-X. Zheng, Z.-Q. Jiang, L.-S. Liao, *Chem. Commun.* **2021**, *57*, 11041.
- [82] W. Yang, N. Li, J. Miao, L. Zhan, S. Gong, Z. Huang, C. Yang, *CCS Chem.* **2022**, *4*, 3463.
- [83] X. Wu, J.-W. Huang, B.-K. Su, S. Wang, L. Yuan, W.-Q. Zheng, H. Zhang, Y.-X. Zheng, W. Zhu, P.-T. Chou, *Adv. Mater.* **2022**, *34*, 2105080.
- [84] Q. Wang, L. Yuan, C. Qu, T. Huang, X. Song, Y. Xu, Y.-X. Zheng, Y. Wang, *Adv. Mater.* **2023**, *35*, 2305125.
- [85] C. Qu, Y. Zhu, L. Liang, K. Ye, Y. Zhang, H. Zhang, Z. Zhang, L. Duan, Y. Wang, *Adv. Opt. Mater.* **2023**, *11*, 2203030.

- [86] W.-C. Guo, W.-L. Zhao, K.-K. Tan, M. Li, C.-F. Chen, *Angew. Chem. Int. Ed.* **2024**, *63*, e202401835.
- [87] L. Yuan, Y.-P. Zhang, Y.-X. Zheng, *Sci. China Chem.* **2024**, *67*, 1097.
- [88] D. Sun, C. Si, T. Wang, E. Zysman-Colman, *Adv. Photonics Res.* **2022**, *3*, 2200203.